

5)

OPTIMIZATION OF THE SEISMIC EARLY WARNING SYSTEM FOR THE TOHOKU SHINKANSEN

by

Achillefs Papadimitriou

Diploma of Civil Engineer
National Technical University of Athens, Greece
(July 1993)

Submitted to the Department of Civil and Environmental Engineering
in Partial Fulfillment of the Requirements for the Degree of

Master of Science in Civil and Environmental Engineering

at the

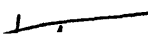
Massachusetts Institute of Technology

September 1995

© 1995 Massachusetts Institute of Technology
All rights reserved

The author hereby grants to MIT permission to reproduce and to distribute publicly paper and
electronic copies of this thesis document in whole or in part.

Signature of Author.....


.....
Department of Civil and Environmental Engineering

June 30th, 1995

Certified by.....


.....
Daniele Veneziano
Professor of Civil and Environmental Engineering
Thesis Supervisor

Accepted by.....


.....
Joseph M. Sussman
Chairman, Department Committee on Graduate Students

MASSACHUSETTS INSTITUTE
OF TECHNOLOGY

OCT 25 1995

LIBRARIES

OPTIMIZATION OF THE SEISMIC EARLY WARNING SYSTEM FOR THE TOHOKU SHINKANSEN

By

Achillefs Papadimitriou

Submitted to the Department of Civil and Environmental Engineering on June 30th, 1995
in Partial Fulfillment of the Requirements for the Degree of Master of Science in Civil
and Environmental Engineering

ABSTRACT

The Tohoku Shinkansen is a high-speed passenger train running along the eastern side of Honshu, the largest of the Japanese islands. The line is about 496km long and links Tokyo to the northern city of Morioka. A seismic early warning system (SEWS) has been in operation since 1978 with the purpose of mitigating the consequences of large destructive earthquakes. The SEWS includes two networks of accelerometers, one along the line (wayside system) and the other dislocated along the eastern coast of Honshu (coastal system), practically midway between the Tohoku line and the highly active offshore seismic sources. By activating the emergency braking system, the SEWS can reduce the distance traveled by trains on potentially damaged tracks, thus reducing the risk of derailments. The current SEWS is however causing a large number of train delays and the level of earthquake protection it provides is unclear. The present study quantifies the current level of seismic risk and indicates ways in which the SEWS can be made more efficient, reducing the rate of earthquake-induced derailments and at the same time reducing the rate of false alarms, unnecessary delays, train cancellations, e.t.c.

The derailment risk is estimated at 2-3 derailments every 100 years over the entire line with the current SEWS. This figure is however influenced greatly by the attenuation model, the local soil conditions and the seismic fragility of the viaduct structure, all of which are uncertain. Changing the way in which the current coastal system operates does not improve the effectiveness of the SEWS by significant amounts. By contrast, changing the seismic intensity parameter used to trigger various actions at the wayside system from peak ground acceleration (used now) to response spectrum acceleration is quite effective. The recommended new setting of the operational parameters for the wayside and coastal systems is estimated to reduce the expected rate of derailment by a factor of 2 and the rate of SEWS-induced delays by a factor of about 40.

Thesis Supervisor : Daniele Veneziano

Title : Professor of Civil and Environmental Engineering

Στην Κατερινα, και στην Αρτεμη της ψυχης μου

Acknowledgments

It is my pleasure to sincerely thank Professor Daniele Veneziano for the close and continuous supervision of this research. His brilliance and his availability to answer questions at all times during the day made these last twelve months a unique learning experience for me. I should also stress that these pages are the only pages of this thesis that Professor Veneziano did not spend a lot of time thoroughly reading and noticeably improving and unfortunately this fact is probably evident to the reader. In addition, I feel compelled to thank Professor Veneziano for introducing me to the field of non-deterministic engineering, which taught me to tolerate and even enjoy uncertainty in life.

Grateful acknowledgments are due to the Safety Research Laboratory at Japanese Railways East for the information gathered and communicated during this last year. In particular, I would like to thank Mr. Shimamura and Mr. Yokoyama for their technical advice and the precious time they devoted to this research project. More importantly, I would like to express my appreciation for the financial support provided during the last ten months, lack of which would have made my life at MIT miserable.

Sincere thanks are also due to the Bodossakis Foundation in Athens, Greece for the financial support it generously provided throughout the two years of my stay at MIT. Their contribution is considered indispensable.

My stay at MIT would have been much poorer academically without the excellently prepared, very instructive and wisely graded courses of Professor C.C. Ladd, the extremely lengthy yet thoroughly didactic homeworks and exams of Professor A.J. Whittle and the time-consuming but enlightening course of Dr. J.T. Germaine that introduced me to the field of experimental geotechnics. It would be inappropriate of me not to express my gratitude for my short yet academically profitable interaction with

Professor R.V. Whitman regarding my most favorite technical subject of “soil dynamics”. Finally, I feel the urge to mention the very informative contributions in the fields of geology, seismology and finite element formulation of Professors H.H. Einstein, N. Toksoz and K.J. Bathe respectively.

I also feel the need to sincerely thank two MIT professors for their non-academic contributions during my stay at MIT. First, my faculty advisor Professor A.J. Whittle whose comments and advice about my academic path at MIT and my future were always very helpful and whose strong belief in my abilities I found inspiring. It is also my pleasure to mention here Kim Mancuso, my acting teacher at MIT, that “scratched the surface” of another world within me.

Many of my friends at MIT have greatly contributed to the completion of this work. At those stressful moments I enjoyed the privilege of their help, now I have the pleasure to sincerely thank them for their time and interest. Thus, in random order, I acknowledge Marika Santagata for her assistance with the figures and the chapter of conclusions, Dianne Newman for her help with the figures and the improvement of my knowledge of the English language over these last “three months”, Elias Vyzas and Caterina Stamoulis for their guidance in managing contouring on Matlab, Alan-Rimm Kaufman, for our long conversations and debates over engineering issues, Joe Sinfield for his innovative solutions to my technical problems, Boonchai “Lek” Uckritchon for his help with programming and plotting in the early stages of this work and Takahiro Aoyagi for his knowledge of Japanese. I should state here that I would really enjoy reciprocating all their help in their academic endeavors in the future.

These last two years many of my friends at MIT have literally changed my life. My hereby expressed acknowledgment is only a small indication of my gratitude. Thus, I sincerely thank: Dan McBrearty for his friendship, his support and his reality checks over my life, Marika Santagata for her advice, her friendship and the fact that she kept the door of 1-343A always open, Amalia Polydoropoulou for her longing for Greece and her

sporadic “mothering”, Elias Vyzas for his everlasting energy and humor, Rachel Brown for her support and her kindness, Petros Komodromos for the beautiful times we spent together especially during the first lonely months at Tang Hall, Miran Rechter for his party attitude and his lessons of chivalry, Caterina Stamoulis for her advice on my first steps at MIT and the Department, Maria Kartalou for the shared moments of our insecurities, all the Greek students for their support and the fact that they did not let me forget my homeland -see Greek dancing at the International Fair, and finally all the Geotech students for their support and the interesting times we had together, highlight of which was the Dirtballs’ win over the Hydros last summer.

Being grateful for the role of Dianne Newman in my life is definitely an understatement. Her sincerity, her brilliance, her friendship and her love have made me a better person. I quit my reference to Dianne here, as I am afraid that words may disrespect my true feelings.

I have reserved the last part of my acknowledgments for my family. I will always thank and respect enormously my parents that went far beyond their financial and sentimental bounds to provide me with the finest education and to make me a worthy human being. Moreover, I am really grateful for the continuous support, encouragement and love from my siblings Caterina, Yannis and Paul during my adventures in the New World.

Αχιλλεας Παπαδημητριου

Table of Contents

Title Page	1
Abstract	2
Dedication	3
Acknowledgments	4
Table of Contents	7
List of Tables	9
List of Figures	11
1. Introduction and Objectives	18
2. The Tohoku Shinkansen and the Present SEWS	23
2.1 The Tohoku Shinkansen	23
2.2 The Present Seismic Early Warning System (SEWS)	25
3. Alternative SEWS Systems	36
3.1 Alternative Coastal SEWS Systems	38
3.2 Alternative Wayside SEWS Systems	42
4. Seismic Environment	51
4.1 Seismicity	51
4.2 Strong Motion Attenuation	53
5. Risk Analysis	66
5.1 Seismic Fragility of the Viaduct Structure	66
5.2 General Procedure of SEWS Performance Evaluation	73
5.3 Conditional Probability of Trigger, $P[T M, \underline{x}, s, \text{SEWS}]$	76
5.4 Conditional Probability of Derailment, $P[DE M, \underline{x}, s, T]$	78
5.5 Conditional Probability of Various Delays, $P[E M, \underline{x}, s, T]$; $E=SD,MD,LD$	82
5.6 Conditional Total Probability of Derailment	83
6. Risk Results	87
6.1 Annual Risk	87

6.2	Scenario-Based Risk Analysis	101
7.	Optimization of the Seismic Early Warning System	121
7.1	Optimization when the Wayside System Operates on a_{\max}	122
7.2	Optimization when the Wayside System Operates on S_a .	124
8.	Conclusions	140
	References	148
	Appendix I: Additional Tables and Figures	151
	Appendix II: Propagation of Delay	172

List of Tables

Table 2.1:	Natural period of horizontal vibration T of the viaduct structure, as a function of viaduct height H .	29
Table 2.2:	Estimated horizontal relative displacement d of the viaduct structure when the piers or the upper beam of the viaduct yield or fail, as a function of height H .	29
Table 2.3:	Soil classification along the Tohoku Shinkansen line.	30
Table 2.4:	Soil classification used in the seismic design of the viaduct structure.	31
Table 2.5:	Soil type, number and aggregate length of tunnels by track segment.	32
Table 2.6:	Frequency of train operation, per track section and time of day. The frequency includes both southbound and northbound trains.	33
Table 3.1:	Stations of the coastal early warning system and track segments they control for system A.	44
Table 4.1:	Gutenberg-Richter parameters for the annual earthquake rate density of the fifteen seismic regions in Figure 4.2 and their correspondence to the seismic sources of Utsu (1974).	58
Table 4.2:	Soil classification used by Kawashima et al. (1984).	58
Table 4.3:	Parameters of the original and the “modified Kawashima” attenuation relations for a_{\max} and S_a (the latter, for $T=0.3$ and 0.5 sec and 5% of critical damping). [Kawashima et al. (1984)]	59
Table 4.4:	Logarithmic standard deviations of a_{\max} and S_a , given earthquake magnitude M and epicentral distance Δ . [Kawashima et al. (1984)]	59
Table 5.1:	Values of x , c and the ductility modification factor $R(\mu)$ for $T = 0.3, 0.4, 0.5$ sec and $\mu = 1, 2, 3, 4$.	84
Table 5.2:	Expected number of continuously damaged (n_1) and undamaged (n_0) viaduct spans for given values of the probability of damage of a single viaduct span P_1 and $c_1=0.03$.	84

Table 7.1:	Performance of alternative SEWS systems. using a_{\max} as the intensity parameter at the wayside stations.	128
Table 7.2:	Performance of alternative SEWS systems, using S_a as the intensity parameter at the wayside stations.	128
Table I-1:	System B: values of $\gamma(i, s, R)$ for earthquakes originating from “sector of origin” R=1. [Columns: coastal station, i=1-8; Rows: segment, s=1-26]	152
Table I-2:	System B: values of $\gamma(i, s, R)$ for earthquakes originating from “sector of origin” R=2. [Columns: coastal station, i=1-8; Rows: segment, s=1-26]	153
Table I-3:	System B: values of $\gamma(i, s, R)$ for earthquakes originating from “sector of origin” R=3. [Columns: coastal station, i=1-8; Rows: segment, s=1-26]	154
Table I-4:	System B: values of $\gamma(i, s, R)$ for earthquakes originating from “sector of origin” R=4. [Columns: coastal station, i=1-8; Rows: segment, s=1-26]	155
Table I-5:	System B: values of $\gamma(i, s, R)$ for earthquakes originating from “sector of origin” R=5. [Columns: coastal station, i=1-8; Rows: segment, s=1-26]	156
Table I-6:	System B: values of $\gamma(i, s, R)$ for earthquakes originating from “sector of origin” R=6. [Columns: coastal station, i=1-8; Rows: segment, s=1-26]	157
Table I-7:	System B: values of $\gamma(i, s, R)$ for earthquakes originating from “sector of origin” R=7. [Columns: coastal station, i=1-8; Rows: segment, s=1-26]	158
Table I-8:	System B: values of $\gamma(i, s, R)$ for earthquakes originating from “sector of origin” R=8. [Columns: coastal station, i=1-8; Rows: segment, s=1-26]	159
Table II-1:	Aggregate delay in terms of minutes for first, second and third order delays along the line, for earthquakes of magnitudes 7 and 8 occurring at 60, 100 and 140km from the center point of the model line.	176
Table II-2:	Factors of increase of the first order delay, after including second or both second and third order delay, for earthquakes of magnitudes 7 and 8 occurring 60, 100 and 140km from the central point of the model line.	177

List of Figures

Figure 1.1:	Tohoku Shinkansen line; location of stations and location of wayside and coastal accelerometers.	22
Figure 2.1:	Sketch of Tohoku Shinkansen viaduct.	34
Figure 2.2:	Map of Japan showing the location of epicenters of earthquakes $M \geq 6$, for the period 1885-1983.	35
Figure 3.1:	Map of “sectors of origin” of earthquakes, R.	45
Figure 3.2:	Expected value of ratio $\gamma(i, s, R)$ between peak ground acceleration at coastal accelerometer i and the spectral acceleration at segment s , for: (a) “sector of origin” of earthquake, $R=1$. (b) “sector of origin” of earthquake, $R=5$.	46
Figure 3.3:	Triggering criteria of the UrEDAS system (Nakamura, 1989).	47
Figure 3.4:	(a) Accuracy of P-wave magnitude estimation in the UrEDAS (b) Accuracy of S-wave magnitude estimation in the UrEDAS (JREast, personal communication).	48
Figure 3.5:	Accuracy in the azimuth estimation using P waves: (a) Nakamura (1988). (b) JREast personal communication.	49
Figure 3.6:	(a) Accuracy of hypocentral distance estimation from S waves in the UrEDAS system (JREast, personal communication). (b) Accuracy of epicentral location estimation in the UrEDAS system using S waves (Nakamura, 1989).	50
Figure 4.1:	Historical seismicity in area of interest for the period 1885-1983.	60
Figure 4.2:	Sources of the proposed earthquake recurrence model for offshore seismicity superimposed on the historical seismicity (1885-1983).	61
Figure 4.3:	Peak ground acceleration at rock sites according to various studies : (a) $M = 5$ and (b) $M=8$.	62
Figure 4.4:	Comparison of peak ground acceleration attenuation relations for $M = 5 - 8$ and for: (a) soil type I, (b) soil type II and (c) soil type III.	63

Figure 4.5:	Comparison of spectral acceleration at $T=0.4\text{sec}$ and 5% damping of critical, for $M = 5 - 8$ and for: (a) soil type I, (b) soil type II and (c) soil type III.	64
Figure 4.6:	(a) Recorded peak ground accelerations during the Kobe earthquake and median values according to the “modified Kawashima” model for soil types I, II, III and $M=7.2$. (b) Estimated spectral accelerations at $T=0.4\text{sec}$ and 5% damping of critical compared to median values according to the “modified Kawashima” model for soil types I, II, III and $M=7.2$.	65
Figure 5.1:	Illustration of a no-derailment event.	85
Figure 5.2:	Shinkansen braking curve (JREast personal communication).	86
Figure 6.1:	(a) Annual rates of derailments and various delays, excluding and including derailment risk due to resumption of operation following short delays, for coastal systems A, B and C and $(a_{t,loc}, A_{insp1}, A_{insp2})=(40, 80, 120\text{gals})$ (b) Coastal trigger parameter versus annual rate of short delays, for coastal systems A, B and C and $(a_{t,loc}, A_{insp1}, A_{insp2})=(40, 80, 120\text{gals})$.	104
Figure 6.2:	Normalized risk decomposition for $(a^*, a_{t,loc}, A_{insp1}, A_{insp2}) = (40, 40, 80, 120\text{gals})$: (a) by earthquake magnitude, (b) along the track, (c) by seismic source, and (d) by epicentral distance.	105
Figure 6.3:	Distribution of risk along the track for $(a^*, a_{t,loc}, A_{insp1}, A_{insp2}) = (40, 40, 80, 120\text{gals})$ for : <u>case 1</u>) same train frequency along entire line, soil type I all along line, no tunnels, <u>case 2</u>) same as case 1, but actual train frequency considered, <u>case 3</u>) same as case 2, but actual soil types considered, <u>case 4</u>) same as case 3 but tunnels considered (most realistic or base-case).	106
Figure 6.4:	Annual rates of derailments and various delays, for coastal systems A, B and C and $(a_{t,loc}, A_{insp1}, A_{insp2})=(40, 80, 120\text{gals})$ for: (1) “modified Kawashima” model, (2) original Kawashima model, and (3) “modified Kawashima” model adjusted to account for the Kobe earthquake. (a) excluding derailment risk due to resumption of service following short delays (b) including derailment risk due to resumption of service following short delays	107
Figure 6.5:	Normalized risk decomposition by earthquake magnitude, for $(a^*, a_{t,loc}, A_{insp1}, A_{insp2}) = (40, 40, 80, 120\text{gals})$ for: (1) “modified Kawashima” model, (2) original Kawashima model and (3) “modified Kawashima” model adjusted to account for the Kobe earthquake.	108

- Figure 6.6:** Annual rates of derailments and various delays, excluding derailment risk due to resumption of operation following short delays for coastal systems A, B and C and $(a_{t,loc}, A_{insp1}, A_{insp2})=(40, 80, 120\text{gals})$, if:
 (a) relative displacement at yielding, $\delta_y = (70\%, 85\%, 100\%)$ of base-case value
 (b) ductility ratio at failure, $\mu = 2, 3, 4(\text{base-case value})$. 109
- Figure 6.7:** Annual rates of derailments and various delays, excluding derailment risk due to resumption of operation following short delays for coastal systems A, B and C and $(a_{t,loc}, A_{insp1}, A_{insp2})=(40, 80, 120\text{gals})$, if:
 (a) uncertainty on resistance, $\sigma_{inR} = 0.3, 0.4(\text{base-case value}), 0.5$. 110
 (b) parameter controlling damage clustering, $c_1=0.015, 0.03(\text{base-case value}), 0.06$
- Figure 6.8:** Normalized derailment risk decomposition, 111
 for $(a^*, a_{t,loc}, A_{insp1}, A_{insp2}) = (40, 40, 80, 120\text{gals})$, if:
 (a) $\delta_y = (70\%, 85\%, 100\%)$ of base-case value, (b) $\mu = 2, 3, 4(\text{base-case value})$,
 (c) $\sigma_{inR} = 0.3, 0.4(\text{base-case value}), 0.5$, (d) $c_1=0.015, 0.03(\text{base-case value}), 0.06$
- Figure 6.9:** Annual rates of derailments and various delays, excluding derailment risk due to resumption of operation following short delays for coastal systems A, B and C and $(a_{t,loc}, A_{insp1}, A_{insp2}) = (40, 80, 120\text{gals})$, if:
 (a) soil type is I, II, III (Table 4.2) all along the line 112
 (b) maximum velocity, $V_o = 210\text{kmh}, 245\text{kmh}(\text{base-case value}), 300\text{kmh}$.
- Figure 6.10:** Normalized risk decomposition by earthquake magnitude, for 113
 $(a^*, a_{t,loc}, A_{insp1}, A_{insp2}) = (40, 40, 80, 120\text{gals})$ if soil all along the line is:
 (1) type I, (2) type II, and (3) type III
- Figure 6.11:** Annual rates of derailments and various delays, excluding derailment risk due to resumption of operation following short delays for coastal systems A, B and C and $(a_{t,loc}, A_{insp1}, A_{insp2})=(40, 80, 120\text{gals})$, if:
 (a) M_{max} of each seismic source is 0.5 higher/lower relative to base-case value 114
 (b) b-value of each seismic source is 0.9, 1.1 or base-case value.
- Figure 6.12:** Annual rates of derailments and various delays, excluding derailment risk due to resumption of operation following short delays for coastal systems A, B and C and $(a_{t,loc}, A_{insp1}, A_{insp2}) = (40, 80, 120\text{gals})$ for : 115
 the UrEDAS system accuracy of P-wave estimation of:
 (a) earthquake magnitude M : $\sigma_{M,P} = 0.5, 1.0(\text{base-case value})$
 (b) epicentral distance Δ : $\sigma_{\Delta,P} = 25\%\Delta, 75\%\Delta(\text{base-case value}), 100\%\Delta$
- Figure 6.13:** Conditional probability $P[E|M, x, s, A]$ of event E along the line, 116
 for $(a^*, a_{t,loc}, A_{insp1}, A_{insp2}) = (40, 40, 80, 120\text{gals})$ and earthquake magnitudes $M = 5 - 9$, [epicenter: 571km from $s=1$ and 135km from $s=26$]
 (a) E = derailment, (b) E = short delay, (c) E = medium delay, (d) E = long delay.

- Figure 6.14:** Expected number of events throughout the line, given earthquake of magnitude $M = 5$ occurring at map location, for $(a^*, a_{t,loc}, A_{insp1}, A_{insp2}) = (40, 40, 80, 120\text{gals})$, where events are: (a) derailments, (b) short delays, (c) medium delays, (d) long delays. 117
- Figure 6.15:** Expected number of events throughout the line, given earthquake of magnitude $M = 6$ occurring at map location, for $(a^*, a_{t,loc}, A_{insp1}, A_{insp2}) = (40, 40, 80, 120\text{gals})$, where events are: (a) derailments, (b) short delays, (c) medium delays, (d) long delays. 118
- Figure 6.16:** Expected number of events throughout the line, given earthquake of magnitude $M = 7$ occurring at map location, for $(a^*, a_{t,loc}, A_{insp1}, A_{insp2}) = (40, 40, 80, 120\text{gals})$, where events are: (a) derailments, (b) short delays, (c) medium delays, (d) long delays. 119
- Figure 6.17:** Expected number of events throughout the line, given earthquake of magnitude $M = 8$ occurring at map location, for $(a^*, a_{t,loc}, A_{insp1}, A_{insp2}) = (40, 40, 80, 120\text{gals})$, where events are: (a) derailments, (b) short delays, (c) medium delays, (d) long delays. 120
- Figure 7.1:** (a) Annual rates of derailments and various delays, excluding and including derailment risk due to resumption of operation following short delays, for coastal systems A, B and C and $(a_{t,loc}, A_{insp1}, A_{insp2})=(40, 80, 120\text{gals})$ (b) Coastal trigger parameter versus annual rate of short delays, for coastal systems A, B and C and $(a_{t,loc}, A_{insp1}, A_{insp2})=(40, 80, 120\text{gals})$. 129
- Figure 7.2:** Annual rates of derailments and various delays, for coastal systems A, B,C and $(a_{t,loc}, A_{insp1}, A_{insp2})=(40, 80, 120\text{gals})$ and $(80, 80, 120\text{gals})$ (a) excluding derailment risk due to resumption of service following short delays (b) including derailment risk due to resumption of service following short delays 130
- Figure 7.3:** Annual rates of derailments and various delays, for coastal systems A, B and C and $(a_{t,loc}, A_{insp1}, A_{insp2})=(80, 80, 120\text{gals})$, $(100, 100, 140\text{gals})$, and $(120, 120, 160\text{gals})$. (a) excluding derailment risk due to resumption of service following short delays (b) including derailment risk due to resumption of service following short delays 131
- Figure 7.4:** Expected number of event E versus A_{insp1} , for coastal system A, $a^* = 80\text{gals}$, $a_{t,loc}=A_{insp1}$ and $A_{insp2}=A_{insp1}+40\text{gals}$ and including derailment risk due to resumption of service following short delays, where E is: (a) E=derailments, (b) E=short delays, (c) E=medium delays, (d) E=long delays. 132

Figure 7.5:	(a) Annual rates of derailments and various delays, excluding and including derailment risk due to resumption of operation following short delays, for coastal systems A, B, C and $(S_{at,loc}, S_{a,insp1}, S_{a,insp2})=(80, 160, 240\text{gals})$ (b) Coastal trigger parameter versus annual rate of short delays, for coastal systems A, B and C and $(S_{at,loc}, S_{a,insp1}, S_{a,insp2})=(80, 160, 240\text{gals})$	133
Figure 7.6:	Annual rates of derailments and various delays, for coastal systems A, B, C and cases $(a_{t,loc}, A_{insp1}, A_{insp2})=(80, 80, 120\text{gals})$ versus $(S_{at,loc}, S_{a,insp1}, S_{a,insp2})=(160, 160, 240\text{gals})$. (a) excluding derailment risk due to resumption of service following short delays (b) including derailment risk due to resumption of service following short delays	134
Figure 7.7:	Annual rates of derailments and various delays, for coastal systems A, B, C and $(S_{at,loc}, S_{a,insp1}, S_{a,insp2}) = (160, 160, 240\text{gals}), (240, 240, 320\text{gals}), (400, 400, 480\text{gals})$. (a) excluding derailment risk due to resumption of service following short delays (b) including derailment risk due to resumption of service following short delays	135
Figure 7.8:	Annual rates of events throughout the line, as a function of a^* and $S_{at,loc}$ ($S_{a,insp1}=S_{at,loc}$ and $S_{a,insp2}=S_{a,insp1}+80\text{gals}$), including derailment risk due to resumption of service following short delays, where events are: (a) derailments, (b) short delays, (c) medium delays, (d) long delays.	136
Figure 7.9:	Annual rates of events throughout the line, as a function of b^* and $S_{at,loc}$ ($S_{a,insp1}=S_{at,loc}$ and $S_{a,insp2}=S_{a,insp1}+80\text{gals}$), including derailment risk due to resumption of service following short delays, where events are: (a) derailments, (b) short delays, (c) medium delays, (d) long delays.	137
Figure 7.10:	Annual rates of events throughout the line, as a function of c^* and $S_{at,loc}$ ($S_{a,insp1}=S_{at,loc}$ and $S_{a,insp2}=S_{a,insp1}+80\text{gals}$), including derailment risk due to resumption of service following short delays, where events are: (a) derailments, (b) short delays, (c) medium delays, (d) long delays.	138
Figure 7.11:	Probability of a train meeting damaged track in 35km, given spectral acceleration at the track, for $c_1 = 0.015, 0.03, 0.06$, i.e. a reasonable range of spatial clustering of damage.	139
Figure I-1:	Normalized risk decomposition for $(b^*, a_{t,loc}, A_{insp1}, A_{insp2}) = (40, 40, 80, 120\text{gals})$: (a) by earthquake magnitude, (b) along the track, (c) by seismic source, and (d) by epicentral distance [Figure similar to Figure 6.2]	160

- Figure I-2:** Normalized risk decomposition for $(c^*, a_{t,loc}, A_{insp1}, A_{insp2}) = (3.0, 40gals, 80gals, 120gals)$: (a) by earthquake magnitude, (b) along the track, (c) by seismic source, and (d) by epicentral distance [Figure similar to Figure 6.2] 161
- Figure I-3:** Normalized risk decomposition for $(a^*, S_{a,tloc}, S_{a,insp1}, S_{a,insp2}) = (40, 80, 160, 240gals)$: (a) by earthquake magnitude, (b) along the track, (c) by seismic source, and (d) by epicentral distance [Figure similar to Figure 6.2; notice the use of S_a at the wayside system] 162
- Figure I-4:** Normalized risk decomposition for $(b^*, S_{a,tloc}, S_{a,insp1}, S_{a,insp2}) = (40, 80, 160, 240gals)$: (a) by earthquake magnitude, (b) along the track, (c) by seismic source, and (d) by epicentral distance [Figure similar to Figure 6.2; notice the use of S_a at the wayside system] 163
- Figure I-5:** Normalized risk decomposition for $(c^*, S_{a,tloc}, S_{a,insp1}, S_{a,insp2}) = (40, 80, 160, 240gals)$: (a) by earthquake magnitude, (b) along the track, (c) by seismic source, and (d) by epicentral distance [Figure similar to Figure 6.2; notice the use of S_a at the wayside system] 164
- Figure I-6:** Annual rates of derailments and various delays, including derailment risk due to resumption of operation following short delays for coastal systems A, B and C and $(a_{t,loc}, A_{insp1}, A_{insp2})=(40, 80, 120gals)$, if: (a) relative displacement at yielding, $\delta_y = (70\%, 85\%, 100\%)$ of base-case value (b) ductility ratio at failure, $\mu = 2, 3, 4$ (base-case value) [Figure corresponds to cases illustrated in Figure 6.6] 165
- Figure I-7:** Annual rates of derailments and various delays, including derailment risk due to resumption of operation following short delays for coastal systems A, B and C and $(a_{t,loc}, A_{insp1}, A_{insp2})=(40, 80, 120gals)$, if: (a) uncertainty on resistance, $\sigma_{InR} = 0.3, 0.4$ (base-case value), 0.5. (b) parameter controlling damage clustering, $c_1=0.015, 0.03$ (base-case value),0.06 [Figure corresponds to cases illustrated in Figure 6.7] 166
- Figure I-8:** Annual rates of derailments and various delays, including derailment risk due to resumption of operation following short delays for coastal systems A, B and C and $(a_{t,loc}, A_{insp1}, A_{insp2}) = (40, 80, 120gals)$, if: (a) soil type is I, II, III (Table 4.2) all along the line (b) maximum velocity, $V_o = 210kmh, 245kmh$ (base-case value), 300kmh [Figure corresponds to cases illustrated in Figure 6.9] 167

- Figure I-9:** Annual rates of derailments and various delays, including derailment risk due to resumption of operation following short delays for coastal systems A, B and C and $(a_{t,loc}, A_{insp1}, A_{insp2})=(40, 80, 120\text{gals})$, if:
 (a) M_{max} of each seismic source is 0.5 higher/lower relative to base-case value
 (b) b-value of each seismic source is 0.9, 1.1 or base-case value
 [Figure corresponds to cases illustrated in Figure 6.11] 168
- Figure I-10:** Annual rates of derailments and various delays, including derailment risk due to resumption of operation following short delays for coastal systems A, B and C and $(a_{t,loc}, A_{insp1}, A_{insp2}) = (40, 80, 120\text{gals})$ for :
 the UrEDAS system accuracy of P-wave estimation of:
 (a) earthquake magnitude $M: \sigma_{M,P} = 0.5, 1.0(\text{base-case value})$
 (b) epicentral distance $\Delta: \sigma_{\Delta,P} = 25\%\Delta, 75\%\Delta(\text{base-case value}), 100\%\Delta$
 [Figure corresponds to cases illustrated in Figure 6.12] 169
- Figure I-11:** Conditional probability $P[E|M, \underline{x}, s, B]$ of event E along the line, for $(b^*, a_{t,loc}, A_{insp1}, A_{insp2}) = (40, 40, 80, 120\text{gals})$ and earthquake magnitudes $M = 5 - 9$, [epicenter: 571km from $s=1$ and 135km from $s=26$]
 (a) E = derailment, (b) E = short delay,
 (c) E = medium delay,(d) E = long delay.
 [Figure similar to Figure 6.13, but for coastal system B] 170
- Figure I-12:** Conditional probability $P[E|M, \underline{x}, s, C]$ of event E along the line, for $(c^*, a_{t,loc}, A_{insp1}, A_{insp2}) = (3.0, 40\text{gals}, 80\text{gals}, 120\text{gals})$ and earthquake magnitudes $M = 5 - 9$, [epicenter: 571km from $s=1$ and 135km from $s=26$]
 (a) E = derailment, (b) E = short delay,
 (c) E = medium delay,(d) E = long delay.
 [Figure similar to Figure 6.13, but for coastal system C] 171
- Figure II-1:** Model line, train and station locations and potential epicenters of earthquakes used in the study of propagation of delay along the line
 [Figure for train frequency of 1 train per segment] 178
- Figure II-2:** Assumed recorded values of peak ground acceleration along the model line for $M = 5-8$, compared to track inspection levels: $A_{insp1}=80\text{gals}$ and $A_{insp2}=120\text{gals}$, for epicentral distances:
 (a) $D=60\text{km}$, (b) $D=100\text{km}$ and (c) $D=140\text{km}$. 179
- Figure II-3:** Train location versus time after resumption of service of trains according to current track inspection levels: $A_{insp1}=80\text{gals}$ and $A_{insp2}=120\text{gals}$. for earthquake of $M=7$ at $D=60\text{km}$.
 [1. Figure presents half the total track and half the trains due to symmetry,
 2. Figure for train frequency of 1 train per segment] 180

Chapter 1

Introduction and Objectives

The Tohoku Shinkansen is a high-speed passenger train running along the eastern side of Honshu, the largest of the Japanese islands; see Figure 1.1. The line is about 496 km long and links Tokyo to the northern city of Morioka, with 14 intermediate stations. The Tohoku Shinkansen is operated by Japanese Railways East (JREast), one of the railway companies that emerged from the privatization of the previously state-owned railways.

Although the Tohoku line does not cross any major known seismogenic area, it is potentially vulnerable to moderate local seismicity and to the more frequent and more intense earthquakes that originate in the subduction zone off the eastern coast of Japan. Seismic risk has long been a concern, not just in the design but also in the operation of the Tohoku Shinkansen. Regarding the latter, a seismic early warning system (SEWS) has been in operation since 1978 with the purpose of mitigating the consequences of large destructive earthquakes. The SEWS includes two networks of accelerometers, one along the line, the other dislocated along the eastern coast of Honshu, roughly midway between the Tohoku line and the more active offshore seismic sources. The purpose of the SEWS is to provide early detection of arriving seismic waves, thus allowing early emergency braking of the trains. The most feared accidents are those associated with derailments, which under seismic conditions occur mainly when a running train encounters a damaged section of the track. Through early braking, the SEWS reduces the distance travelled by trains on potentially damaged tracks and therefore reduces the risk of severe accidents.

Several issues have been raised about the effectiveness of the SEWS system. Specifically, questions have been posed on whether the effectiveness of the system could be improved:

1. by modifying the way in which the system operates,
2. by modifying the earthquake intensity parameters used to trigger emergency train stopping (the parameter currently used at both the coastal and wayside accelerometers is peak ground acceleration, a_{\max}),
3. by changing the level of seismic intensity at which various actions are taken (emergency braking, track inspection, resumption of operation).

The problem is not just to achieve the maximum possible level of earthquake protection, but to balance safety with the monetary and non-monetary costs associated with false alarms, long delays, train cancellations, e.t.c.

Studies on seismic early warning systems around the world include the following : Fujiwara et al.(1980), a study of a system which was at the time under development for the Tohoku Shinkansen and performed a three-point estimation of earthquake magnitude and epicentral location, Heaton (1985), a study of a system that performs an estimation of location, time of origin and amplitude of ground shaking through information from a dense array of broadband seismometers, Nakamura (1988 and 1989), studies of a system named UrEDAS which performs a single-point estimation of earthquake magnitude and epicentral location. These studies present technical characteristics and the triggering philosophy of these early warning systems but they do not include estimates of cost/benefit effectiveness of these systems in actual applications.

The objectives of the present study are to quantify the level of seismic safety of the Tohoku line and to compare the effectiveness of alternative SEWS systems and SEWS operational strategies. From the results of this study, we have derived a set of recommendations on the most efficient way to operate the early warning system. In essence, we have found that :

1. by changing the way in which the current system operates one can gain only minor improvements in seismic effectiveness;

2. changing the intensity parameters used to trigger various actions (we specifically propose to replace a_{\max} to response spectrum acceleration S_a at an appropriate frequency and damping ratio) produces significant improvements in the sense of reducing both the rate of earthquake-induced derailments and the rate of train delays and potential cancellations;
3. changing the levels of seismic intensity at which various actions take place (emergency braking, track inspection, resumption of service) also produces significant improvements over the current operation of the system.

Another set of recommendations is reached in this study regarding the reduction of uncertainty on the actual level of seismic risk. We have found that seismic safety of the Tohoku Shinkansen is particularly sensitive to : (a) seismic attenuation and local attenuation effects and (b) earthquake vulnerability of the viaduct structure that supports most of the line. Both elements are at present time highly uncertain. We suggest that JREast undertakes additional studies to reduce these uncertainties. Such studies could also lead to the identification of segments of the line that are especially vulnerable to earthquakes and that should be retrofitted on a priority basis. The Tohoku line is primarily subjected to destructive earthquakes originating in the subduction zone off the eastern coast of Honshu while the inland seismicity is comparatively less significant. This is the reason that led us to consider only the offshore seismicity in this study.

Chapter 2 of this thesis describes the Tohoku Shinkansen as a transportation and structural system and gives the main characteristics of the current SEWS system and its historical performance. Alternative coastal and wayside SEWS systems are discussed in Chapter 3. The seismic environment of the Tohoku Shinkansen is characterized in Chapter 4 in terms of earthquake recurrence laws and seismic attenuation models, including local amplification effects. Chapter 5 presents the general methodology used in this study to evaluate earthquake risk. This includes a description of the seismic

vulnerability of the viaduct structure which is an element of primary importance in determining seismic risk. Numerical results are presented in Chapter 6, where the performance of the SEWS is estimated, the main factors contributing to seismic risk are identified and uncertainty on the actual level of risk is quantified. Chapter 7 presents a detailed numerical comparison of the various seismic early warning systems under different operational policies. Specific recommendations to JREast for the future operation of the system and proposed areas of further study are included in Chapter 8. Appendix I presents additional risk results that are complementary to results included in Chapters 6 and 7. Appendix II addresses the issue of propagation of delay along the Tohoku line.

Station

- Detecting Point along the wayside
- :Sub Station (SS)
- :Sectioning Post (SP)
- ▲ :Sub Sectioning Post (SSP)
- ★ Detecting Point on the coast :★

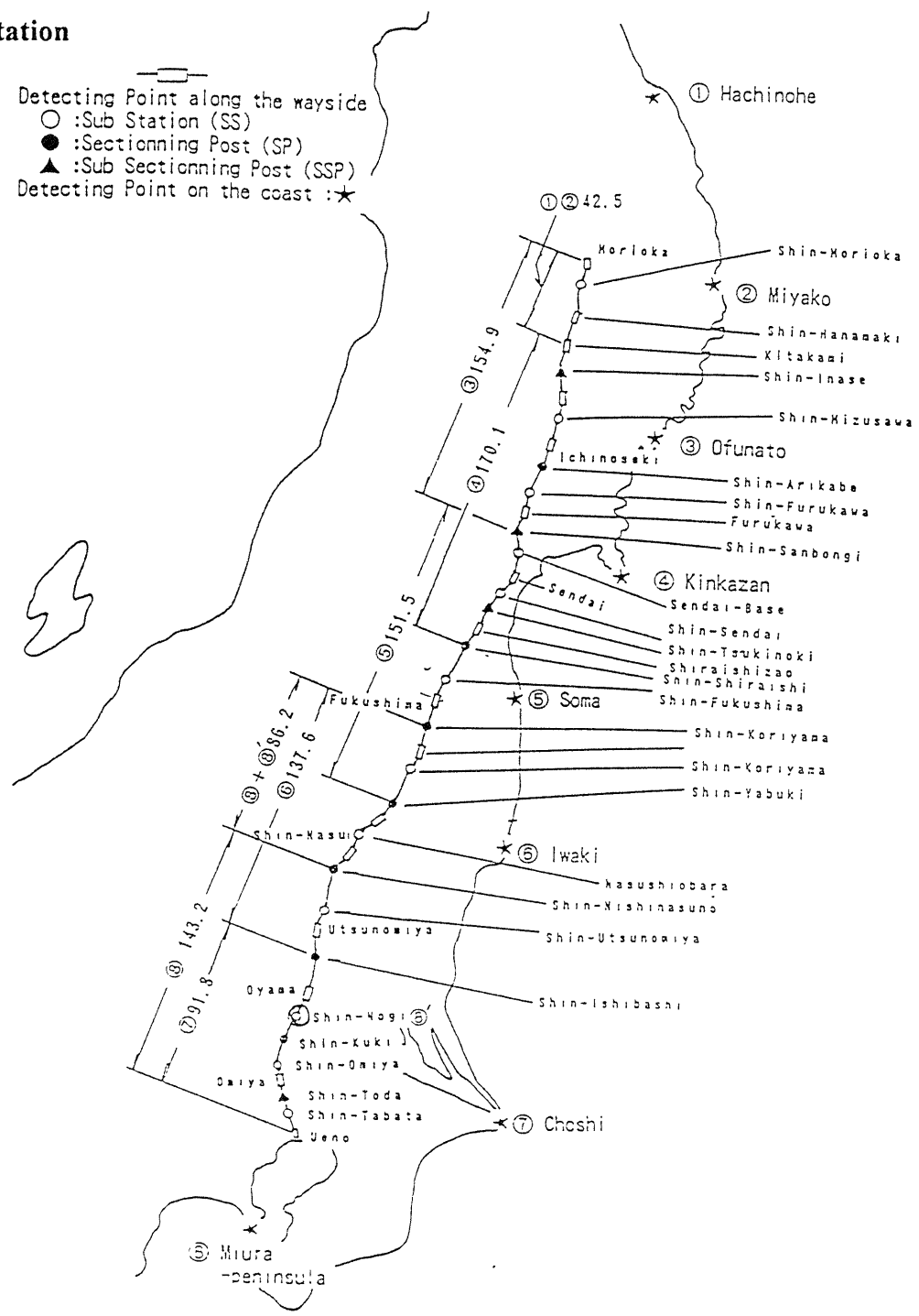


Figure 1.1: Tohoku Shinkansen line; location of stations and location of wayside and coastal accelerometers.

Chapter 2

The Tohoku Shinkansen and the Present SEWS

2.1 The Tohoku Shinkansen

The Tohoku Shinkansen travels not on an embankment as most conventional lines in Japan do, but on a continuous viaduct structure except, for tunnels in rocky parts of the line. The viaduct is a reinforced concrete-continuous beam frame structure that carries a double track. The typical span between piers is 7 meters and the height of the structure ranges between 7 and 14 meters, with a typical value of 10 m; see Figure 2.1.

An important parameter for the seismic behavior of the structure is the natural period of vibration of the viaduct, T , which has been estimated by JREast (personal communication) as shown in Table 2.1. The values of T in the table correspond to horizontal vibration in the direction perpendicular to the track. According to JREast engineers, vibration in the vertical and horizontal directions may be considered harmless to the viaduct; these components of motion are therefore ignored in the present study.

A second important parameter in the study of seismic vulnerability is the displacement of the deck relative to the ground, d , at which the column pier or the upper beam yield. JREast engineers have estimated these values of d as given in Table 2.2, for different viaduct heights.

Earthquake loads on the viaduct structure are influenced significantly by the local geologic/soil conditions along the line. Such local conditions may amplify or de-amplify the ground motion relative to standard (e.g. bedrock). Table 2.3 presents a crude soil

classification along the Tohoku Shinkansen line. In this table, N is the representative SPT-value for the material above bedrock and t is the thickness of the soil layer. The soil classes in Table 2.3 correspond to those used for seismic design of the viaduct structure and are defined in Table 2.4. Specifically, the soil coefficient is the one used in the design of the viaduct structure to scale the seismic design relative to “normal” conditions. It should be kept in mind that, this soil coefficient is only a rough estimate of the local amplification effects and that in reality amplification (or de-amplification) may vary substantially along the line depending on specific local conditions.

Next we mention a few miscellaneous characteristics of the Tohoku line which will be used later in the analysis of seismic safety :

- Location and extent of tunnels : The line includes a total of 115 tunnels, which range in length from 20 to 11,705 meters. Most of the tunnels are shorter than 1,000 m and their aggregate length is 116,450 m or 23% of the total length of the line. Table 2.5 gives the total length and number of tunnels within each of 26 non-overlapping track segments into which the line is divided. The segments correspond to operational track units and are associated each to one of the 26 wayside accelerometers. A more detailed description of this system will be given in section 2.2. The distance from Tokyo reported in Table 2.5 is the distance along the track of the starting location of the track segment.

- Frequency of train passages : The frequency of train operation varies with track segment and time of day, as reported in Table 2.6. Notice that Sendai station is approximately 325 km from Tokyo. The Shinkansen trains are on average 250 m long and their operational speed is at the moment set at 245 kmh. Assuming an average speed of 200 kmh (including occasional stops at stations along the line) and using the frequency data in Table 2.6, one concludes that, at a generic point in time, the expected number of trains between Tokyo and Sendai is 11.47 and between Sendai and Morioka is 2.95.

As was mentioned briefly above and as described in detail in Section 2.2, the track is divided into 26 segments, which are relevant to the operational control of the wayside earthquake detection system. The track section from Tokyo to Sendai (T-S) includes 16 segments while that from Sendai to Morioka (S-M) is divided into 10 segments. Assigning a uniform train density in each of these two track sections, the expected number of trains per segment is 0.72 from Tokyo to Sendai and 0.30 from Sendai to Morioka. This change in train density will be found to be a factor in the variability of risk along the Tohoku line.

The aforementioned characteristics provide a physical and technical picture of the Tohoku Shinkansen as a transportation system. For the protection of this transportation system against earthquakes, JREast is operating a Seismic Early Warning System (SEWS) that automatically induces a train to stop when a potentially destructive earthquake is detected at a wayside or coastal seismic station. The present study focuses on the risk reduction capabilities of this system and the optimization of its future operation. The next section gives a detailed description of the exact purpose, configuration and operation of the present SEWS.

2.2 The Present Seismic Early Warning System (SEWS)

Before the Tohoku Shinkansen, other Shinkansen lines in Japan had been provided with a seismic early warning system. The Tokaido Shinkansen had such a system as early as 1966. The concept of SEWS had been around also before that time, but it was the disastrous Niigata earthquake of 1964 that promoted its development. Based on the experience gained from the Tokaido and Sanyo Shinkansen, a new SEWS was developed for the Tohoku Shinkansen, which became operational in 1978. This is the system described here. Very recently, the effectiveness of the existing system has been questioned and alternative schemes have been proposed. Possible changes will be described in detail in Chapter 3.

The earthquake activity in the region surrounding the Tohoku line may be broadly divided into offshore Pacific Ocean seismicity and inland seismicity. This division can be observed in the map of earthquake epicenters, shown in Figure 2.2. Offshore earthquakes contribute 80% to 90% of the earthquake occurrence rate in the area and are often of larger magnitude. However, these events occur at a distance of at least 80-100 km from the line and therefore are subjected to higher attenuation. These characteristics of the regional seismicity motivate the following philosophy of the seismic early warning system for the Tohoku Shinkansen :

- (1) Protect against offshore earthquakes is obtained through a coastal earthquake detection;
- (2) Protect against inland earthquakes through accelerometers installed along the track.

The wayside accelerometers operate also as a second line of defense against offshore earthquakes that might not be triggered by the coastal stations. Moreover, the intensity of ground motion recorded at the wayside stations is the basis for operational decisions about post-earthquake track inspection and resumption of service. The way in which the coastal and wayside systems operate is described next in greater detail.

(1) Coastal System

Accelerometers are installed on rock at eight (8) coastal locations, chosen to provide the longest lead time possible at the track for offshore earthquakes; see Figure 1.1. At present, the accelerometers are set to trigger when a pre-specified level of peak ground acceleration is exceeded. The eight locations are : *Hachinoche, Miyako, Ofunato, Kinkasan, Soma, Iwaki, Choshi* and *Miura peninsula*. A ninth accelerometer is located along the track at *Shinnogi* and is operated as part of the coastal system. This last location was chosen to provide trains running in the central portion of the line with lead time relative to inland earthquakes from the area south of Tokyo. As mentioned before, this

analysis takes considers the risk from the offshore seismicity only, therefore this ninth accelerometer is not taken into account.

In the current early warning system, each coastal accelerometer controls a preset track segment, as shown in Figure 1.1. Therefore, as the horizontal ground acceleration at a coastal station exceeds the chosen threshold level (currently, 40 gals), emergency braking is automatically activated for all trains running in the corresponding track segment.

(2) Wayside System

The wayside system consists of 26 accelerometers installed at nearly equal intervals between Tokyo and Morioka. The locations correspond to substations (S.S), section points (S.P) and subsection points (S.S.P), all of which have a dual role : (a) detect the incoming earthquake strong motion and possibly cause trains in the adjacent segments to stop, and (b) measure the intensity of the ground motion close to the line, to decide upon post-earthquake actions. Because the average spacing between the accelerometers is 20 km, each wayside station controls trains over a track segment of about 40 km. In a simplifying approximation, it is assumed in the present analysis that each location along the line is controlled by only one wayside accelerometer. Therefore, the track is divided into 26 non-overlapping segments. We refer to such non-overlapping segments as *operational track segments*. The location of the starting point of these operational segments is provided, with other information, in Table 2.5. At present, the wayside instruments are set to trigger emergency train braking when the local peak ground acceleration exceeds 40 gals.

Historical Operation of the SEWS

During the period from 1982 to the end of 1993, the seismic early warning system triggered in 144 earthquakes: the coastal system alone issued 63 warnings, the wayside system triggered alone 54 times, while the two systems triggered simultaneously in 27 cases. The 144 events in which the SEWS was triggered resulted in the following consequences for the operation of Shinkansen trains :

- (a) There were 31 trains that did not resume regular operation after being stopped by the SEWS. This was due to the fact that track inspection was considered necessary. This number corresponds to a rate of 2.82 stopped trains/year.
- (b) There were 796 trains that were delayed but were allowed to resume operation after being stopped by the SEWS. This number corresponds to a rate of 72.36 delayed trains/year.

The temporal distribution of these stopped and delayed trains is far from uniform within the 11 years of the record. Specifically, all 31 stopped trains were stopped during 1993. Moreover, during 1983, 1987 and 1993 the SEWS caused 116, 112 and 186 train delays respectively, while during 1982 and 1991 the numbers of delayed trains were 24 and 19 respectively.

H (m)	7.0	8.5	10.0	12.0	14.0
T (sec)	0.30	0.33	0.32	0.32	0.36

Table 2.1: Natural period of horizontal vibration T of the viaduct structure, as a function of viaduct height H.

H(m)	d(cm)	failure mode
7.0	2.2	column pier failure
8.5	3.1	column pier yielding
8.5	5.2	upper beam yielding
10.0	3.1	upper beam yielding
10.0	3.4	column pier yielding
12.0	4.1	upper beam yielding
14.0	2.0	upper beam yielding

Table 2.2: Estimated horizontal relative displacement d of the viaduct structure when the piers or the upper beam of the viaduct yield or fail, as a function of height H.

Section (km from Tokyo)	Length (km)	Soil Type (see Table 2.4)
3 - 13	10	II
13 - 30	17	III
30 - 37	7	II
37 - 43	6	III
43 - 51	8	II
51 - 61.5	10.5	III
61.5- 100	38.5	II
100 - 181	81	I
181 - 263	82	II
263 - 293	30	II
293 - 298	5	III
298 - 329	31	II
329 - 335	6	III
335 - 356	21	II
356 - 367	11	III
367 - 498	131	II

Table 2.3: Soil classification along the Tohoku Shinkansen line.

Soil Type	Soil Name	Soil Description	Ground Coefficient
I	Rock	Tertiary and pretertiary rock	0.8
II	Normal	Dilluvium or alluvium(except soft alluvium)	1.0
II	Soft	N=0 and t > 2m N<3 and t > 5m N<5 and t > 11m	1.2

Table 2.4: Soil classification used in the seismic design of the viaduct structure.

Track Segment	Distance from Tokyo (km)	Segment Length (km)	Soil Type (Table 2.4)	Length in Tunnel (km)	No. of Tunnels
1	0.000	3.875	II	2.052	2
2	3.875	8.228	II	1.495	1
3	12.103	14.440	II	0.585	1
4	26.543	14.641	II	0.000	0
5	41.184	15.964	II	0.000	0
6	57.148	23.060	II	0.000	0
7	80.208	25.282	II	0.000	0
8	105.490	25.726	II	1.019	2
9	131.216	22.420	II	1.145	4
10	153.636	23.523	II	10.862	6
11	177.159	23.667	III	11.230	18
12	200.826	22.124	II	0.000	0
13	222.950	22.427	II	16.150	11
14	245.377	24.726	II	0.692	1
15	270.103	26.466	II	17.624	9
16	296.569	16.735	II	10.826	12
17	313.304	15.667	II	0.000	0
18	328.971	21.078	I	9.308	14
19	350.049	18.280	I	3.170	9
20	368.329	19.204	I	3.140	7
21	387.533	26.902	I	17.588	8
22	414.435	21.551	II	6.656	8
23	435.986	18.850	III	0.000	0
24	454.836	19.042	II	2.908	2
25	473.878	15.541	III	0.000	0
26	489.419	7.061	II	0.000	0

Table 2.5: Soil type, number and aggregate length of tunnels by track segment.

Time Range	Tokyo-Sendai (trains / hr)	Sendai-Morioka (trains / hr)
06:00 - 12:00	10	4.5
12:00 - 18:00	10	6
18:00 - 24:00	8.2	3.3

Table 2.6: Frequency of train operation, per track section and time of day. The frequency includes both southbound and northbound trains.

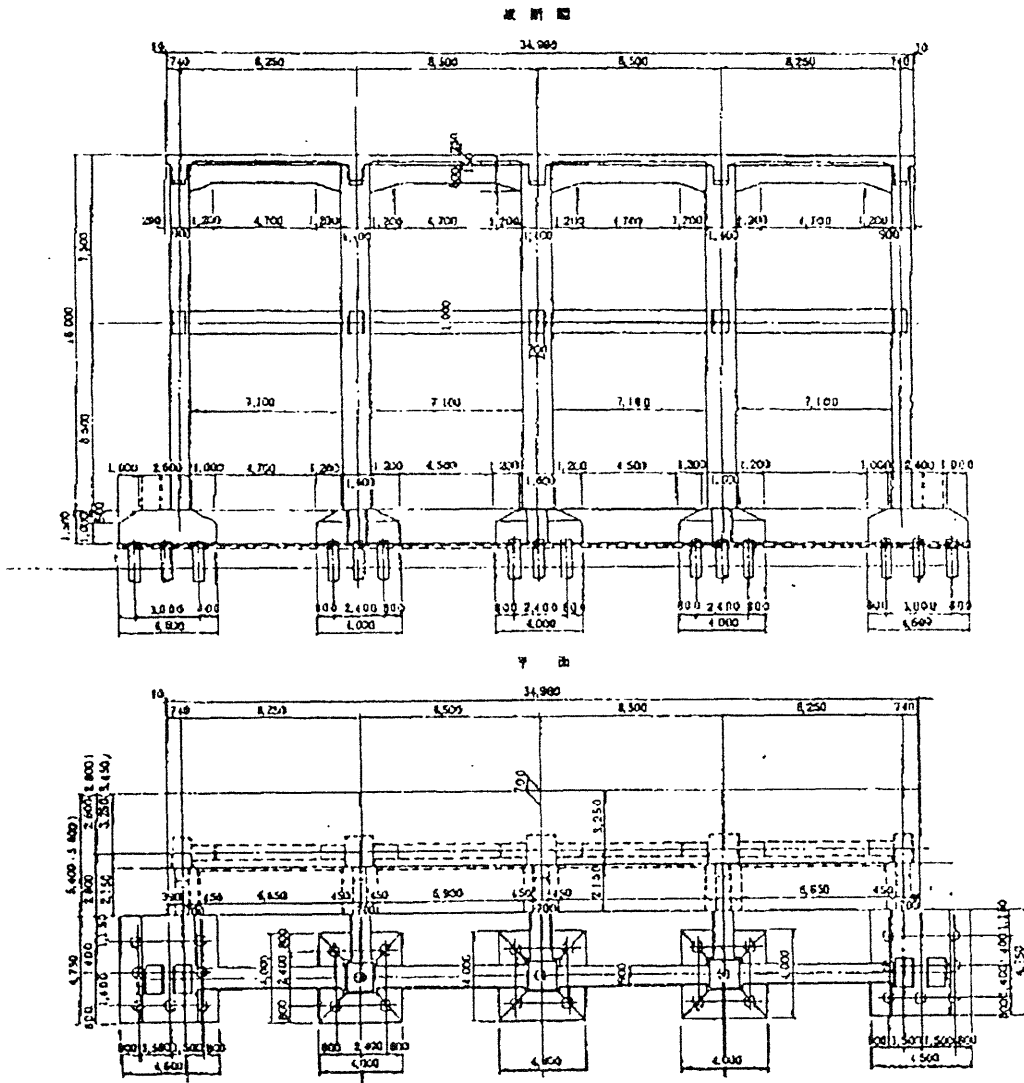


Figure 2.1: Sketch of Tohoku Shinkansen viaduct.

Chapter 3

Alternative SEWS systems

The performance of the current seismic early warning system appears sub-optimal in several respects. First, the trigger levels of the system are causing on average six trains every month to be delayed from schedule because they are stopped unnecessarily. Furthermore, the system causes one train every four months not to resume immediately regular operation to allow for track inspection; see section 2.2. This average rate of train delays and stops is considered high for a system that has never experienced any earthquake-induced accident. To remedy the current inefficiency of the seismic early warning system we study the effect of changing three different aspects of the SEWS : First, the scope of control of each of the coastal accelerometers, then the intensity parameter used at the wayside detecting systems for issuing warnings and deciding post-earthquake resumption of train operation, and finally the trigger levels of both detecting systems. Regarding the first issue, we consider three different coastal systems A, B and C. System A is the current system, while systems B and C implement the potential for any of the coastal accelerometers to order emergency braking of trains anywhere along the Tohoku line, if the level of ground shaking calls for such an action. This kind of operational rules are hereafter referred to as *continuous rules*. The difference between systems B and C is that the latter assumes that at the location of each of the coastal accelerometers there will be the potential for issuing an earlier warning, i.e. upon the arrival of the P waves. The system that is capable of performing such an early operation is called UrEDAS; see Nakamura (1988 and 1989). Another important aspect that controls the performance of the seismic early warning system is the intensity parameter used at the wayside system. In this study we study the efficiency of the system by using either peak ground acceleration, as is currently performed, or alternatively response

spectrum acceleration at an appropriate frequency and damping ratio. Finally, we study the effect of different trigger levels of both coastal and wayside systems in the overall performance of the SEWS system.

In describing alternative system configurations, we use the following notations :

- i = generic coastal accelerometer (any of eight accelerometers),
- j = location along the track,
- s = operational track segment (a subset of locations j that are simultaneously controlled in terms of the operation of the SEWS; any of the twenty-six operational segments),
- M = earthquake magnitude (JMA),
- x = epicentral location,
- Δ = epicentral distance from x to the location of interest j along the track,
- a_{\max} = peak ground acceleration.
- S_a = maximum acceleration experienced by a 1-DOF structure with a given natural period T and damping ratio β . S_a is referred to as response spectrum acceleration.

General characteristics of all SEWS systems considered here are :

- (1) The coastal system can cause a train in operational segment s to brake until complete stop. The coastal system operates on S waves (systems A and B) or, for system C on either P or S waves.
- (2) The wayside system can order a train in segment s to stop upon the arrival of the S waves at track segment s .

(3) Braking orders are generated four seconds after the first arrival of the wave phase of interest (P or S), at the site of the accelerometer. Indeed, four seconds into the motion is typical of the time when the peak ground shaking intensity is reached; see for example Murakami et al. (1975), Ejiri et al.(1988) and Der Kiureghian et al. (1989).

(4) Seismic waves are assumed to propagate isotropically and at constant and isotropic velocity. The velocity of the S waves, V_s is assumed equal to 3.80 km/sec (JREast, personal communication). Based on elastic wave theory (Gubbins, 1990), the velocity of the P waves, V_p is related to V_s as :

$$V_p = \sqrt{\frac{\lambda + 2\mu}{\mu}} V_s \quad (3.1)$$

where λ , μ are the Lamé constants. Since a reasonable assumption is that $\lambda = \mu$ in the crust (Gubbins, 1990), equation (3.1) gives $V_p = 6.58$ km/sec.

3.1 Alternative Coastal Seismic Early Warning Systems

System A

This is the system that is currently in operation. It assigns a specific track segment to each of the eight coastal accelerometers, as shown in Figure 1.1. These eight preset sections, hereafter referred to as “shut-down” sections, cover the entire line with some overlap. Each “shut-down” section is composed of neighboring operational segments; see Table 3.1. The principle underlying this system is that when the earthquake motion at a coastal accelerometer exceeds a preset intensity, then the earthquake is considered potentially dangerous for the corresponding “shut-down” section. A limitation of this system is that, if one of the coastal accelerometers records high ground motion levels, it should be able to trigger automatic braking also outside its designated proximal track section. Doing so

could increase significantly the lead time of warning at locations along the line far away from the coastal station.

System A operates on S waves and triggers automatic braking when peak ground acceleration exceeds a threshold value a^* , which is currently set at **40gals**. In analyzing seismic risk under system A, we shall make the simplifying assumption that, if an operational segment s can be controlled by more than one coastal station, in an earthquake of given epicentral location it is actually controlled by the coastal station that is closest to the epicenter.

System B

This system maintains the geographic configuration of the coastal accelerometers of system A, but introduces a new operational philosophy. In this case there is no preset “shut-down” section assigned to each coastal accelerometer. Rather, it is the intensity of the earthquake motion recorded at the station and a roughly estimated epicentral location area that determines the length of the “shut-down” section. Therefore, as the recorded intensity increases the “shut-down” section of the track becomes larger. Compared to system A, system B aims at gaining lead time for the braking of trains, as such action can be caused at all locations along the track by the coastal accelerometer closest to the epicenter, if the recorded ground motion intensity justifies such action.

Implementation of this system requires the definition of a set of trigger ground acceleration levels at each coastal station i , which depend on track location s and on the “sector of origin” of the earthquake R . The latter is defined as the subset seismogenic regions that is closest to each coastal accelerometer; see Figure 3.1. These trigger accelerations a_t have the form :

$$a_t(i,s,R)=b^* \gamma(i,s,R) \quad (3.2)$$

where b^* is a scaling factor with units of acceleration and $\gamma(i, s, R)$ is ideally the ratio between the peak ground acceleration at coastal detector i and the spectral acceleration at track segment s , for earthquakes that occur within “sector of origin” R . Because the above ratio is uncertain and further depends on magnitude M and on the actual epicentral location \underline{x} within R , γ is evaluated as follows :

$$\gamma(i, s, R) = \frac{\int_{\underline{x} \in R} \int_6^{M_{\max}} \frac{a_{\max}(M, \Delta(\underline{x}, i))}{S_a(M, \Delta(\underline{x}, s))} 10^{-bM} dM}{\int_{\underline{x} \in R} \int_6^{M_{\max}} 10^{-bM} dM} \quad (3.3)$$

In equation (3.3), a_{\max} and S_a are median attenuated values of peak ground acceleration and of spectral acceleration at the period and damping of the viaduct structure. Also notice that integration over M is limited to values from 6 to the maximum possible magnitude from location \underline{x} , as smaller magnitudes do not pose significant threat to the Shinkansen system. Figure 3.2 presents the values of γ as functions of i and s for earthquakes originating from different “sectors of origin”. The estimated values of $\gamma(i, s, R)$ for all coastal stations i and operational segments s for earthquakes originating from all “sectors of origin” R are presented in Appendix I and more specifically in Tables I-1 through I-8. Parameter b^* has the meaning of estimated spectral acceleration at track location s above which emergency braking is considered appropriate. System B operates on S waves. In evaluating the performance of system B, we make the simplifying assumption that any automatic braking action is caused by the coastal accelerometer that is closest to the epicenter.

System C

The idea behind system C is that more accurate warnings can be issued by estimating the magnitude M and epicentral location \underline{x} of the earthquake and then deciding about the

action to take based on M and \underline{x} . A system like this is the UrEDAS system; see Nakamura (1988 and 1989). In the UrEDAS system, M and \underline{x} are estimated from a single station using P waves or S waves. The obvious advantage of using P waves is the increase in lead time. Emergency braking may or may not be ordered depending on these first estimates of M and \underline{x} . The procedure is then repeated using S waves. The S-based estimates of M and \underline{x} have increased accuracy. The benefit of this system in added lead time is counter-balanced to some degree by the limited estimation accuracy of M and \underline{x} especially when using P waves.

Following estimation of (M, \underline{x}) , the UrEDAS system evaluates the destructive potential at all locations along the track. This is done using historical data on damage and non-damage events, depending on magnitude and epicentral distance $\Delta(\underline{x}, s)$; see Figure 3.3. The shaded area in that figure indicates (M, Δ) combinations that are considered potentially damaging. For our analysis, only epicentral distances above about 80km are of interest and the boundary between damage and non-damage conditions is linear in M and $\log_{10}\Delta$: $0.71M - \log_{10}\Delta = 3.20$, as shown in Figure 3.3. Accordingly, we have considered System C to trigger emergency braking if :

$$\text{TRIG}=(0.71M-\log_{10}[\Delta(\underline{x},s)]-c^*)\geq 0 \quad (3.4)$$

where c^* is a scaling parameter that controls the degree of conservatism in when using System C.

The effectiveness of System C depends on the estimation accuracy of M and \underline{x} . Figures 3.4a and 3.4b compare earthquake magnitudes estimated by the UrEDAS system using P and S waves with actual magnitudes (JREast, personal communication). The plots show that the S estimates are more accurate (all such estimates within ± 0.5 of the actual values) whereas for the P estimates the average is ± 1.0 . The latter value agrees with Figure 3.4c, which includes larger earthquake magnitudes for which the reported

accuracy is somewhat smaller (Nakamura, 1988). Based on these figures and indications from JREast, we consider the following as reasonable values for the standard deviation of the earthquake magnitude estimation error :

$$\begin{aligned} \sigma_{M,P} &= 1.0 \text{ (JMA)} && \text{Magnitude estimation from P wave arrival} \\ \sigma_{M,S} &= 0.5 \text{ (JMA)} && \text{Magnitude estimation from S wave arrival} \end{aligned}$$

Regarding the estimation accuracy of epicentral location, the information available is not very conclusive. First, the azimuth and hypocentral distance are estimated from P and S waves. Nakamura (1988) presents evidence that all estimates of the azimuth lie within a range of $\pm 20^\circ$ of their actual values; see Figure 3.5a. This range is larger in Figure 3.5b (JREast, personal communication). The estimation of hypocentral from P waves is not very accurate (Nakamura, 1989), but accuracy increases (all estimates within ± 20 km of actual values) after the arrival of the S waves; see Figure 3.6a. Finally, Figure 3.6b presents an illustration of the accuracy of the earthquake location estimation after the S waves (Nakamura, 1989). This information, and personal communication with JREast, lead us to estimate as follows the standard deviation of the estimation error for epicentral distance of the earthquake:

$$\begin{aligned} \sigma_{\Delta,P} &= 75\% \Delta && \text{Epicentral distance estimation from P wave arrival} \\ \sigma_{\Delta,S} &= 25 \text{ km} && \text{Epicentral distance estimation from S wave arrival} \end{aligned}$$

where Δ is the epicentral distance in km. Due to the limited data available, these accuracy values are highly uncertain. The sensitivity of seismic risk to such accuracy parameters will be assessed in Chapter 6.

3.2 Alternative Wayside SEWS Systems

Use of System to Reduce Seismic Risk

A wayside accelerometer may cause trains in the corresponding operational segment s to stop if the intensity of ground motion exceeds a given threshold. At present, ground motion intensity is measured in terms of peak ground acceleration a_{\max} . In this study, we have considered as an alternative the use of spectral acceleration S_a at the period of the viaduct (about 0.4sec) and for 5% of critical damping. The latter parameter is much better related to structural damage than a_{\max} . The associated trigger levels are denoted by $a_{t,loc}$ and $S_{a,t,loc}$. At present, $a_{t,loc}$ is set to **40gals**.

Use of System to Determine Inspection Needs and to Resume Operation

After trains have been stopped by either the coastal or the wayside system, a decision must be made regarding resumption of operation and possibly the need for track inspection. Such decisions are based on the earthquake intensity at the wayside station that is closest to the location of the stopped trains. Again, the intensity measure may be a_{\max} or S_a .

The system currently operates with two threshold levels, A_{insp1} and A_{insp2} : If $a_{\max} < A_{insp1}$, the trains resume regular high-speed operation immediately after stopping, without inspection of the tracks. We refer to these events as *short delays*. If $A_{insp1} \leq a_{\max} \leq A_{insp2}$, the trains resume operation at a reduced speed (30-50 kmh) to perform on board inspection of the tracks. We refer to these events as *medium delays*. Finally, if A_{insp2} is lower or equal to a_{\max} , an on-foot inspection of the tracks is performed prior to restoration of service (*long delays*). In the same manner, if the intensity parameter used is S_a the associated track inspection levels are denoted by $S_{a,insp1}$ and $S_{a,insp2}$.

The current wayside system, operates in terms of a_{\max} and the inspection levels are $A_{insp1}=80\text{gals}$ and $A_{insp2}=120\text{gals}$.

No	Location of accelerometer	From location along track	To location along track	Track section (km)	Control of segments
1	Hachinoche	Shin-Kitakami	Morioka Station	42.5	1 - 3
2	Miyako	Shin-Kitakami	Morioka Station	42.5	1 - 3
3	Ofunato	Shin-Kozuruzawa	Morioka Station	154.9	1 - 8
4	Kinkazan	Shin-Shiraishi	Shin-Kitakami	170.1	4 - 12
5	Soma	Shin-Yabuki	Shin-Kozuruzawa	151.5	9 - 16
6	Iwaki	Shin-Ishibashi	Shin-Nihonmastu	137.6	14 - 20
7	Chosi	Tokyo Station	Shin-Ishibashi	95.4	20 - 26
8	Miura penins.	Tokyo Station	Shin-Nishinasuno	146.8	18 - 26

Table 3.1: Stations of the coastal early warning system and track segments they control (system A).

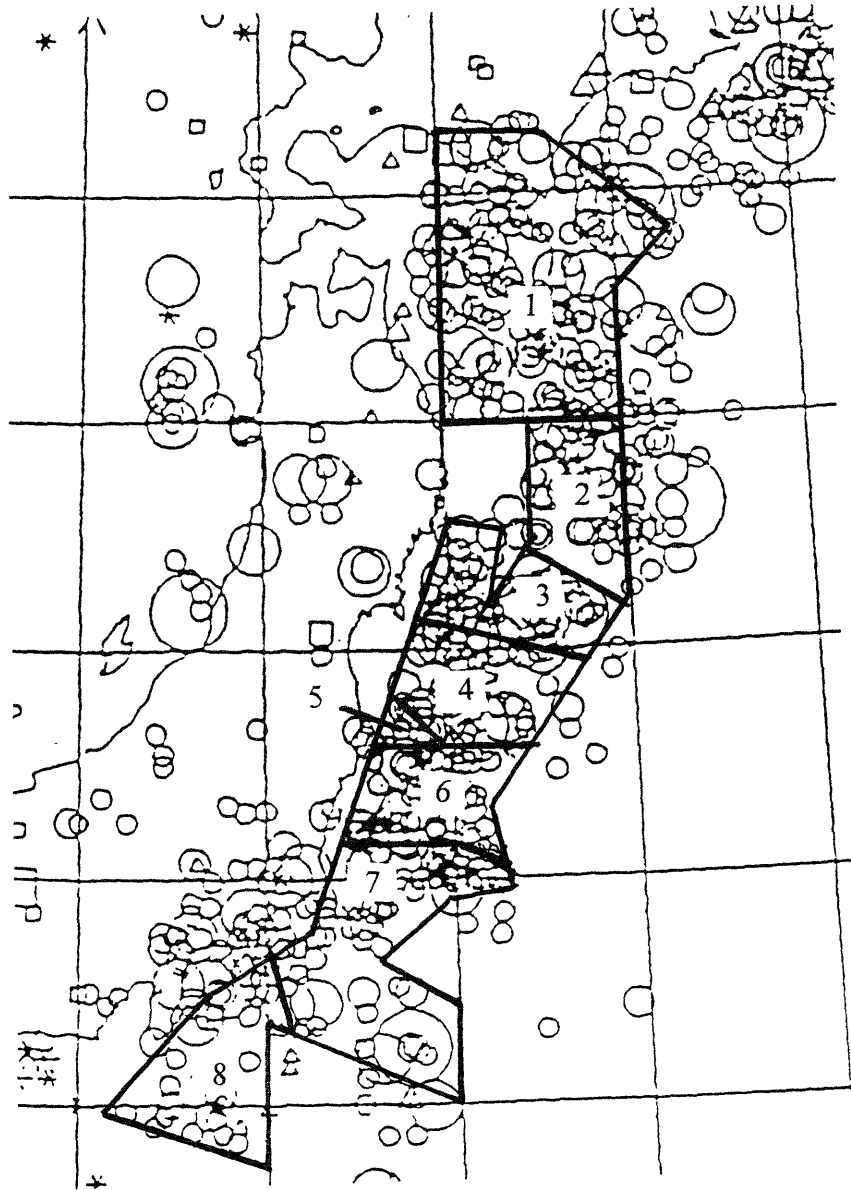


Figure 3.1: Map of "sectors of origin" of earthquakes, R.

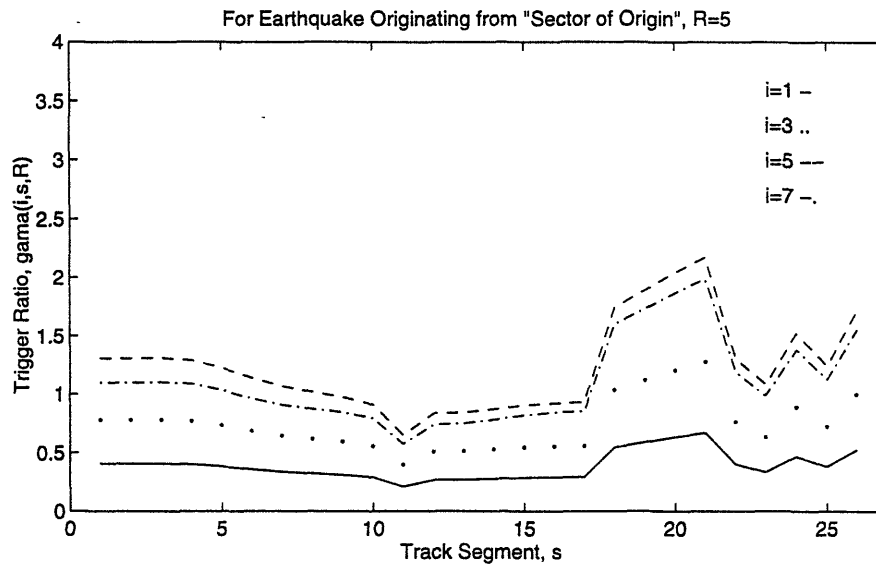
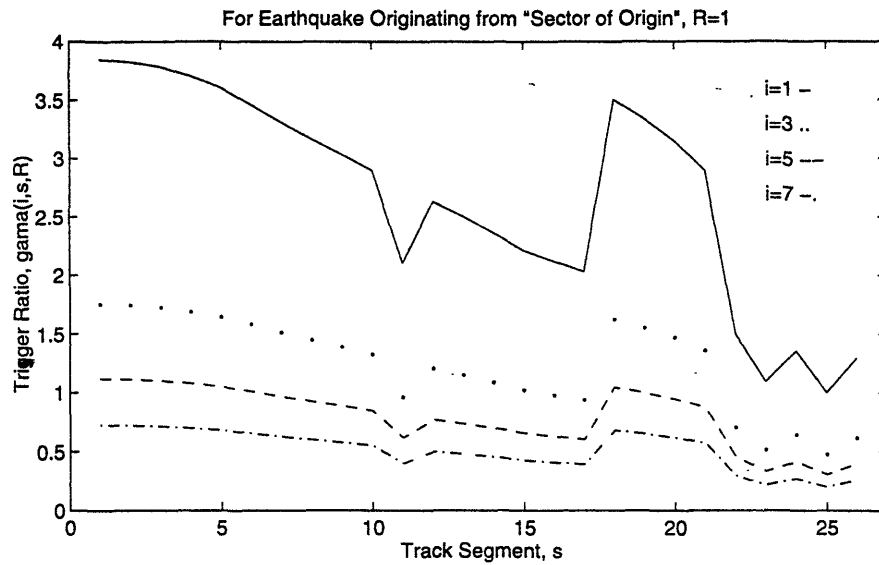


Figure 3.2: Expected value of ratio $\gamma(i, s, R)$ between peak ground acceleration at coastal accelerometer i and the spectral acceleration at segment s , for:
 (a) "sector of origin" of earthquake, $R=1$.
 (b) "sector of origin" of earthquake, $R=5$.

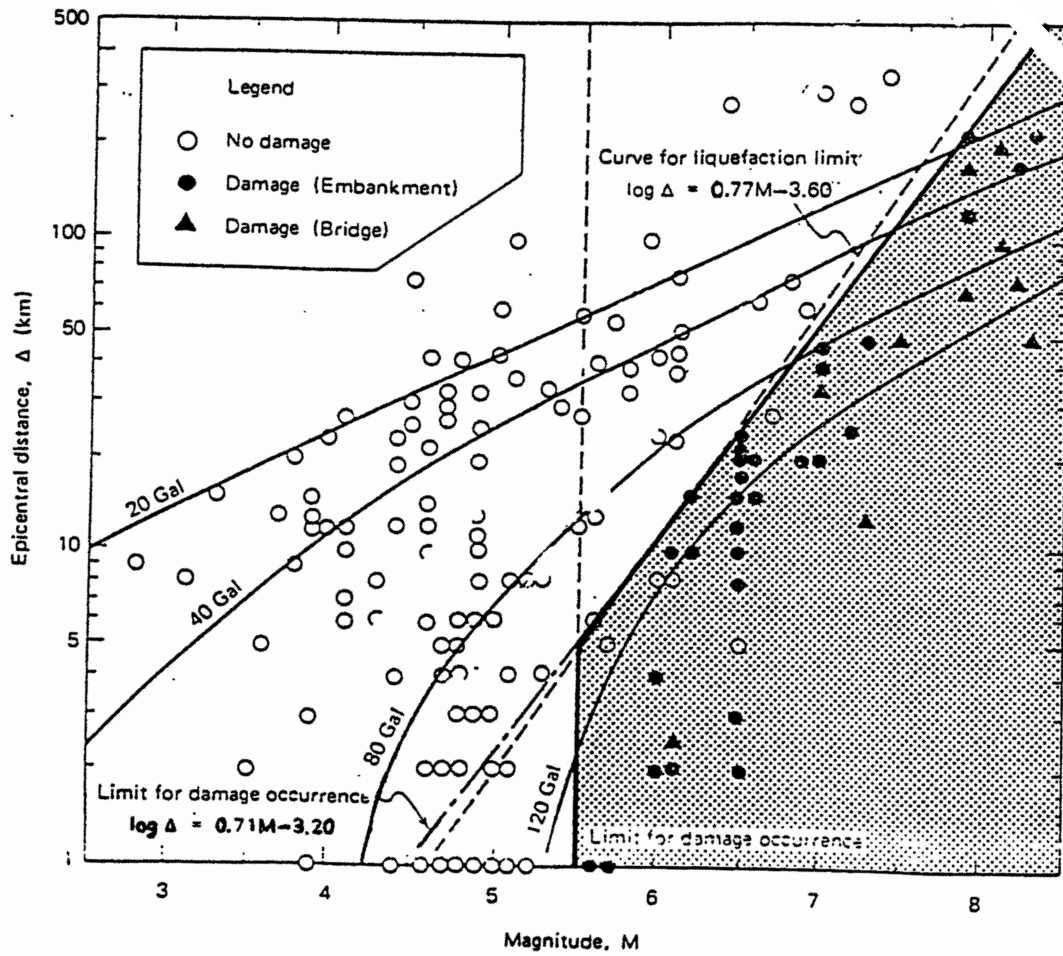


Figure 3.3: Triggering criteria of the UrEDAS system (Nakamura, 1989).

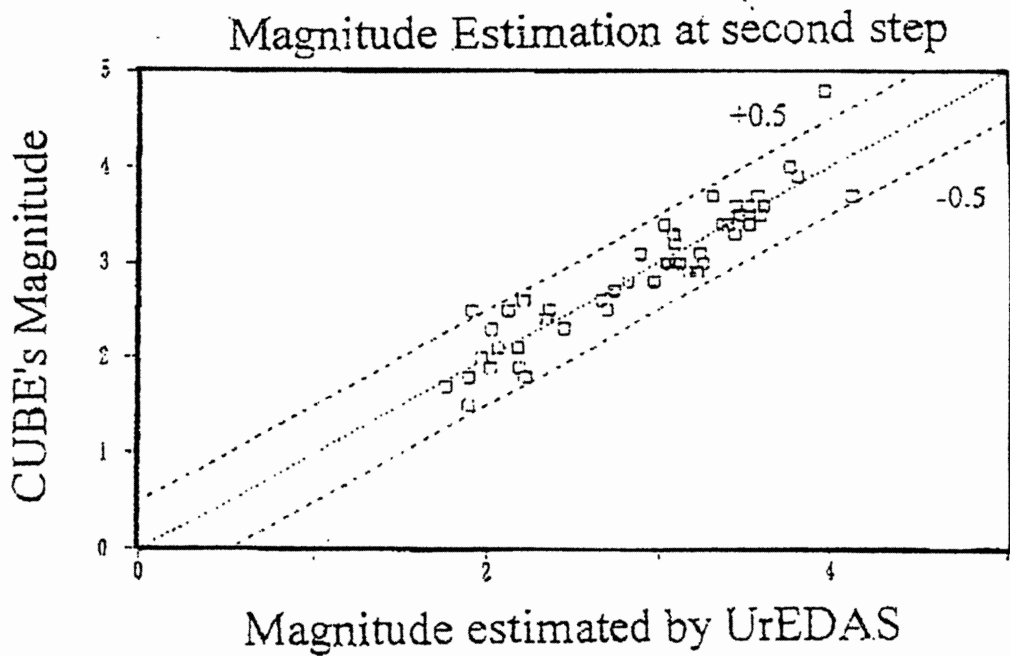
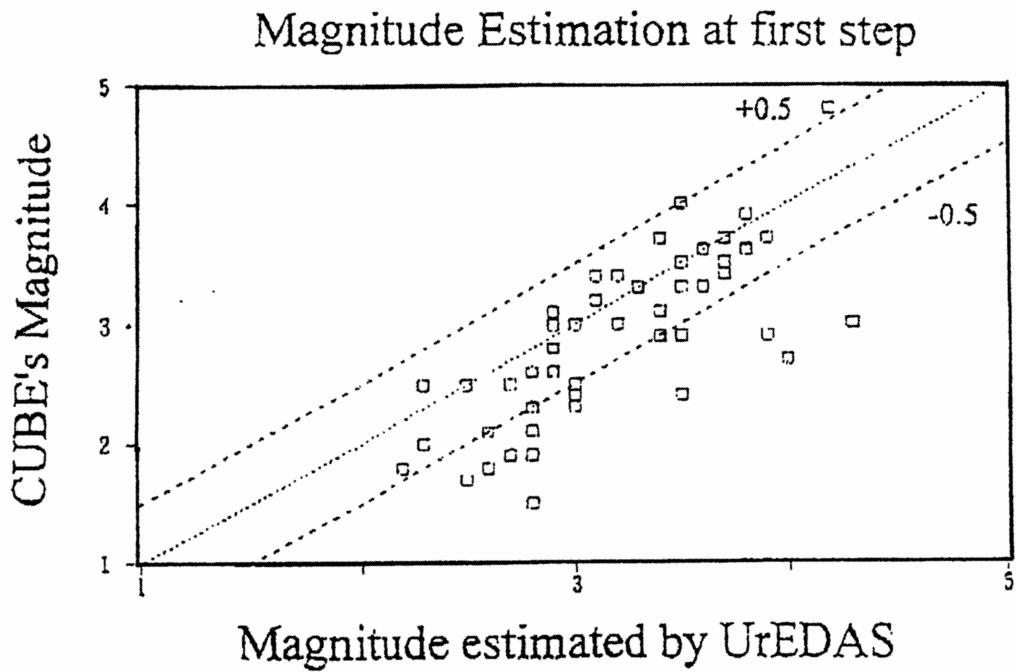


Figure 3. : (a) Accuracy of P-wave magnitude estimation in the UrEDAS
 (b) Accuracy of S-wave magnitude estimation in the UrEDAS
 (JREast, personal communication).

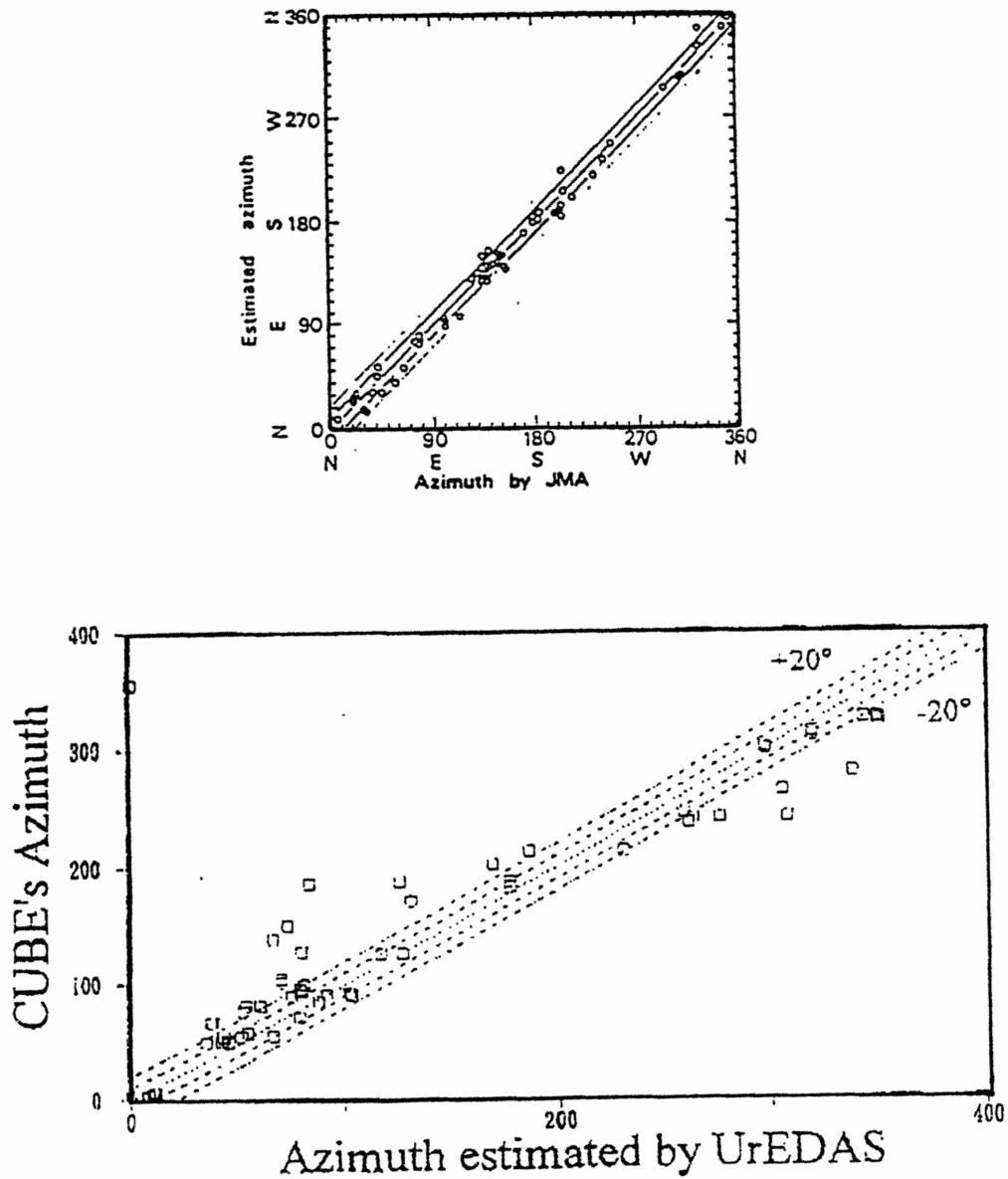


Figure 3.7: Accuracy in the azimuth estimation using P waves:
 (a) Nakamura (1988).
 (b) JREast personal communication.

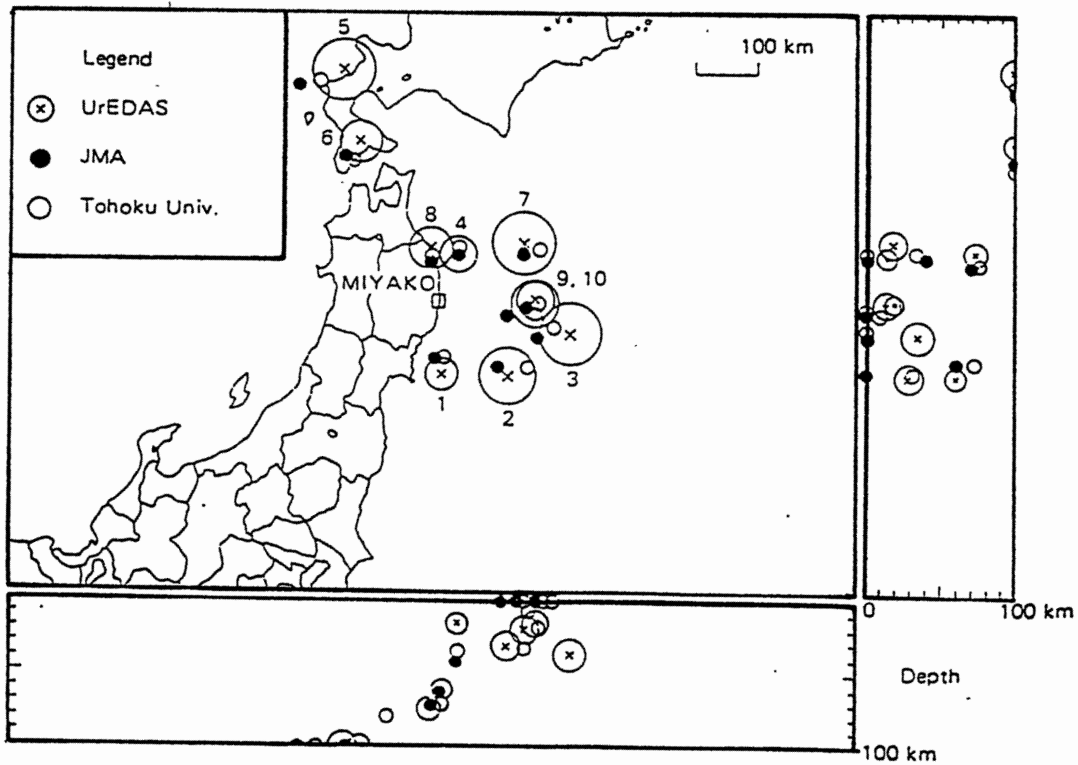
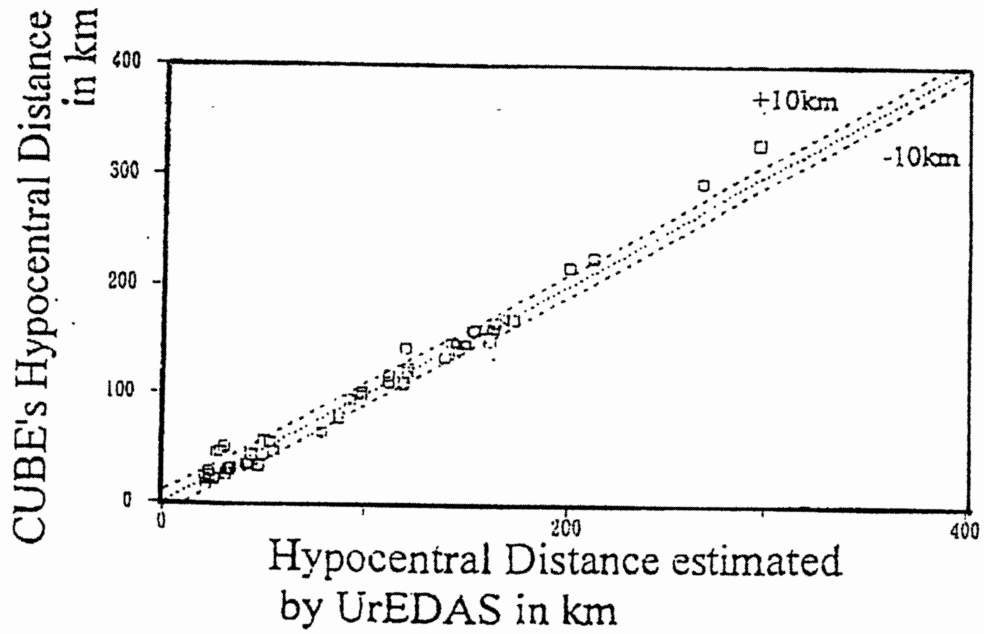


Figure 3.6: (a) Accuracy of hypocentral distance estimation from S waves in the UrEDAS system (JREast, personal communication).
 (b) Accuracy of epicentral location estimation in the UrEDAS system using S waves (Nakamura, 1989).

Chapter 4

Seismic Environment

In this Chapter, we consider models of earthquake recurrence in the offshore region that may potentially affect the Tohoku Shinkansen line, as well as strong motion attenuation. In each case, we briefly review the literature and then develop models for this study.

4.1 Seismicity

The literature on the seismicity of Japan is very extensive. Studies that cover the area of interest include Takemura et al. (1989) for the area southwest of Tokyo, Kanda et al. (1988) for the greater Tokyo region, Annaka et al. (1988) for the Kanto district, Utsu (1974) for offshore northeastern Japan and Umino et al. (1993) for northeastern Japan in general. Unfortunately, none of these studies covers completely the whole area of interest to us. The model used in this study is based mainly on Utsu (1974) and is complemented with information from Annaka et al. (1988).

Figure 4.1 shows the historical seismicity in the area of interest. As it is clear from this figure, offshore seismicity, which is the focus of the present study, is far more intense than inland seismicity. We have modeled offshore seismicity through fifteen seismogenic regions (“sources”), within which earthquake activity is considered uniform. The sources correspond for the most part to those of Utsu (1974), except for the fact that some of Utsu’s seismogenic regions have been split into several sources. The main reason for this operation is computational expedience. Figure 4.2 shows the fifteen seismic regions of the proposed model superimposed on historical seismicity. A statistical analysis of the historical data produces estimates of the rate density $\lambda(M)$, where $\lambda(M)dM$ is the rate in

events/year of earthquakes of magnitude between M and $M+dM$ in a seismic source. We assume that, $\lambda(M)$ has the following form :

$$\lambda(M)=10^{a-b(M-6)} \quad ; \quad M \leq M_{\max} \quad (4.1)$$

where a is a measure of the overall seismicity (10^a is the rate density of earthquakes of magnitude M around 6)

b is a parameter that controls the relative frequency of events of different magnitudes and

M_{\max} is the maximum earthquake magnitude that can possibly be generated by the seismic source.

Table 4.1 gives for each of the fifteen seismic sources, estimates of the parameters (a , b , M_{\max}), the area, and the correspondence with the seismic sources of Utsu (1974).

Before discussing how the estimates of the seismicity parameters were obtained, we observe that Utsu (1974) based his results on shallow earthquakes (focal depth ≤ 80 km) with magnitude $M \geq 6$ during the period 1926 - 1973. On the other hand, the analysis of Annaka et al. (1988) is based on shallow earthquakes (focal depth ≤ 70 km) with magnitude $M \geq 6$ during the period 1885 - 1986.

Seismic Sources 1, 2, 4, 5, 6, 8, 9 : The rate density parameters a , b and M_{\max} were directly derived from these of Utsu (1974), considering that the parameters a in that study refer to 47 years of data.

Seismic Sources 10, 11, 12 : These sources are parts of source L of Utsu. Their annual rate density has been obtained by distributing the total rate proportionally to source areas. M_{\max} is the same as for Utsu's source L.

Seismic Source 3: This source corresponds to a part of Utsu's source H. Utsu gives no clear information on the seismicity level of source H. Furthermore, this seismogenic region is not studied in Annaka et al. (1988). Thus, the rate density per km² of the neighboring source E (Utsu, 1974) for M=6 is assigned to source H and adjusting for the area of source 3. Because no large earthquake has occurred in source H during the period 1926 - 1973, we assumed $M_{\max} = 8.0$, which is a value somewhat smaller than that of source E.

Seismic Source 7: We assign to this source a rate density per km² equal to that of the neighboring sources K and L, as no clear information on the a parameter given by Utsu on the corresponding source J. We take $M_{\max} = 8.5$, mainly because of a series of large earthquakes in 1938.

Seismic Source 13: According to Utsu, source M is tectonically similar to source L. Therefore the b-value for the corresponding region 13 was assumed equal to the value for source L. Also the rate density and the maximum magnitude for source 13 have been taken from Utsu's source L.

Seismic Source 14: No clear information is provided in Utsu (1974) for this region. We have based our estimate on information from the geographically close zones 16 and 20 in Annaka et al. (1988), adjusting for the area of region 14. The value of M_{\max} is also taken from the latter publication.

Seismic Source 15: As for region 14, we estimate the values of the seismicity parameters from information on zone 27 in Annaka et al. (1988), adjusting for areas.

Clearly, the parameters in Table 4.1 are just point estimates. Sensitivity of the risk to the values of b and M_{\max} will be presented in Chapter 6.

4.2 Strong Motion Attenuation

Several studies of strong motion attenuation have been made using data from the region of interest and from other seismically active areas of the world. For our analysis, we are

interested in the attenuation of peak ground acceleration a_{\max} and response spectrum acceleration S_a with 5% damping of critical. For a_{\max} pertinent studies include Yamabe et al. (1988), Tomatsu et al. (1988), Kobayashi et al. (1988) and Kawashima et al. (1984) based on earthquakes in Japan, Boore et al. (1993) based on western North American earthquakes and Fukushima et al. (1988) based on worldwide earthquakes. Selected recent studies on S_a attenuation are those of Annaka et al. (1988), Kawashima et al. (1984) based on earthquakes in Japan and Boore et al. (1993) based on western North American earthquakes.

Most of these studies refer to specific subsoil conditions (usually “firm ground” or “rock”). Only the last two studies take into account the amplification effect from different local soil conditions. As local amplification may have a significant effect on damage, we have included the influence of soil conditions in our analysis although in a simplified categorical manner. Kawashima et al. (1984), has derived different attenuation relations for different soil types. The latter are defined as in Table 4.2, based on geological characteristics of the site and on the natural period of the soil layer above bedrock, T_G . This period is :

$$T_G = \frac{4H}{V_s} \quad (4.2)$$

where H is the thickness of the soil layer above bedrock,

V_s is a representative value of the shear wave velocity of the soil layer.

The soil classification presented in Table 4.2 is assumed to correspond to that included in the standard design code of the Japanese National Railways (Table 2.4), that was used in the design of the Tohoku viaduct structure. This assumption is reasonable for the following reasons : (a) soil types I, II in Tables 2.4 and 4.2 have similar geologic descriptions and (b) the very low SPT values for soil type III in Table 2.4 correspond, in general, to soft alluvium and reclaimed land, that is soil type III in Table 4.2.

Figure 4.3a compares median attenuated values of a_{\max} , for earthquake magnitude $M = 5$ and rock conditions, according to various studies. It appears from this and other comparisons that the Kawashima et al. (1984) attenuation yields too high values of a_{\max} at such low magnitudes, while the median values from Boore et al. (1993) are consistent with those from other Japanese studies. Figure 4.3b makes a similar comparison for earthquake magnitude $M = 8$ and rock conditions. In this case, the attenuated median value of a_{\max} according to Kawashima et al. (1984) is a reasonable upper bound value, while the value from Boore et al. (1993) appears unrealistically low for eastern Japan. Based on comparisons of this type, we have specified attenuation relations for the area of interest of the general type :

$$Y = a 10^{bM} (\Delta + 30)^{-c} \quad (4.3)$$

where Y is the median attenuated value of the seismic intensity parameter of interest
(either peak ground acceleration a_{\max} or spectral acceleration S_a with 5%
damping in a random horizontal direction),

Δ is epicentral distance in km and

(**a**, **b**, **c**) are parameters that depend on the soil conditions for a_{\max} and on
both soil conditions and the natural period T for S_a .

This relation is based on the attenuation of Kawashima et al. (1984), but the values of the attenuation parameters are calibrated to account for what we believe is an overprediction of Y at low magnitudes, as suggested by Figure 4.3. The calibration was performed for different soil conditions and natural periods so as to produce values of Y similar to those of Boore et al. (1993) at low magnitudes. More specifically, parameters **a** and **b** of equation (4.3) were adjusted from the original values of Kawashima et al. (1984) to yield:

- The value of Y according to Boore et al. (1993) for $M = 5$ and $\Delta = 100$ km.
- The value of Y according to Kawashima et al. (1984) for $M = 8$ and $\Delta = 100$ km.

This modification resulted generally in smaller values of a and larger values of b . The resulting law is referred to here as the “modified Kawashima” attenuation model. The parameters of the original and modified Kawashima et al. (1984) attenuation relations for a_{\max} and S_a (the latter, for periods $T = 0.3$ and 0.5 sec that are of greatest interest for this study) are given in Table 4.3.

The values of a_{\max} and S_a given earthquake magnitude M and epicentral distance Δ are typically found to follow a log-normal distribution. The dispersion of the distribution is usually given in terms of the logarithmic standard deviation $\sigma_{\ln y}$, estimates of which from Kawashima et al. (1984) are given in Table 4.4. These estimates have been retained also in the “modified Kawashima” attenuation model.

In the study of seismic risk of the Tohoku Shinkansen, it is necessary to specify an attenuation model of S_a for natural periods between $T = 0.3$ sec and $T = 0.5$ sec. As such intermediate periods are not considered in the original study of Kawashima et al. (1984), we have used a log-linear interpolation scheme of the attenuated parameter between periods 0.3 and 0.5 sec.

Figures 4.4 and 4.5 compare median attenuated values of a_{\max} and S_a per soil type, according to Boore et al. (1993), Kawashima et al. (1984) and the modified Kawashima model. Comparison of S_a is for $T = 0.4$ sec, which is a period of particular importance in the seismic risk study of the Shinkansen viaduct.

The very large accelerations and velocities recorded during the January 17, 1995 Hyogo-ken-Nambu Earthquake (the “Kobe earthquake”) of January 17, 1995 has raised questions regarding the accuracy of the attenuation model proposed in this study. Figure 4.6 compares recorded values of a_{\max} and estimated values of S_a with 5% damping during this earthquake of JMA magnitude 7.2 ($M_w=6.8$) at different epicentral distances (JREast, personal communication), to the median attenuated values according to the modified

Kawashima model. This comparison shows that the model underestimates the recorded accelerations at small epicentral distances, whereas better agreement is found at larger distances. This discrepancy is attributed for the most part to the combined effect of the near-field radiation pattern and the amplification from local soil conditions. The latter was especially large in the reclaimed land of the Kobe port and Awaji island (NCEER Bulletin, 1995). A sensitivity analysis relative to the attenuation parameters will be reported later in this study.

Seismic Region (Sources: Utsu, 1974)	a	b	M_{max}	AREA (10 ⁴ km ²)
1 (D)	- 0.05	0.87	7.5	2.25
2 (E)	0.16	0.82	8.5	1.86
3 (H)	- 0.29	0.82	8.0	0.58
4 (F)	0.60	1.15	8.0	2.64
5 (G)	- 0.18	1.01	7.5	1.47
6 (I)	0.10	0.90	8.0	1.00
7 (J)	- 0.74	1.06	8.5	0.23
8 (J)	0.07	1.06	8.5	1.69
9 (K)	- 0.07	1.06	7.5	0.95
10 (L)	- 0.59	1.06	7.5	0.28
11 (L)	- 1.14	1.06	7.5	0.09
12 (L)	- 0.28	1.06	7.5	0.32
13 (M)	- 0.33	1.06	7.5	0.33
14 (N)	- 0.27	1.00	8.0	2.82
15 (O)	- 0.33	1.00	8.0	2.03

Table 4.1: Gutenberg - Richter parameters for the annual earthquake rate density of the fifteen seismic regions in Figure 4.2 and their correspondence to the seismic sources of Utsu (1974).

Soil Type	Geological Description	Definition by Natural Period, T_G
I	Tertiary rock - Diluvium with H < 10 m	T _G < 0.2 sec
II	Diluvium (H ≥ 10m) - Alluvium (H < 25m)	0.2 < T _G < 0.6 sec
III	Soft Alluvium - Reclaimed Land	T _G > 0.6 sec

Table 4.2: Soil classification used by Kawashima et al. (1984)

Soil Type (Table 4.2)	I		II		III	
	Original Kawashima et al.(1984)	Modified Kawashima et al.(1984)	Original Kawashima et al.(1984)	Modified Kawashima et al.(1984)	Original Kawashima et al.(1984)	Modified Kawashima et al.(1984)
a (a_{max})	987.4	90.0	232.5	138.1	403.8	412.5
b (a_{max})	0.216	0.346	0.313	0.341	0.265	0.264
c (a_{max})	1.218	1.218	1.218	1.218	1.218	1.218
a ($S_a; T=0.3s$)	574.8	22.1	266.8	37.9	1263	240.2
b($S_a; T=0.3s$)	0.273	0.450	0.345	0.451	0.224	0.314
c ($S_a; T=0.3s$)	1.178	1.178	1.178	1.178	1.178	1.178
a ($S_a; T=0.5s$)	211.8	12.2	102.2	14.8	580.6	58.1
b($S_a; T=0.5s$)	0.299	0.454	0.388	0.493	0.281	0.406
c ($S_a; T=0.5s$)	1.178	1.178	1.178	1.178	1.178	1.178

Table 4.3: Parameters of the original and modified Kawashima et al.(1984) attenuation relations for a_{max} and S_a (the latter, for $T = 0.3$ and 0.5 sec and 5% of critical damping).

Soil Type (Table 4.2)	I	II	III
$\sigma_{lny} (a_{max})$	0.497	0.516	0.454
$\sigma_{lny} (S_a; T = 0.3sec)$	0.555	0.622	0.500
$\sigma_{lny} (S_a; T = 0.5sec)$	0.640	0.573	0.553

Table 4.4: Logarithmic standard deviations of a_{max} and S_a , given earthquake magnitude M and epicentral distance Δ (Kawashima et al., 1984).

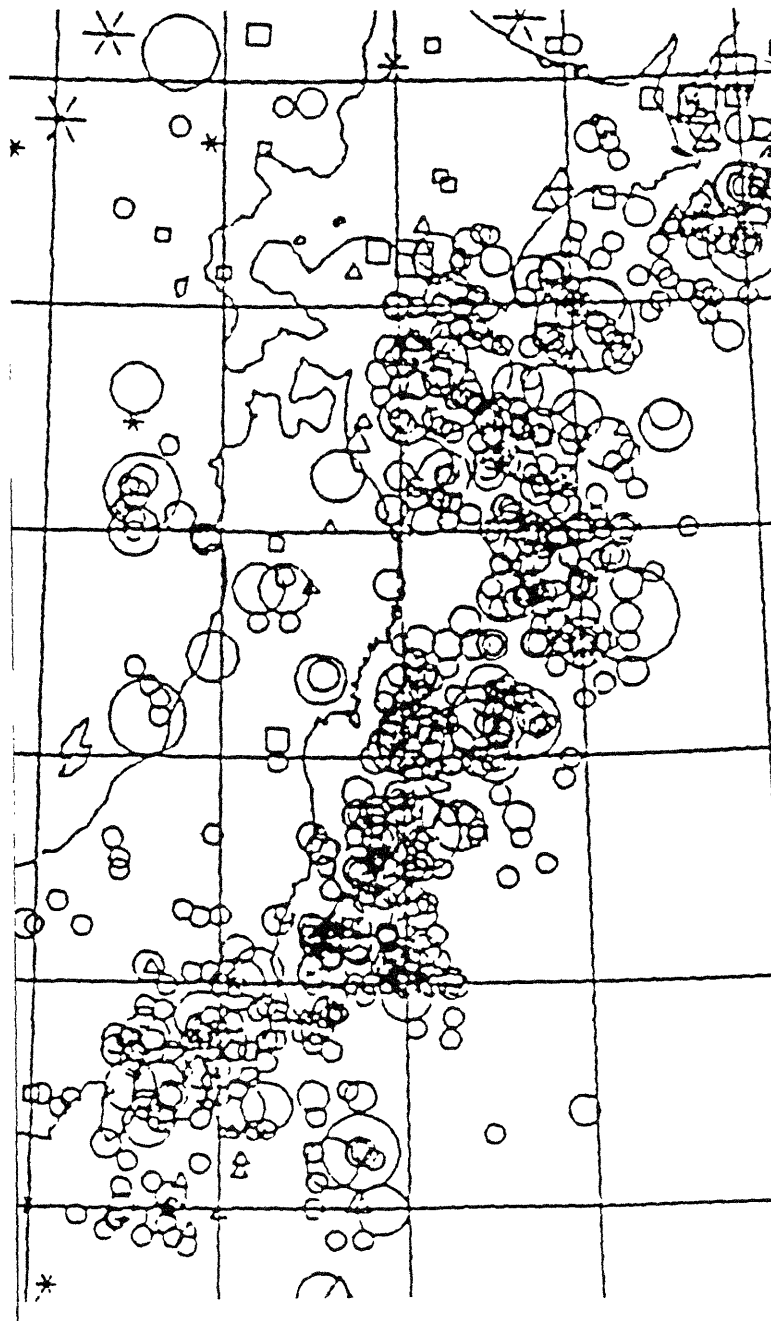


Figure 4.1: Historical seismicity in area of interest for the period 1885-1983

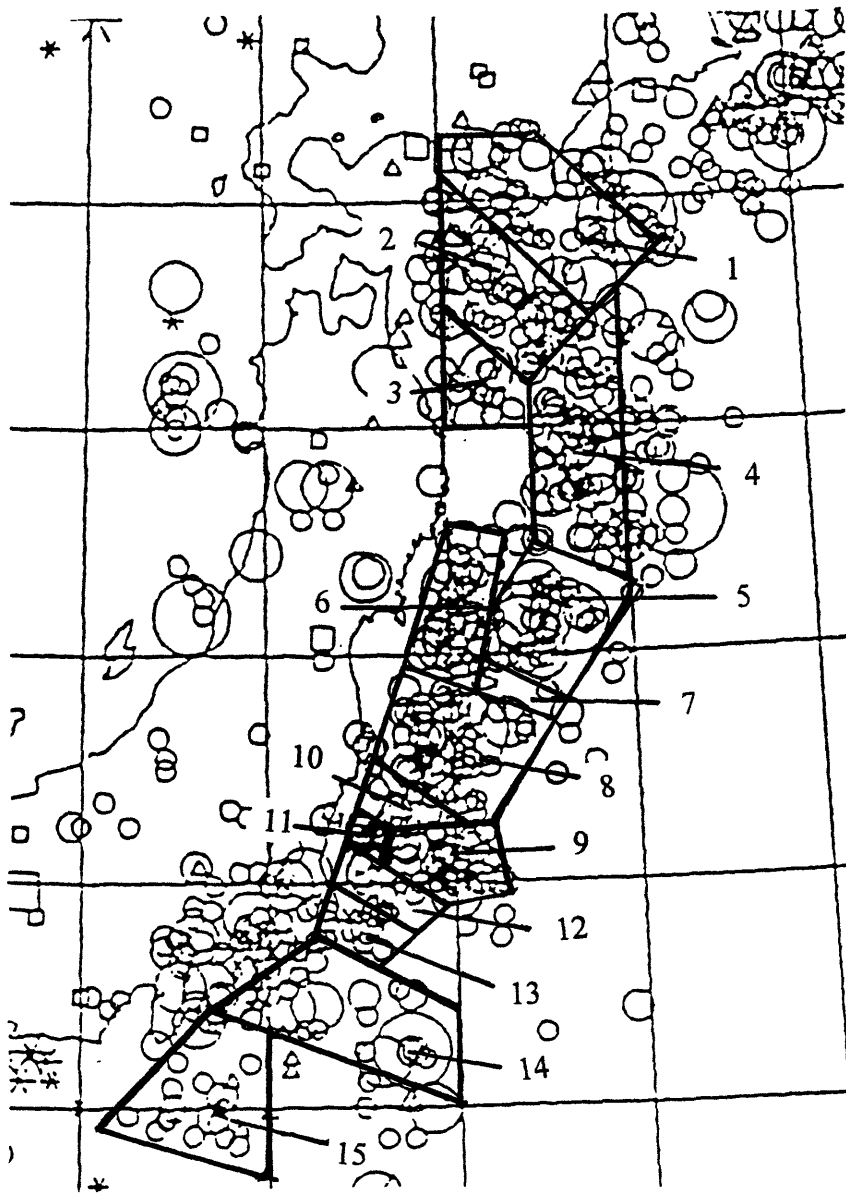


Figure 4.2: Sources of the proposed earthquake recurrence model for offshore seismicity superimposed on the historical seismicity (1885-1983).

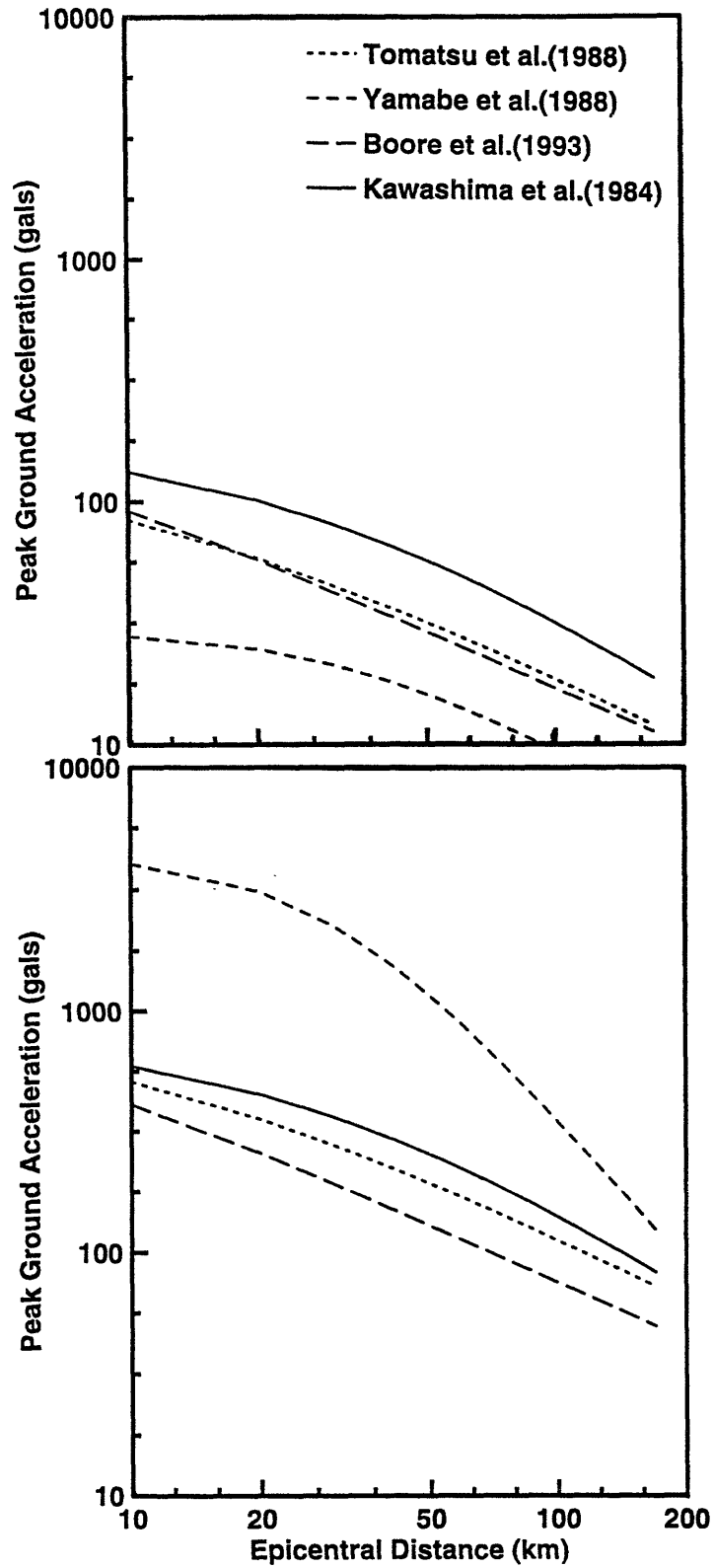


Figure 4.3: Peak ground acceleration at rock sites according to various studies :
 (a) $M = 5$ and (b) $M = 8$.

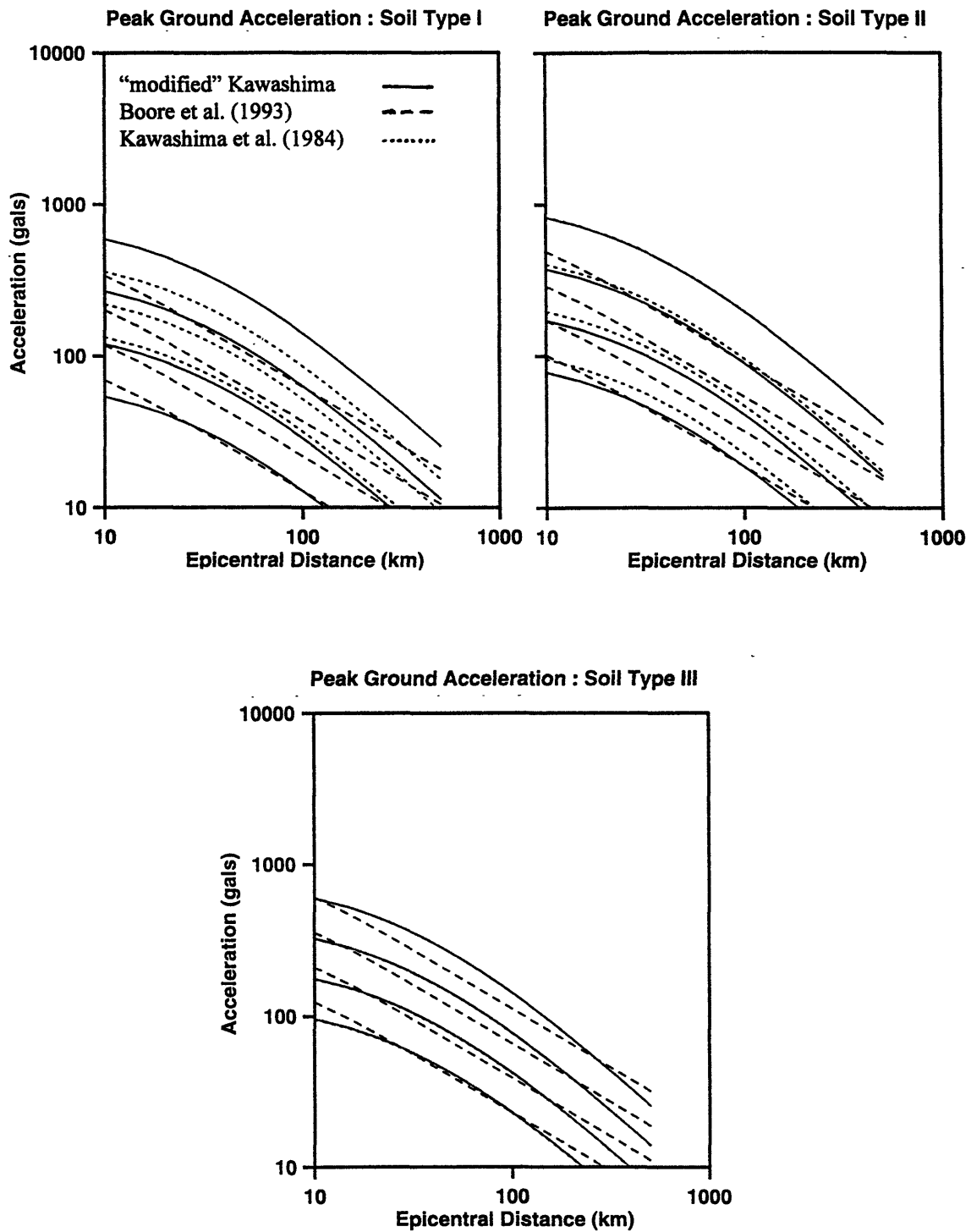


Figure 4.4: Comparison of peak ground acceleration attenuation relations for $M = 5 - 8$ and for: (a) soil type I, (b) soil type II and (c) soil type III.

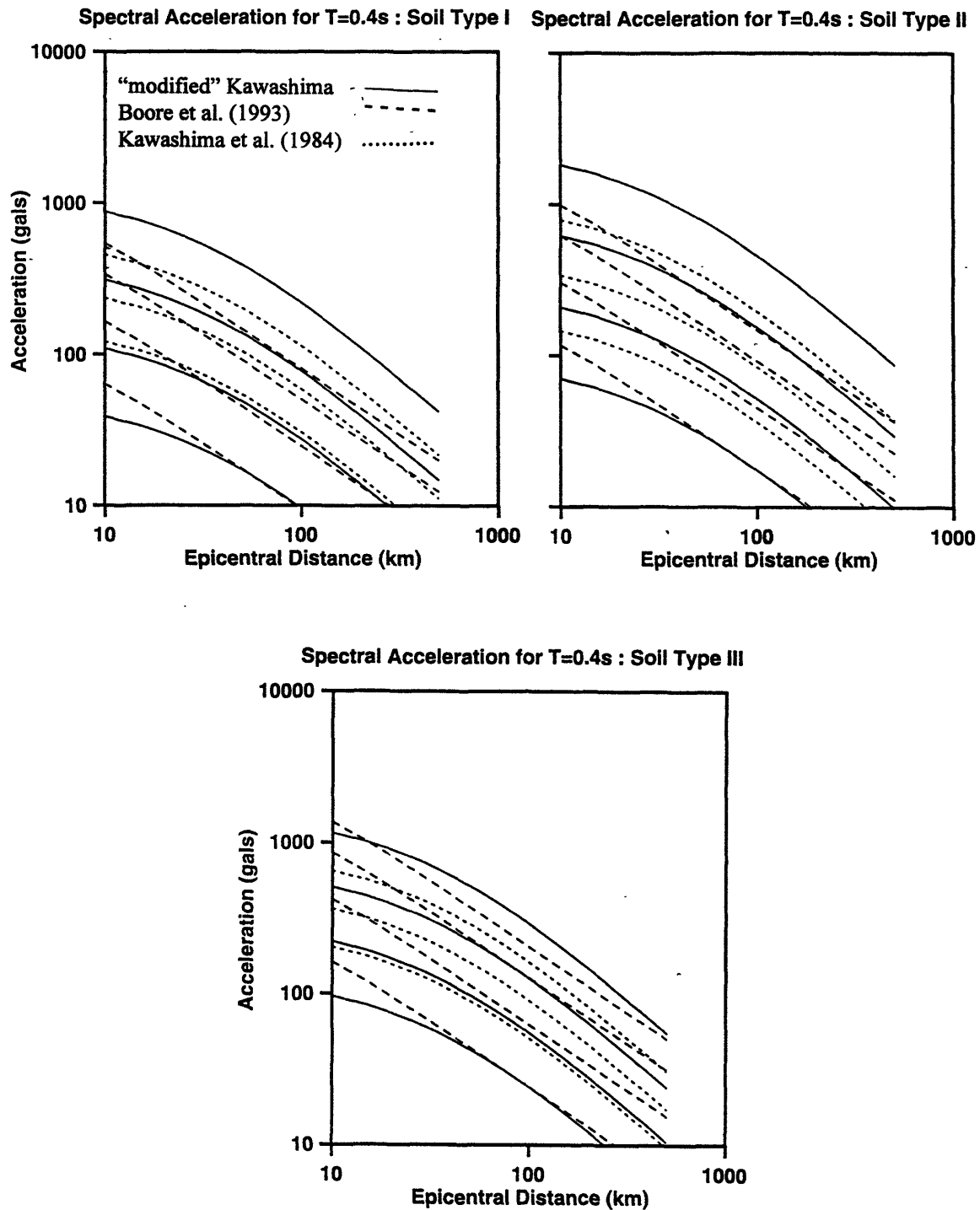


Figure 4.5: Comparison of spectral acceleration at T=0.4sec and 5% damping of critical, for M = 5 - 8 and for: (a) soil type I, (b) soil type II and (c) soil type III.

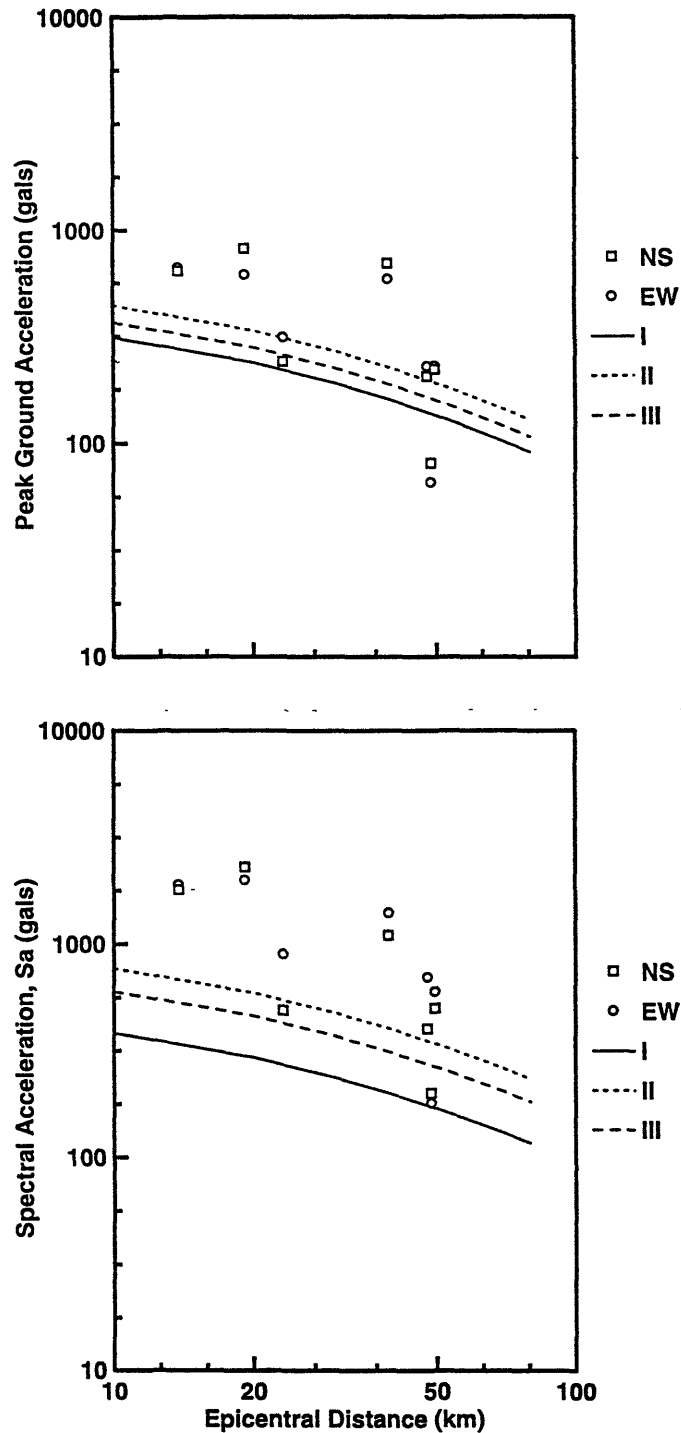


Figure 4.6: (a) Recorded peak ground accelerations during the Kobe earthquake and median values according to the “modified Kawashima” model for soil types I, II, III and $M=7.2$.
 (b) Estimated spectral accelerations at $T=0.4\text{sec}$ and 5% damping of critical compared to median values according to the “modified Kawashima” model for soil types I, II, III and $M=7.2$.

Chapter 5

Risk Analysis

In this chapter, we describe the method used to assess the rate of earthquake-induced derailments and trains delays, as functions of the type of seismic early warning system (System A, B or C) and of the operational parameters (choice of intensity parameter and trigger and inspection levels). A seismic fragility model for the viaduct structure is described first, followed by a discussion of the performance measures of the effectiveness of the seismic early warning system and by the general procedure for their evaluation. The last three sections of this Chapter address the specific problem of calculating the conditional probabilities of SEWS trigger, train derailment and train delay.

5.1 Seismic Fragility of the Viaduct Structure

A key component of the seismic risk analysis is the evaluation of the probability of viaduct damage in an operational segment s , given earthquake magnitude M and epicentral location x . This probability is used in the calculation of the risk of earthquake-induced derailments. First, we consider the probability of damage “at a point” (for a single viaduct span) and then proceed to the estimation of damage anywhere along a line segment, including the effect of damage clustering.

Probability of Damage of a Single Viaduct Span, $P_1(S_a)$

There is ample evidence from the literature that, for structures like the Shinkansen viaduct, a good measure of the destructiveness of earthquake motion is spectral acceleration at an appropriate period and for an appropriate damping ratio. We denote by

$P_1(S_a)$ the probability that a single viaduct span is damaged, given that it experiences a spectral acceleration S_a . In calculating $P_1(S_a)$, we assume that structural resistance in terms of S_a follows a log-normal distribution (NIBS Technical Manual, 1994). This resistance distribution has a median value R_m which depends on structural and geotechnical parameters. In evaluating R_m , we proceed as follows:

(1) Assess the viaduct top relative displacement at yielding, $\delta_{y,v}$: According to JREast, for a viaduct height of 10m (this is the average as well as the most common height), designed under normal soil conditions, this displacement is $\delta_y = 3.1 - 3.4\text{cm}$.

(2) Evaluate the median spectral acceleration at yielding, $S_{a,y}$: For three values of the natural period T of the structure and using the relationship : $S_{a,y} = \omega^2 S_{d,y}$, these median values are :

$$T = 0.3\text{sec}: S_{a,y} = 1.36g - 1.49g$$

$$T = 0.4\text{sec}: S_{a,y} = 0.76g - 0.84g$$

$$T = 0.5\text{sec}: S_{a,y} = 0.49g - 0.54g$$

(3) Take into account the effect of structural ductility μ , to obtain the median spectral acceleration $S_{a,u}$ that causes the ductility capacity of the viaduct to be exceeded. We assume that derailment due to track damage does not occur unless the viaduct structure has accumulated permanent deformation in excess of its ductility capacity. Denoting by $R(\mu) = S_{a,u}/S_{a,y}$ the factor by which the median resistance relative to first yielding is increased to produce ultimate ductility conditions, we evaluate $R(\mu)$ as :

$$R(\mu) = (c\mu - c + 1)^{1/x} \tag{5.1}$$

$$x = 1.78 + \frac{0.157}{T} \tag{5.2}$$

$$c = 1.80 - \frac{0.0422}{T} \tag{5.3}$$

The above expressions are taken from a study of elasto-plastic 1-DOF systems by Osteraas et al. (1990). The function $R(\mu)$ in equation (5.1) was also used by Takada et al.(1988 and 1989). Values of x , c , and $R(\mu)$ for μ ranging from 1 to 4, and for $T=0.3, 0.4$ and 0.5sec are listed in Table 5.1.

(4) Consider the effect of local soil conditions : All previous values of $S_{a,y}$ refer to normal soil conditions. Soil conditions were considered in the design of the Tohoku Shinkansen by scaling the design strength of the structure by a coefficient that depends on soil type; see Table 2.4. One can thus calculate the median resistance R_m of the structure depending on soil conditions, ductility level and natural period. According to JREast, the expected ductility of the structure is $\mu=4$. This level of ductility means that the structure must undergo considerable deformation and softening before failing, which leads us to increase the effective natural period from $T = 0.30 - 0.36$ sec for the structure in the elastic range to $T = 0.4 - 0.5$ sec for a heavily damaged structure. For $T=0.4\text{sec}$, which is the equivalent period we have used in base-case calculations, and for $\mu = 4$, R_m has the following values:

Rock : $R_m = 1.48g$

Normal soil : $R_m = 1.85g$

Soft soil : $R_m = 2.22g$

The above refers to the median resistance of the structure in terms of spectral acceleration at the effective period T . In order to define the log-normal distribution of R , one needs in addition the logarithmic standard deviation $\sigma_{\ln R}$. Based on results from an extensive statistical analysis for railway bridges in the Continental US (NIBS Technical Manual, 1994) and on literature on the seismic fragility of framed reinforced concrete structures, we have set that $\sigma_{\ln R} = 0.40$.

It should be noted that the train could derail also without track damage, due to excessive vibratory motion. This cause of derailment might in fact become dominant over portions

of the viaduct founded on soft soil, because of the higher structural resistance under such conditions. Our estimates of the probability of local structural damage and JREast estimates of the probability of derailment due to vibratory motion for $S_a = 1.0, 1.5, 2.0g$ are as follows :

Conditional Probabilities (given S_a)	$S_a = 1.0g$	$S_a = 1.5g$	$S_a = 2.0g$
Probability of local structural damage	0.095	0.261	0.436
Probability of derailment due to vibratory motion	0.010	0.100	0.250

For the epicentral distances of 80 km or larger in which we are interested in this study, the values of S_a that are responsible for most of the derailment events are below 1.0g and for these levels of vibration, the risk of derailment due to shaking is negligible relative to that from structural damage. Therefore, we have decided to exclude vibratory motion as a cause of derailment.

Spatial Dependence of Damage

The viaduct structure of the Tohoku Shinkansen is composed of a series of short spans (with length $SP=7m$). In order to include clustering of the damaged/non-damaged spans (as for example was observed in the recent Kobe earthquake) one may model the alternation of undamaged-damaged spans as a Markov 0-1 model. According to the model, the number of continuously damaged or continuously undamaged spans has a geometric (essentially exponential) distribution. The parameters of the model are :

$n_0(S_a)$ = mean number of continuously undamaged spans, given that the local level of spectral acceleration is S_a

$n_1(S_a)$ = mean number of continuously damaged spans, given that the local level of spectral acceleration is S_a .

An equivalent parameterization of the Markov model is in terms of the marginal probability of damage of the generic single span, $P_1(S_a)$, and the conditional probability $P_{1|1}(S_a)$, which is the probability that a span is damaged given that the previous span is damaged and given the level S_a of ground motion. Hence, the latter is defined as,

$$P_{1|1}(S_a) = P[\text{span } i+1 \text{ is damaged, given that span } i \text{ is damaged and } S_a \text{ occurred}]$$

The relation between the two parameterizations is as follows :

$$n_1(S_a) = \frac{1}{1 - P_{1|1}(S_a)} \quad (5.4)$$

$$n_0(S_a) = n_1(S_a) \frac{1 - P_1(S_a)}{P_1(S_a)} \quad (5.5)$$

Also, it is convenient to simplify the model by setting:

$$P_{1|1}(S_a) = 1 + c_1 \log_{10}[P_1(S_a)] \quad ; \quad 0 \leq c_1 \leq 0.1 \quad (\text{for } P_1(S_a) \geq 10^{-10}) \quad (5.6)$$

Equation (5.6) formulates the physical phenomenon of clustering of earthquake damage. This is why the value of the conditional probability is much higher than the value of the corresponding marginal probability. Moreover, both marginal and conditional probabilities increase with an increase of the level of the local spectral acceleration. The value of parameter c_1 in equation (5.6) governs the extent of the conditionally damaged track, given a specific value of P_1 . We have found that reasonable estimate of c_1 is $c_1=0.03$. This choice of c_1 corresponds to the values of n_1 and n_0 in Table 5.2. Such values of n_1 and n_0 are consistent with the damage caused by the Kobe earthquake to local Shinkansen viaduct : North of the exit of the tunnel through the Rokko Mountain, the viaduct suffered damage over four major sections within a length of approximately 3 km (NCEER Bulletin, 1995). Within this clustered damage region, there were approximately 30 - 35 collapsed spans. From Figure 4.6 one may estimate that the local S_a value may

have been around 1g. For normal soil conditions, this corresponds to P_1 of about 0.12 and an expected number of continuously damaged spans of about 36.

Probability of Derailment

Suppose, for the moment, that the spectral acceleration S_a at the track reaches its maximum value instantly. Assume that a train of length L travels a distance LE after the arrival of the S waves. We define the probability of derailment P_d as the probability that the train meets damaged track (see previous section for the less significant contribution from vibratory motion). Under these simplifying assumptions, the event of no-derailment occurs only if (a) the last point of the train, coming from undamaged conditions (before the strong motion arrives at the track), encounters no damage in track length LE and stops instantly, and if (b) the instant before stopping, the section of track of length L occupied by the train is entirely undamaged given that it is undamaged at the location where the train terminates; see Figure 5.1 for illustration of event of no-derailment. From the fact that the distribution of undamaged and damaged sections is exponential and using equation (5.5) we define the probabilities of the aforementioned events a, b as :

$$P_a(S_a) = e^{-[LE/(SP)]/n_o(S_a)} \quad (5.7)$$

$$P_b(S_a) = e^{-[L/(SP)]/n_o(S_a)} \quad (5.8)$$

where $SP=7m$, is the length of a single viaduct span. Based on equations (5.7) and (5.8) and assuming independence of events a and b, the probability of no-derailment given S_a is given by :

$$P_{no\ d}(S_a) = P_a(S_a) P_b(S_a) = e^{-[(LE+L)/(SP)]/n_o(S_a)} \quad (5.9)$$

Based on equation (5.9) and given that the events of derailment and no-derailment are complementary, we define the probability of derailment given S_a as follows :

$$P_d(S_a) = 1 - P_d(S_a) = 1 - e^{-[(LE+L)/(SP)]/no(S_a)} \quad (5.10)$$

According to equation (5.10), the probability of derailment, $P_d(M, \underline{x}, s)$ of a train running in operational segment s , given the occurrence of an earthquake of magnitude M at epicentral location \underline{x} , is given by :

$$P_d(M, \underline{x}, s) = 1 - E_{S_a|M, \underline{x}, s} [e^{-[(LE+L)/(SP)]/no(S_a)}] \quad (5.11)$$

Because tunnels protect trains from derailing (e.g. see the good performance of the Rokko Mountain tunnel during the Kobe earthquake), we incorporate this in the analysis by a risk reduction factor, $trf(s)$ of the probability of derailment reflecting the assumption that tunnels are considered safe havens for running trains in segment s . When the S waves arrive at operational segment s , we assume that trains can be anywhere along that segment with equal probability. Thus, the actual location of trains and tunnels within an operational segment is not important in this analysis. In this perspective, risk reduction due to the fact that a train may be in a tunnel when the S waves arrive at the track is analogous to the fraction of the segment length in tunnels. Hence, this parameter is considered through $trf(s)$ which is defined as follows :

$$trf(s) = 1 - \frac{tun(s)}{seg(s)} \quad (5.12)$$

where $tun(s)$ is the total tunnel length in segment s and $seg(s)$ is the length of segment s (see Table 2.5). According to equations (5.11) and (5.12), the probability of derailment $P_d(M, \underline{x}, s)$ is as in equation (5.13) :

$$P_d(M, \underline{x}, s) = (1 - E_{S_a|M, \underline{x}, s} [e^{-[(LE+L)/(SP)]/no(S_a)}]) (1 - \frac{tun(s)}{seg(s)}) \quad (5.13)$$

Equation (5.13) provides the general fragility model used in this study. However, the early warning system may cause the train to start braking before the intense phase of ground motion arrives at the track. One might envision cases when, at the time of arrival of the strong motion, the train has completely stopped or is decelerating, cases when braking takes place after the strong motion has reached its peak at the track, and cases when no braking takes place because the early warning system did not trigger. Moreover, the site intensity S_a is varying and the train speed is not constant. How these various conditions affect the conditional probability of derailment in a general form in equation (5.13), will be shown in Section 5.4.

5.2 General Procedure of SEWS Performance Evaluation

In order to avoid derailments, the present early warning system tends to stop trains at a high rate. In a few cases such actions may turn out to be justified (they indeed result in derailment avoidance), but in most cases they produce “false alarms” and unnecessary delays of various durations. Hence, a reasonable way to characterize the performance of the early warning system is to calculate the rate of derailments that were not prevented and the rate of delays of various magnitudes. More specifically, we define four rates :

- λ_{DE} = annual rate of earthquake-induced *derailments*. This is the expected number of trains per year that derail due to earthquakes, anywhere along the line.
- λ_{SD} = annual rate of earthquake-induced *short delays*. This is the expected number of trains per year that, after being stopped by the SEWS system, are immediately allowed to resume operation without any inspection of the tracks.

- λ_{MD} = annual rate of earthquake-induced *medium delays*. This is the expected number of trains per year that, after being stopped by the SEWS system, resume operation at low speed (30 - 50 kmh) to perform on board inspection of the tracks.
- λ_{LD} = annual rate of earthquake-induced *long delays*. This is the expected number of trains per year that, after being stopped by the SEWS system, are not allowed to resume operation until on-foot inspection of the tracks has been completed.

Whether a stopped train experiences a short, medium or long delay depends on the intensity of ground motion recorded along the track and on the threshold levels A_{insp1} and A_{insp2} for track inspection; see Chapter 3. Trains that experience short delays face the possibility of derailing after resuming operation since no track inspection is performed in that case. This is not true for trains experiencing medium and long delays, as the track inspection procedure is assumed to identify any track damage and eliminate any possibility of derailment. The added derailment risk following short delays is taken into account in the present analysis and has led to two definitions of λ_{DE} , one before and the other after the resumption of service following short delays.

Considerable simplification in the evaluation of the delay rates follows from considering each train in isolation, thus neglecting train interaction in the form of propagation of delays, train cancellations, e.t.c. In this and the following chapters we use this simplifying assumption. The effect of interactions can be estimated through corrective factors, as discussed in Appendix II.

Mathematical Formulation

The general procedure to calculate the rates λ_{DE} , λ_{SD} , λ_{MD} , λ_{LD} for a given early warning system is as follows: Let E be the event of interest (E can be DE, SD, MD, or LD, where the symbols stand for derailment, short delay, medium delay and long delay events). Then the annual rate λ_E is given by :

$$\lambda_{E|SEWS} = \int \int_{M \underline{x} s} (\sum \lambda(M, \underline{x}) E[N_s] P[E|M, \underline{x}, s, SEWS]) d\underline{x} dM \quad (5.14)$$

where $\lambda(M, \underline{x})$ is the rate density per year of earthquakes of magnitude M at epicentral location \underline{x} . This rate density is given by

$$\lambda(M, \underline{x}) = \frac{10^{a-b(M-6)}}{AREA}, \quad M < M_{max} \quad (5.15)$$

where a and b are the Gutenberg-Richter parameters for the seismic source to which \underline{x} belongs (see Chapter 4) and $AREA$ is the area of that seismic source.

$E[N_s]$ is the expected number of trains running at a random point in time in operational segment s . Values of $E[N_s]$ for the 26 operational segments of the Tohoku Shinkansen line are given in Section 2.1.

$P[E|M, \underline{x}, s, SEWS]$ is the probability of event E occurring under the given early warning system for a train running in operational segment s , an earthquake of magnitude M and epicentral location \underline{x} . This probability may in turn be written as :

$$P[E|M, \underline{x}, s, SEWS] = \sum_T P[T|M, \underline{x}, s, SEWS] P[E|M, \underline{x}, s, T] \quad (5.16)$$

where T is the generic trigger/no-trigger status of the early warning system . T has the following logical values: $T=T_c$ for automatic braking triggered by the coastal system, $T=T_{loc}$ for automatic braking triggered by the local (wayside) system, and $T=$ “No T ” in the case of no triggering. In the remainder of this chapter, we show how the probabilities in the right hand side of equation (5.16) are evaluated for different E , T and $SEWS$ systems.

5.3 Conditional Probability of Trigger, P[T|M, x, s, SEWS]

Here we consider how one can evaluate the probability of various triggering events T , for a train running in segment s , when an earthquake of magnitude M occurs at epicentral location \underline{x} . Automatic braking may be caused by first triggering the coastal or the wayside system. We denote such events by T_c and T_{loc} , respectively. “No T ” means that neither T_c nor T_{loc} occurs, hence that automatic braking is not activated.

For $P[T_c|M, \underline{x}, s, SEWS]$ we must differentiate among the different coastal systems, for which we use the symbols A (current system), B (modification of current system) and C (UrEDAS system); see Chapter 3 for details on such systems. Systems A and B trigger on horizontal acceleration a , whereas for the wayside system we consider either horizontal (perpendicular to track) acceleration a or response spectrum acceleration S_a at the natural period of the viaduct. Due to the location of the earthquake sources relative to the coastal and wayside accelerometers, it is safe to assume that, if both the coastal and the wayside systems trigger, then the coastal system is the one that triggers first (T_c occurs). A second simplifying assumption is that, if systems B and C cause trains in segment s to stop, then the event occurs due to triggering of the coastal station that is closest to the epicenter. Under these conditions, $P[T_c|M, \underline{x}, s, SEWS]$ for coastal systems A and B is obtained as follows :

For System A operating with trigger horizontal acceleration a^* ,

$$P[T_c|M, \underline{x}, s, A] = P[a_{\max}(M, \Delta(\underline{x}, i)) \geq a^*] \quad (5.17)$$

where $\Delta(\underline{x}, i)$ is the distance between \underline{x} and the coastal accelerometer i that controls operational segment s and $a_{\max}(M, \Delta(\underline{x}, i))$ is the attenuated peak ground acceleration at the i -th coastal station. The correspondence between coastal detectors and operational

track segments was shown earlier in Chapter 2. At present, JREast is operating the coastal system using policy A with $a^*=40\text{gals}$.

For System B operating with trigger horizontal accelerations $a_t(i, s, R)$,

$$P[T_c|M, \underline{x}, s, B] = P[a_{\max}(M, \Delta(\underline{x}, i)) \geq a_t(i, s, (\underline{x} \in R_i))] \quad (5.18)$$

where i is now the coastal station that is closest to the epicenter and R_i is the corresponding sector of origin. The trigger accelerations a_t for system B are calculated from equations (3.2) and (3.3) and therefore depend on a single operational parameter b^* , which corresponds to a given predicted value of S_a along the track.

System C may trigger upon the arrival of either P or S waves. For given estimates of M and Δ , the system causes trains to stop if the parameter TRIG defined in equation (3.4) is positive. Considering uncertainty on the estimates of (M, \underline{x}) , given the corresponding true values, TRIG may be modelled as a random variable with normal distribution, mean value given by equation (3.4) and variance

$$\sigma_{\text{TRIG}}^2 = (0.71\sigma_M)^2 + \left(\frac{\sigma_\Delta}{\Delta \ln 10}\right)^2 \quad (5.19)$$

The formulation of the variance of parameter TRIG in equation (5.19) is consistent with the definition of that parameter in equation (3.4). Denoting by $\text{TRIG}_{P,S}$ the values of TRIG obtained using the estimates of (M, \underline{x}) from P and S waves and assuming that $(\text{TRIG}_P | M, \underline{x})$ and $(\text{TRIG}_S | M, \underline{x})$ are independent, the conditional probability of trigger under system C is found as :

$$P[T_c|M, \underline{x}, s, C] = P[\text{TRIG}_P \geq 0] + (1 - P[\text{TRIG}_P \geq 0]) P[\text{TRIG}_S \geq 0] \quad (5.20)$$

Note that the mean values of $(TRIG_p | M, \underline{x})$ and $(TRIG_s | M, \underline{x})$ depend on a single operational parameter c^* .

The probability of triggering by the wayside system is given by the following equations:

$$P[T_{loc}|M, \underline{x}, s, SEWS] = P[a_{max}(M, \Delta(\underline{x}, s)) \geq a_{t,loc}] (1 - P[T_c|M, \underline{x}, s, SEWS]) \quad (5.21)$$

$$P[T_{loc}|M, \underline{x}, s, SEWS] = P[S_a(M, \Delta(\underline{x}, s)) \geq S_{at,loc}] (1 - P[T_c|M, \underline{x}, s, SEWS]) \quad (5.22)$$

respectively for the cases when the system operates with peak ground acceleration a_{max} or spectral acceleration S_a . Here, $\Delta(\underline{x}, s)$ is the distance between the epicentral location \underline{x} and the operational segment s , and $a_{t,loc}$ and $S_{at,loc}$ are the preset trigger levels of the wayside system.

Under the assumption of independence, the probability of no-trigger by either the coastal or the wayside system is as given by the following equation:

$$P[\text{noT}|M, \underline{x}, s, SEWS] = (1 - P[T_c|M, \underline{x}, s, SEWS]) (1 - P[T_{loc}|M, \underline{x}, s, SEWS]) \quad (5.23)$$

5.4 Conditional Probability of Derailment, $P[DE|M, \underline{x}, s, T]$

Next we consider the probabilities of derailment given (M, \underline{x}) and given different trigger/no trigger events, i.e. for $T=T_c$, T_{loc} or “no T”. These specific expressions are all based on equation (5.12), which gives the probability of derailment in general.

If emergency braking of the train is caused by the coastal system, then the probability of derailment is given by the following equation (5.24) :

$$P[DE|M, \underline{x}, s, T_c] = (1 - E S_a | M, \underline{x}, s [e^{-[(L/(SP)]/n_o(S_{a,stop})}])(e^{-[D/(SP)]/n_o'(S_a)}]) (1 - \frac{\tan(s)}{\sec(s)})$$

where D is the distance traveled from the time of strong motion arrival at the train location until complete stop.

$S_{a,stop}$ is the maximum horizontal spectral acceleration normal to the track, prior to complete stopping of the train. Because we are conditioning on coastal triggering (T_c), there is some lead time of train braking before strong motion arrives at the track. This is why potentially, $S_{a,stop}$ could be smaller than S_a .

$n_o'(S_a)$ is a single representative value of the mean number of undamaged viaduct spans, n_o , from the time when the strong motion arrives at the train location until complete train stopping. This representative value is calculated as :

$$n_o'(S_a) = \frac{D}{\int \frac{V(t)}{n_o(S_a(t))} dt} \quad (5.25)$$

where $V(t)$ is the train speed at time t since emergency braking started. The function $V(t)$ has been obtained from the braking curve in Figure 5.2, which has the following analytical expression :

$$V(t)[\text{km/sec}] = \frac{V_{\max}[\text{kmh}] - 2.85t[\text{sec}]}{3600} \quad (5.26)$$

where V_{\max} is the speed of the train when braking starts.

The formulation of $n_o'(S_a)$ in equation (5.25) considers the concurrent time-variability of the speed of the train and of the level of S_a . Through time-

integration, the denominator takes into account the distance traveled by the train from the time of strong motion arrival at the train location until complete stop (distance D). In order for $n_0'(S_a)$ to represent continuous undamaged viaduct spans, we formulate equation (5.25) with distance D in the numerator.

If emergency braking of the train is caused by the wayside system, then the probability of derailment, based again on equation (5.13), is given by the following equation:

$$P[DE|M, \underline{x}, s, T_{loc}] = (1 - E S_a | M, \underline{x}, s [e^{-[(L+D_{tot})/(SP)]/n_0'(S_a)}]) (1 - \frac{\tan(s)}{\sec(s)}) \quad (5.27)$$

where D_{tot} is the track length traveled by the train from full speed until complete stoppage. D_{tot} is obtained by an integration of equation (5.26), which gives approximately:

$$D_{tot} [km] = \frac{0.1754}{3600} V_{max}[kmh]^2 \quad (5.28)$$

Equation (5.27) sets simply length LE of equation (5.13) equal to D_{tot} . This is because in this case braking begins after the maximum level of S_a has been reached and therefore the total distance traveled is equal to D_{tot} . The track section of length D_{tot} is potentially damaged from the maximum level of local intensity S_a , since emergency braking starts after this level has been reached.

If no braking of the train occurs, then based on equation (5.13) the conditional probability of derailment is given by the following equation:

$$P[DE|M, \underline{x}, s, noT] = (1 - E S_a | M, \underline{x}, s [e^{-\{L+SEC(s)\}/(SP)]/n_0(S_a)}]) (1 - \frac{\tan(s)}{\sec(s)}) \quad (5.29)$$

where $SEC(s)$ is the length of track that a train in operational segment s covers, if it is not ordered to stop from either detection system. $SEC(s)$ is evaluated as half the distance between trains travelling in s in the same direction, and is a function of the expected number of trains in that segment. Notice that, after the train has travelled a distance $SEC(s)$, the track ahead has already been covered by other trains and, if such trains have not derailed, is safe.

Equation (5.29) sets simply length LE of equation (5.13) equal to $SEC(s)$. This is because we assume that, according to the aforementioned reasoning, that the train travels this distance under risk of derailment after the maximum level of seismic intensity S_a has been reached.

5.4.1 Conditional Probability of Derailment following Resumption of Service following a Short Delay, $P[DE|M, \underline{x}, s, SD]$

After a train has been stopped, if the first track inspection level A_{insp1} has not been exceeded, the train is allowed to resume immediately normal operation. Because, with a small probability, the track ahead may have been damaged (especially if the first inspection level is set high), it is necessary to evaluate the probability of derailment following a short delay event. For the cases when the wayside system operates with peak ground acceleration or peak spectral acceleration, this probability of derailment is given by the following equations (5.30a) and (5.30b) :

$$P[DE|M, \underline{x}, s, SD] = (1 - E_{S_a|M, \underline{x}, s} [e^{-\{L + SEC(s) - D_{tot}\} / (SP)} / n_o(S_a)]) \left(1 - \frac{t_{un}(s)}{seg(s)}\right)$$

$$P[DE|M, \underline{x}, s, SD] = (1 - \sum_{S_a \leq S_{a, insp1}} [e^{-\{L + SEC(s) - D_{tot}\} / (SP)} / n_o(S_a)]) \left(1 - \frac{t_{un}(s)}{seg(s)}\right)$$

where we have assumed that the length of potentially damaged tracks travelled after resumption of service is $(SEC(s) - D_{tot})$, i.e. is the potentially damaged length travelled if

the train was not ordered to brake (see equation 5.29) minus the distance already covered during braking (see equation 5.27).

Equation (5.30a) is obtained under the assumption that, S_a and a_{\max} are conditionally independent, given M, \underline{x}, s . More specifically, the fact that it was a short delay, i.e. a_{\max} was below the first track inspection level, does not yield any information regarding the value of S_a ; therefore we take the expected value of the exponential term as the best estimate. This is not the case for equation (5.30b) where we consider only the values of S_a below the first inspection level. The assumption of conditional independence of S_a and a_{\max} leads probably to a slight overestimation of the derailment probability in equation (5.30a) but there is no conclusive evidence of their correlation.

5.5 Conditional Probability of Various Delays, $P[E|M, \underline{x}, s, T] ; E=SD, MD, LD$

Delays can be caused by either the coastal or the wayside system; these events are denoted by T_c and T_{loc} , as indicated earlier in Section 5.3. The wayside system can operate on either a_{\max} , or S_a , but here we give formulas just for the former, for reasons of brevity. For an S_a -based operation of the wayside system, the equations are completely analogous.

Short Delays

$$P[SD|M, \underline{x}, s, T_c] = P[a_{\max}(M, \Delta(\underline{x}, s)) \leq A_{insp1}] \quad (5.31)$$

$$P[SD|M, \underline{x}, s, T_{loc}] = P[a_{t, loc} \leq a_{\max}(M, \Delta(\underline{x}, s)) \leq A_{insp1}] \quad (5.32)$$

$$P[SD|M, \underline{x}, s, noT] = 0 \quad (5.33)$$

Medium Delays

$$P[MD|M, \underline{x}, s, T_c] = P[A_{insp1} \leq a_{\max}(M, \Delta(\underline{x}, s)) \leq A_{insp2}] \quad (5.34)$$

$$P[MD|M, \underline{x}, s, T_{loc}] = P[A_{insp1} \leq a_{\max}(M, \Delta(\underline{x}, s)) \leq A_{insp2}] \quad (5.35)$$

$$P[MD|M, \underline{x}, s, noT] = 0 \quad (5.36)$$

Long Delays

$$P[LD|M, \underline{x}, s, T_c] = P[A_{insp2} \leq a_{max}(M, \Delta(\underline{x}, s))] \quad (5.37)$$

$$P[LD|M, \underline{x}, s, T_{loc}] = P[A_{insp2} \leq a_{max}(M, \Delta(\underline{x}, s))] \quad (5.38)$$

$$P[LD|M, \underline{x}, s, noT] = 0 \quad (5.39)$$

5.6 Conditional Total Probability of Derailment

Equations (5.14) and (5.16) provide the means to calculate the annual rate of derailments for any given seismic early warning system, $\lambda_{DE|SEWS}$. This is the annual rate of derailments excluding derailments during resumption of operation following short delays. Similar expressions give the total annual rate of derailments, including this additional risk of derailment. This is introduced by the following equation (5.40) :

$$P_i[DE|M, \underline{x}, s, SEWS] = P_e[DE|M, \underline{x}, s, SEWS] + P[DE|M, \underline{x}, s, SD]P[SD|M, \underline{x}, s, SEWS]$$

where $P_i[DE|M, \underline{x}, s, SEWS]$ is the conditional probability of derailment including resumption of operation following short delays, and

$P_e[DE|M, \underline{x}, s, SEWS]$ is the conditional probability of derailment before resumption of operation, as calculated from equations (5.16) through (5.24), and (5.27), (5.29).

Parameter	T = 0.3 sec	T = 0.4 sec	T = 0.5 sec
x	2.303	2.173	2.094
c	1.659	1.695	1.716
R(μ), $\mu = 1$	1.000	1.000	1.000
R(μ), $\mu = 2$	1.529	1.578	1.611
R(μ), $\mu = 3$	1.887	1.975	2.036
R(μ), $\mu = 4$	2.174	2.296	2.381

Table 5.1: Values of x, c and the ductility modification factor R(μ) for T = 0.3, 0.4, 0.5sec and $\mu = 1, 2, 3, 4$.

P ₁	P _{1/1}	n ₀	n ₁
0.00001	0.85	666660	6.67
0.00010	0.88	83325	8.33
0.00100	0.91	11100	11.11
0.01000	0.94	1650	16.67
0.10000	0.97	300	33.33

Table 5.2: Expected number of continuously damaged (n₁) and undamaged (n₀) viaduct spans for given values of the probability of damage of a single viaduct span P₁ and c₁=0.03.

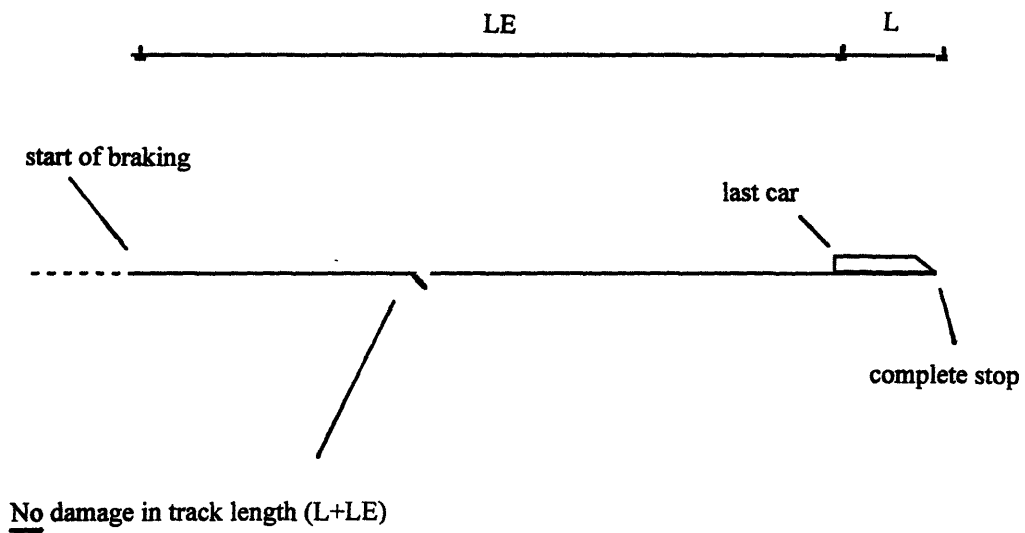


Figure 5.1: Illustration of a no-derailment event.

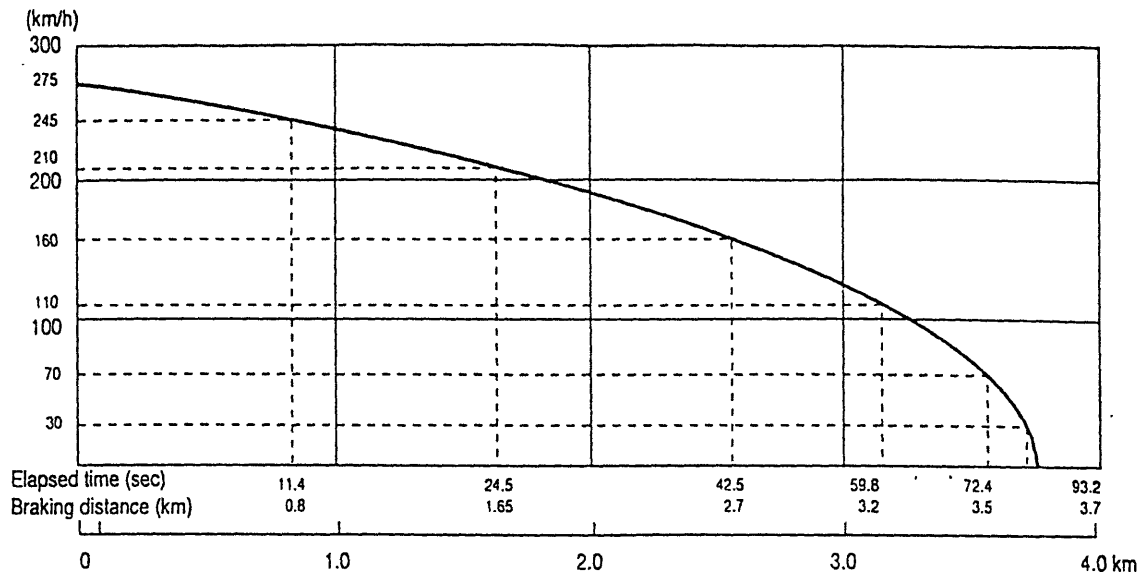


Figure 5.2: Shinkansen braking curve (JREast personal communication).

Chapter 6

Risk Results

In this chapter we obtain numerical results, primarily in the form of the annual rate of derailments and the rates of various delay events for different SEWS systems. These results are presented in section 6.1 and they are for different coastal systems, while the wayside system is operating as at present. To aid interpretation, the total rates are decomposed by earthquake magnitude M , track location s , seismic source, and epicentral distance. The sensitivity of the total rates to various physical and modeling parameters is displayed at the end of this section. A scenario-based approach to the risk is presented in section 6.2. In this case, the results are in terms of the expected number of various events (derailments and delays) along the track, given that an earthquake of given magnitude occurs at a specific location.

The effects of different modes of operation of the wayside system are described in Chapter 7, where the issue of the optimization of the SEWS is addressed.

6.1 Annual Risk

Annual Rates of Derailments and Delays and their Decomposition

This section shows in some detail the performance characteristics of different SEWS systems while the wayside system is operated as at present, with parameters $(a_{t,loc}, A_{insp1}, A_{insp2}) = (40, 80, 120 \text{ gals})$. The trigger parameters of the coastal system, \mathbf{a}^* (System A), \mathbf{b}^* (System B), and \mathbf{c}^* (System C) are varied. For derailments (rate λ_{DE}), we present results including or excluding the contribution from resumption of service after short

delays. The rates are plotted in Figure 6.1a and the corresponding parameters a^* , b^* and c^* are shown in Figure 6.1b. Notice that the rates λ_{MD} and λ_{LD} do not depend on either the type of coastal system or its operational parameters (they depend only on the operation of the wayside system). These rates are therefore just listed. The two sets of plots in Figure 6.2a correspond to including (upper plots) or excluding (lower plots) derailments following short delays. For the current coastal system (System A, with $a^* = 40$ gals), the rates are :

- $\lambda_{DE} = 0.017 / 0.033$ trains/year (for exclusion/inclusion of derailments following short delays)
- $\lambda_{SD} = 82.6$ trains/year
- $\lambda_{MD} = 3.38$ trains/year
- $\lambda_{LD} = 1.20$ trains/year

The performance of the system during the past eleven years shows an annual average of 2.8 stopped and 72.4 delayed trains; see Chapter 2. These “delayed trains” correspond to the sum of short and medium delays when trains resume regular or low-speed operation respectively. “Stopped trains” correspond to long delays when trains stop to allow for on-foot track inspection. Therefore, we conclude that our theoretical results for the various delays are consistent with the historical record. The annual rate of derailments cannot be verified historically because such events are rare. Other observations on the results of Figure 6.1 are as follows :

Effect of Coastal System

Coastal system A (the present system) is consistently outperformed by systems B and C. This is due to the fact that, allowing any coastal station to stop trains (as systems B and C do) increases the lead time relative to the arrival of the strong phase of ground motion at the track. The lead time of system A is short and the reduction in the rate of derailments relative to operating only the wayside system (leftmost points in the plots) is small. At the

same time, the low threshold value ($a^* = 40\text{gals}$) produces many short delays. In general, System C (UrEDAS) performs best, because of the added lead time when triggering occurs upon the arrival of P waves. This is actually true for values of the threshold parameter $c^* \leq 3.1$. For less conservative values of c^* (when the coastal system is not expected to issue frequent warnings), the large uncertainty in the estimation of earthquake magnitude and location makes the UrEDAS system somewhat less efficient than System B.

Quantitatively, the differences noted above are hardly significant, especially if the systems are operated with higher trigger levels. At most, system B reduces the derailment risk by 50% compared to system A and system C may potentially add a further 10% reduction to this risk. These are, however, upper limits and correspond to very conservative operation of the systems (rightmost points in the plots). More realistic settings of the trigger parameters make the benefits smaller. Even smaller percentile differences are found if the risk of derailment after resumption of service following short delays is included (top plots in Figure 6.1a). This is because the added risk is independent of the type of coastal system.

The small gains from changing the type of coastal system are attributed to the fact that, in spite of the lead time from operation of the coastal system (up to approximately 30 sec for the UrEDAS), the braking trains cover a large part of their braking distance course after the arrival of the strong motion phase at the track (for a speed of 245kmh, the total braking time is approximately 85 sec).

Effect of Wayside Policy

The wayside system can potentially cause the trains to brake after the arrival of the strong phase of ground motion at the track. Even such action, without lead time, is effective as it causes trains to cover approximately 3 km while braking as opposed to half the distance between trains running in the same direction when trains are not stopped. For example,

the distance between consecutive trains traveling in the same direction between Tokyo and Sendai is approximately 28 km. Thus, the trigger level of the wayside system, if set conservatively, as it now is, largely controls the risk of derailment. The coastal policy may reduce that risk, but not by a large amount.

The inspection levels at the track control completely the medium and long delays, while the short delays are controlled by both the coastal and wayside systems.

The added risk due to the resumption of operation after short delays is a function of the wayside system. Figure 6.1a shows that this added risk may be very significant. The reason is that, given M and \underline{x} , the quantities a_{\max} and S_a at the track are treated as conditionally independent. Therefore, low recorded values of a_{\max} that produce short delays do not necessarily imply that S_a (which is better related to damage) is also small. It should be noted that, although conservative, the assumption of conditional independence of a_{\max} and S_a is consistent with observations from strong ground motions. Later in this study, we shall present results for the case in which the wayside system operates in terms of S_a . In that case, the resumption of operation after short delays does not contribute significant risk.

Next we analyze how the annual rates λ_E for various events E (derailments and various delays) are contributed by earthquakes of different magnitudes and with different distances from the track, how they are contributed by different earthquake sources, and how they are distributed along the track. Illustrated in Figure 6.2 is the risk decomposition for the current operation of the SEWS, i.e. $(\mathbf{a}^*, a_{t,loc}, A_{insp1}, A_{insp2}) = (40, 40, 80, 120 \text{ gals})$ excluding the added risk of derailments following short delays. More specifically, we present the annual rates of each event type E decomposed according to earthquake magnitude, track segment, seismic source and epicentral distance. For more effective comparison, the rates are presented normalized.

Decomposition by earthquake magnitude

Derailments are mostly caused by earthquakes magnitudes from 7 to 8.5, whereas, long, medium and short delays are produced mainly by earthquakes of magnitudes 7 ± 0.5 , 6.5 ± 0.5 and 5.5 ± 0.5 , respectively. There is no contribution to the risk from earthquakes of magnitude $M \geq 8.5$, because it is believed that there are no seismic sources that can produce such large magnitude earthquakes in the area of interest; see Table 4.1. Furthermore, there are “jumps” in the contribution to the risk from earthquakes immediately smaller and larger of 7.5 and 8, because these values correspond to our estimates of maximum magnitude for several seismic sources. Therefore, as the magnitude of the earthquake gets larger, there are fewer seismic sources that can potentially produce earthquakes of that magnitude.

Distribution along the track

The area of operational segments 12-16 is the one where most derailments and delays are expected to occur. Segments 18-21 are those where derailments and delays have the lowest rate of occurrence.

The significant variability of the risk along the line is due to the following site-specific parameters : (a) proximity to seismic sources, (b) traffic load, (c) length of tunnels, and (d) local soil conditions. The effects of these parameters are studied via comparative analysis of the following cases :

- case 1 : Same train frequency along the entire line ($E[N_s] = 0.295$)
Soil Type I everywhere.
No tunnels.
- case 2 : Same as case 1, but actual train frequency considered.
- case 3 : Same as case 2, but actual soil types along the Tohoku line considered.
- case 4 : Same as case 3, but tunnels considered (most realistic or base-case)

Figure 6.3 presents the distribution along the track of the rates of all events for the four cases listed above. Case 1 shows that seismicity alone causes a relatively uniform distribution of the risk along the track (at the most, the local rate of derailments varies by a factor of 3). The density of train traffic induces variations by up to a factor of 2.5. Inclusion of soil type alters significantly the spatial distribution of risk. Specifically, soil type III reduces the rate of derailments by a factor of almost 10 while it increases insignificantly the rates of all delays, whereas soil type II increases the risk of both derailments and delays by a factor of at the most 4. These large differences are due to local amplification effects; see Figures 4.4 and 4.5. The amplification by soil type II is consistent at all magnitudes for both a_{\max} and S_a . Soil type III causes small amplifications of a_{\max} at the small magnitudes that generally cause delays. On the other hand, soil type III does not amplify the value of S_a at the large magnitudes that cause derailments. In addition, the viaduct has been constructed expecting an amplification of motion for soil type III (soil coefficient 1.2; see Table 2.4). Therefore, the risk of derailment is reduced significantly in operational segments where there is predominantly soil type III. Finally, the tunnels along the line reduce locally the derailment risk by a factor up to 3, but have no effect on the delay rates.

Decomposition by seismic source

Seismic sources 6 and 8 contribute by far the most to the annual rate of all events. This is a combined effect of their relative proximity to the track and their high seismic activity; see Figure 4.2 and Table 4.1. By contrast, seismic sources 1 and 15 contribute very little to the risk mainly because of their large distance from the track, sources 7 and 11 contribute little because of their low seismicity and seismic source 5 contributes insignificantly because of both low seismic activity and large distance.

Decomposition by epicentral distance

Derailments and long delays are mostly caused by earthquakes that originate about 130km from the track. Medium and short delays are predominantly produced by earthquakes with epicentral distances around 150 and 160 km, respectively. In general,

the range of crucial epicentral distances for all rates is from 100 to 170 km. Shorter distances are not significant because there are no seismically active offshore sources that are closer to the track. Larger distances are unimportant due to attenuation.

Sensitivity of Annual Risk

Uncertainty on the value of model parameters was discussed in detail in previous chapters. In this section, we present the potential effect of the estimation errors on the results in Figures 6.1 and 6.2. Sensitivity analyses are made relative to: (a) attenuation parameters, (b) the seismic fragility of the viaduct structure, (c) the soil classification along the Tohoku line, (d) the speed of Shinkansen, (e) seismicity parameters and (f) the (M, \mathbf{x}) estimation accuracy of the UrEDAS system.

This study shows that annual risk is very sensitive to parameters (a), (b) and (c) listed above. In more detail, we have:

Sensitivity to attenuation coefficients

The attenuation model used in the previous analysis is a modification of the model of Kawashima et al.(1984) to account for an apparent overestimation of the motion at small magnitudes; see Figure 4.3a. Yet, the records from the recent Kobe earthquake suggest that the model may underestimate grossly the strong motion at relatively high magnitudes; see Figure 4.6. Therefore, in a sensitivity analysis we consider a calibration of the median attenuated value of both a_{\max} and S_a , to the values recorded during the Kobe earthquake: we maintain the form of the previous models (see equation 4.3) but the parameters a and b of the equation are estimated so as to: (a) reproduce the median values of the modified-Kawashima model for $M = 5$, and (b) increase by a factor of 1.8 the values for $M = 7.2$ (the magnitude of the Kobe earthquake).

Figure 6.4 presents the sensitivity of the annual risk to the attenuation coefficients. Three sets of coefficients are considered; coefficients corresponding to (1) the “modified Kawashima” model (Table 4.3), (2) the original Kawashima model (Table 4.3) and, (3)

the “modified Kawashima” model adjusted to account for accelerations recorded during the Kobe earthquake, as discussed above. Figure 6.4a gives the rates excluding the added risk of derailments following resumption of service after short delays, whereas in Figure 6.4b this risk is included. Figure 6.5 shows the sensitivity of the annual risk decomposition by earthquake magnitude to the attenuation coefficients.

The value of the attenuation coefficients affects significantly the annual rate of derailments (by a factor of 2 to 8) and long delays (by a factor of 1.5 to 3.6). However, the sensitivity for medium and short delays is much lower (1.9 and 1.3 respectively). The original Kawashima model estimates larger median accelerations at small magnitudes ($M=5 - 6$) than any of the other two models. Therefore, it produces a higher annual rate of short delays. The “adjusted to Kobe” model estimates larger median accelerations at high magnitudes ($M=7 - 8$) than any of the other two models. Thus, it estimates that the annual rates of derailments and long delays are higher than what assessed by the other two models. For medium delays, both the original Kawashima and the “adjusted to Kobe” model produce values higher than the modified Kawashima model, because of the higher median accelerations predicted for intermediate magnitudes ($M=6 - 7$).

The added risk of derailments following the resumption of service after short delays does not alter significantly the sensitivity to the attenuation coefficients. In general, sensitivity analysis results are similar for cases that exclude or include this added risk. Therefore, for the rest of this sensitivity analysis we present and comment only on results when this added risk is excluded. Corresponding results including this risk are presented in Appendix I.

Sensitivity to the seismic fragility of the viaduct structure

In this case, uncertainty lies in the values of the following parameters : (a) the relative displacement of the top of the viaduct at yielding, δ_y , which might be smaller than originally estimated (values 15 and 30% smaller are considered), (b) the ductility ratio at

failure, μ , which again may be smaller than the base-case value of 4 (sensitivity values of 2 and 3 are considered), (c) the logarithmic standard deviation of the seismic resistance of the structure, $\sigma_{\ln R}$, which is varied by ± 0.1 relative to the base-case of 0.4 and, (d) the parameter c_1 in equation (5.6), which controls the clustering of damage along the line; for c_1 , we consider a 2fold decrease and increase relative to the base-case value of 0.03. A 2fold increase in the value of c_1 corresponds to a 2fold decrease in the length of the continuously damaged track sections.

Figures 6.6 and 6.7 show the sensitivity of the annual risk to the values of the relative displacement at yielding δ_y , the ductility μ , the value of $\sigma_{\ln R}$ and finally the value of c_1 . The rates of various delays are not influenced by the uncertainty in the fragility of the viaduct structure of the Tohoku line. Therefore, Figure 6.8 gives only the sensitivity of the decomposition by earthquake magnitude of the rate of derailments.

The derailment risk is mostly influenced by the values of δ_y and $\sigma_{\ln R}$, as the uncertainty in their value produces risks different by factors up to 4 and 3.5. The sensitivity to the values of μ and c_1 may lead to values of risk different by factors up to 2.8 and 1.5 respectively. The sensitivity of the annual risk to the value of δ_y and μ is attributed to the uncertainty in the values of these fragility parameters which influences accordingly the value of the median resistance of the structure. In addition, the difference in the values of the considered fragility parameters causes mainly a uniform scaling of the contribution of all earthquake magnitudes. The caused change in the relative contribution of different earthquake magnitudes is less important.

Sensitivity to soil classification along the Tohoku line

Tables 2.3, 2.4 introduce the soil classification along the line code used for the construction of the Tohoku Shinkansen continuous viaduct structure. Table 2.5 gives the approximate soil classification per operational segment used in this analysis. In Chapter 4, the soil types of the proposed attenuation model are presented; see Table 4.2. Based on

information in these tables, there are three possible sources of uncertainty in the soil classification along the line: (a) The three soil types of the JNR code (Table 2.4) do not coincide exactly with the three soil types of the proposed attenuation model (Table 4.2), (b) the seismic design recommendations of the JNR code (Table 2.4) imply a specific expected influence of soil type on the acceleration, somewhat different than what the attenuation model estimates (see Chapter 4), and least importantly (c) the soil classification along the line, as provided from a personal communication with JREast (Table 2.3), is rather crude and engineering judgment was necessary for the implementation of this classification in the risk analysis as presented in Table 2.5.

In order to assess the sensitivity of the annual rates to the soil classification along the line, we performed the following analyses that essentially bracket the possible effect : given that the viaduct is constructed according to the soil classification and design recommendations of the JNR seismic code, we assumed that the whole track is soil type I, II or III according to the attenuation model; this effect is presented in Figure 6.9a. The performance of the SEWS under these uniform soil conditions is compared to the performance of the system presented in Figure 6.1, that corresponds to the soil classification presented in Table 2.5, which is predominantly soil type II. To enhance our understanding of the sensitivity of the annual rates to the soil classification, we present Figure 6.10 that illustrates the decomposition by earthquake magnitude of all rates for the studied uniform soil classifications. Important for gaining insight in these effects of soil type are Figures 4.4 and 4.5, where the median attenuated values of a_{\max} and S_a for all soil types and earthquake magnitudes are presented.

Of all measures of performance of the early warning system, the annual rate of derailments is the most sensitive to the soil classification along the line (up to a factor of 7). The various delays are less sensitive: long, medium and short delays have factors of difference as large as 3, 2.8 and 2.5 respectively. All these large sensitivities correspond to the case that, the soil classification is uniformly type I and lead to relatively lower values for both rates of derailments and delays. This because the median values of both

a_{\max} and S_a for soil type I are consistently lower than those for soil type II, i.e. the predominant soil type along the line.

For soil type II the factors of influence for derailments, short, medium and long delays are 1.75, 1.14, 1.09 and 1.01 respectively, i.e. smaller than those for soil type I. The influence is smaller because the proposed soil classification is predominantly soil type II. Moreover, for this soil type derailments, long, and medium delays are relatively larger than the values for the proposed soil classification, while the effect is reversed for short delays. This is due to the fact that the latter are mainly caused by small magnitudes ($M < 6$), as opposed to the rest that are primarily produced by larger magnitudes ($M > 6$) and the influence of soil type on the median values of small magnitudes is different than that for large earthquake magnitudes.

Finally, for soil type III the factors of influence for derailments, short, medium and long delays are 1.3, 1.18, 1.20 and 1.1. In this case, the annual rate of long delays is estimated larger than for the proposed soil classification. This is due to the relatively higher attenuated values of a_{\max} for large magnitudes and soil type III as opposed to those for soil type II. This is not the case for S_a and large earthquake magnitudes that controls the rate of derailments, nor for a_{\max} and smaller magnitudes that control the other types of delays. For these cases, soil type II is estimated to amplify the motion more than soil type III.

In conclusion, sensitivity to the attenuation coefficients, the seismic fragility of the viaduct structure and the soil classification along the Tohoku line is very significant (factors of influence up to 8, 4 and 7). Therefore, accurate estimations of the attenuation law, the seismic fragility and the soil classification are considered much needed endeavors, which are however beyond the scope of the present study.

In contrast, it is found that annual risk is relatively insensitive to the Shinkansen operating speed, to the seismicity parameters and the (M, x) estimation accuracy of the UrEDAS system. More specifically:

Sensitivity to Shinkansen operating speed

In order to investigate the effect of the train operating speed on the performance of the SEWS, we performed an analysis for the following cases : (a) $V_o = 210$ kmh, to study how much benefit in the risk would be introduced by a reduction of the current operating speed ($V_o=245$ kmh), and (b) $V_o = 300$ kmh, to study the effect on the seismic risk along the line if JREast decided to increase the operational speed of the Shinkansen for more efficient transportation of its passengers. Figure 6.9b displays the sensitivity of the annual rates of derailment and various delays to the value of the operating speed. This analysis assumes that a train derails if it meets damaged track, independent of the speed of the train at the time when it reaches the damaged section of the track. In this perspective :

The operating speed has no effect on the delays produced by the operation of the early warning system. This is because the system orders emergency braking based on the recorded ground acceleration, that is not related to the speed of the Shinkansen. For the rate of derailments, an increase of the operating speed to 300kmh would cause an increase of 35%, whereas a decrease of the speed to 210kmh would produce a reduction of the risk of approximately 25%. This is because a train running at 300kmh has a braking distance of 4.4 km (see equation 5.28), as opposed to the braking distances of 2.9 km for $V_o=245$ kmh and 2.1 km for $V_o=210$ kmh. It is obvious that, the larger the braking distance of the train, the larger the probability that it travels over a damaged portion of the track and thus the larger the annual rate of derailments.

Sensitivity to seismicity parameters

The main uncertain parameters of the earthquake recurrence model are maximum earthquake magnitudes M_{max} and the b-values of the Gutenberg-Richter relation. To evaluate sensitivity to these parameters, analyses were performed assuming that, relative

to the base-case values : (a) the maximum magnitude M_{\max} of each seismic source is 0.5 (JMA units) higher/lower and (b) $b = 0.9$ or 1.1 for all seismic sources (as opposed to an overall average of about 1.0).

Figure 6.11a shows sensitivity of the annual rates to the value of M_{\max} . The rate of derailments is the one most sensitive to M_{\max} , with increase/decrease factor of about 2. This is because derailments are induced by large accelerations that originate from large magnitude earthquakes. Short, medium and long delays are relatively insensitive to M_{\max} .

Sensitivity of the annual rates to the b -parameter is shown in Figure 6.11b. Notice that, according to equation (4.1), the earthquake rate density is independent of b for $M = 6$. Therefore, an increase of b corresponds to both an increase in the rate of earthquakes with $M < 6$ and a decrease in the rate of earthquakes with $M > 6$. Because of this “pivoting effect”, changing b affects significantly the rate of very large earthquakes and therefore the rate of derailments.

Sensitivity to (M , x) estimation accuracy of the UrEDAS system

As presented in Chapter 4, the estimation accuracy of the UrEDAS system is an issue of considerable uncertainty. In order to study the sensitivity of the annual risk to this parameter, we consider the following cases for the P waves estimation (the S waves estimation is not considered as this system provides relative benefit if it adds lead time with respect to the arrival of the S waves) :

- $\sigma_{M,P} = \sigma_{M,S} = 0.5$ (JMA units), assuming an improvement of the P waves estimation of the earthquake magnitude to the levels of the current estimation accuracy of the S wave.
- $\sigma_{\Delta,P} = 25\% \Delta$ or $100\% \Delta$, assuming that the P waves epicentral distance estimation is 3 times more or 1.3 times less accurate than the base-case value.

The sensitivity of the annual rates to the accuracy of the UrEDAS system is presented in Figure 6.12a and 6.12b. The former plot gives the effect of the magnitude estimation accuracy and the latter the effect of the epicentral distance estimation. More specifically,

The annual risk is sensitive to the UrEDAS estimation accuracy only for relatively non conservative operation of the system, i.e. for $c^* \geq 2.2$; see Figure 6.1. For smaller values of the coastal parameter, the uncertainty on the prediction of (M, x) does not affect the system, as the latter is set to trigger often enough that the estimation accuracy of the system does not reduce the probability of triggering. Moreover, the sensitivity to the magnitude estimation accuracy is relatively more important than that to the epicentral location estimation. This is because the UrEDAS system triggers based on the estimated values of M and $\log_{10}\Delta$ and thus the importance of the epicentral distance is smaller given that it is $\log_{10}\Delta$ and not Δ itself that causes the potential emergency braking.

The rate of medium and long delays are not influenced by the UrEDAS estimation accuracy, because these measures of performance of the early warning system are controlled completely by the wayside system; see initial discussion of section 6.1. Moreover, derailments are practically insensitive to the estimation accuracy of the UrEDAS, whereas for the rate of short delays an improvement in the M estimation upon the arrival of the P waves, would reduce the short delays by 65%. The considered large range of the accuracy of the epicentral distance estimation causes only a 25% decrease/increase in the rate of short delays.

In conclusion, sensitivity to the Shinkansen operating speed, the seismicity parameters and the (M, x) estimation accuracy of the UrEDAS system is relatively unimportant (factors of influence up to 1.35, 2.0 and 1.65 respectively).

6.2 Scenario-Based Risk Analysis

Probability of event occurring at a specific track segment s , given M , \underline{x} and SEWS

Figure 6.13 presents the conditional probabilities $P[E|M, \underline{x}, s, A]$ for events $E = DE$ (derailment), SD (short delay), MD (medium delay) or LD (long delay). The location of the earthquake \underline{x} , is fixed at ($E142^{\circ}15'$, $N40^{\circ}12'$), that is off shore North-East of Morioka. Actually, the epicenter is located 571 km from Tokyo and just 135 km from Morioka. Moreover earthquake magnitude M is varied between 5 and 9 (JMA units), and the segment number from $s = 1$ (Tokyo) to $s = 26$ (Morioka). The case portrayed corresponds to the current SEWS, the setting of which can be summarized by : $(\mathbf{a}^*, a_{t,loc}, A_{insp1}, A_{insp2}) = (40, 40, 80, 120 \text{ gals})$, where \mathbf{a}^* , $a_{t,loc}$ are the coastal and wayside trigger parameters and A_{insp1} , A_{insp2} are the track inspection levels. The probability of derailment does not include derailment events after resumption of service following short delays. The following features of Figure 6.13 should be noted :

As earthquake magnitude increases, the probabilities of derailment and long delay increase throughout the line. This is because such events require high ground accelerations. On the other hand, the probabilities of short and medium delays, which occur at lower accelerations, the effect of magnitude is not monotonic.

Although all probabilities show general trends along the line, there are sharp peaks and valleys in these curves due mainly to (a) local soil conditions, (b) the fraction of segment length in tunnels and, for the case of derailments and short delays, (c) the assignment of track segments to coastal stations. For example, the decrease in the probability of derailment in operational segment 11 is mainly due to the fact that in this segment the soil is relatively soft (soil type III) as opposed to the neighboring segments where the soil is normal (soil type II). This sensitivity to local soil conditions can be seen in Figure 4.5 which shows that, at large magnitudes, the median S_a for soil type II is higher than that for soil type III.

These qualitative features of $P[E|M, x, s, \text{SEWS}]$ are common to all SEWS systems and trigger level settings. Similar plots for all alternative coastal systems and equivalent, in terms of risk, trigger levels are included in the Appendix I for further reference.

Expected number of events occurring throughout the line, given M , x and SEWS.

In this section, we estimate the expected number of derailments, short, medium and long delays that would occur throughout the line for a specific setting of the SEWS, given an earthquake of magnitude M that takes place at an epicentral location x . This is performed by taking into account the conditional probabilities presented in the previous section, as well as the expected number of trains per track segment (Table 2.6). The results of this study are presented in the following format : Each point of a map of the region yields the number of derailments and different kinds of delays caused along the line, if an earthquake of magnitude M occurred at that given point. For ease of presentation, these results are presented with the use of contours. Hence, Figures 6.14 through 6.17 present the expected number of derailments, short, medium and long delays for the current SEWS system, i.e. $(a^*, a_{t,loc}, A_{insp1}, A_{insp2}) = (40, 40, 80, 120\text{gals})$, and for earthquakes of magnitudes M 5 up to 8 respectively. There is a certain limitation to the accuracy of these figures, because the area of seismic interest is offshore and thus we have ignored the inland seismicity. This assumption results in no illustrated effects from potential inland earthquakes, as well as in a series of “artificial” contours between the zero inland activity and the maximum values estimated in the geographic areas closest to the line.

This approach may be misleading in the attempt to identify the most potentially dangerous seismic areas, as it does not take into account the historical seismicity of each area. Thus, the location of the most or least potentially dangerous seismic areas could change if the latter parameter is taken into account. Nevertheless, it provides a more tangible estimate of the risk than what is conveyed by the annual rates. At any generic moment of time, there are approximately 14 trains all along the line. This number is the maximum potential value of the sum of short, medium and long delays at any epicentral location and for any earthquake magnitude. Hence,

Regarding the expected number of derailments, the relatively most dangerous area for the Tohoku line is south of Tokyo (around E140°, N35°). Somewhat smaller risk causes the area south-east of Sendai (around E141°30', N37°). The expected number of derailments decreases consistently with epicentral distance from the track.

For magnitudes between 5 and 7, the most short delays are produced by an area northeast of Sendai (around E141°30', N38°). In this magnitude range, the expected number of short delays decreases consistently with epicentral distance from the line. This trends reverses for larger magnitudes ($M = 8$), because short delays occur for low peak ground accelerations which for an earthquake of magnitude 8 can occur only for relatively larger epicentral distances.

Similarly, the expected number of medium delays decreases with epicentral distance for earthquakes of magnitudes between 5 and 7, while this tendency is inverted for earthquakes of magnitude 8 for the reason mentioned above. For earthquakes in the range between 5 and 7, most medium delays are caused by earthquakes in the areas described as the most dangerous in terms of short delays. In contrast, for an earthquake of magnitude 8, it is the area around (E142°, N36°), almost 160km from the track that may cause a maximum of 3 medium delays.

The area that produces the most long delays is the area south-east of Sendai, while the area south of Tokyo produces fewer. In this case, the expected number of long delays decreases consistently with epicentral distance from the line.

The qualitative features of the expected number of events, conditional to M and x , are common to all SEWS systems and trigger level settings.

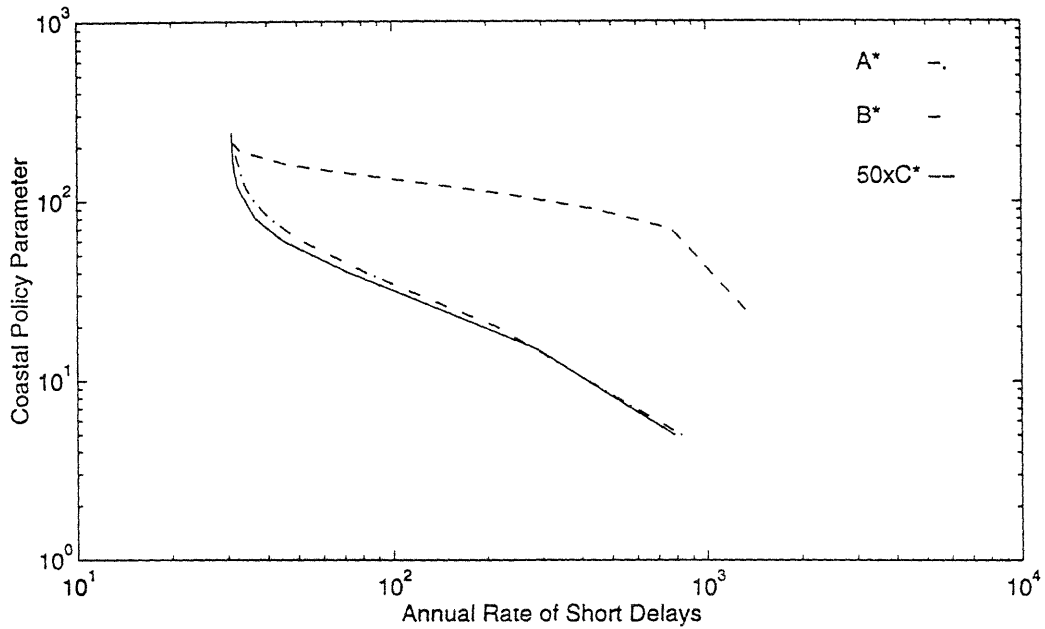
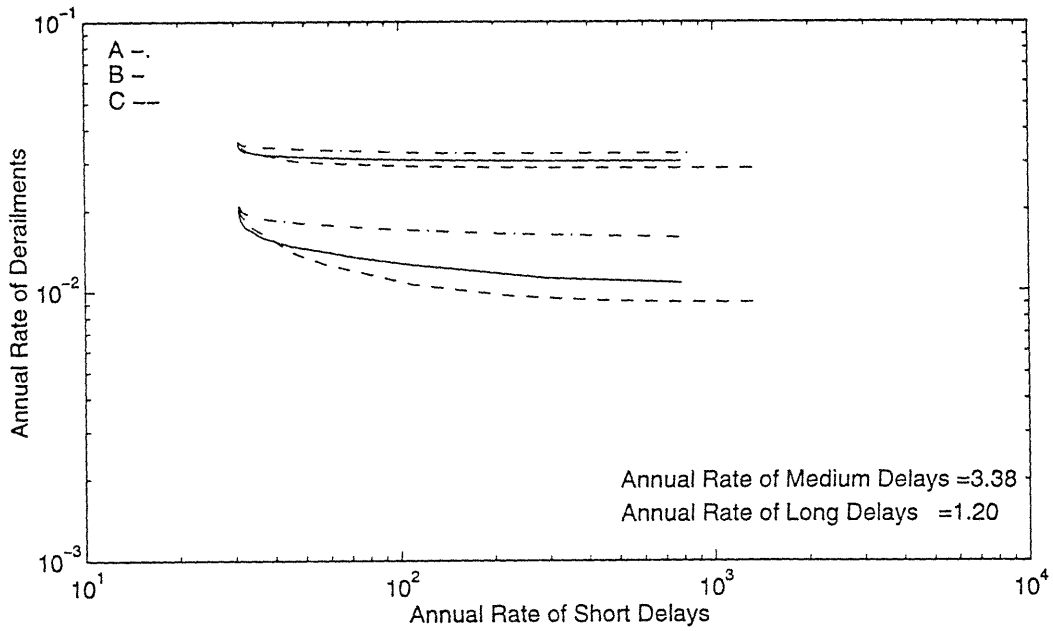


Figure 6.1: (a) Annual rates of derailments and various delays, excluding and including derailment risk due to resumption of operation following short delays, for coastal systems A, B and C and $(a_{t,loc}, A_{insp1}, A_{insp2})=(40, 80, 120\text{gals})$
(b) Coastal trigger parameter versus annual rate of short delays, for coastal systems A, B and C and $(a_{t,loc}, A_{insp1}, A_{insp2})=(40, 80, 120\text{gals})$.

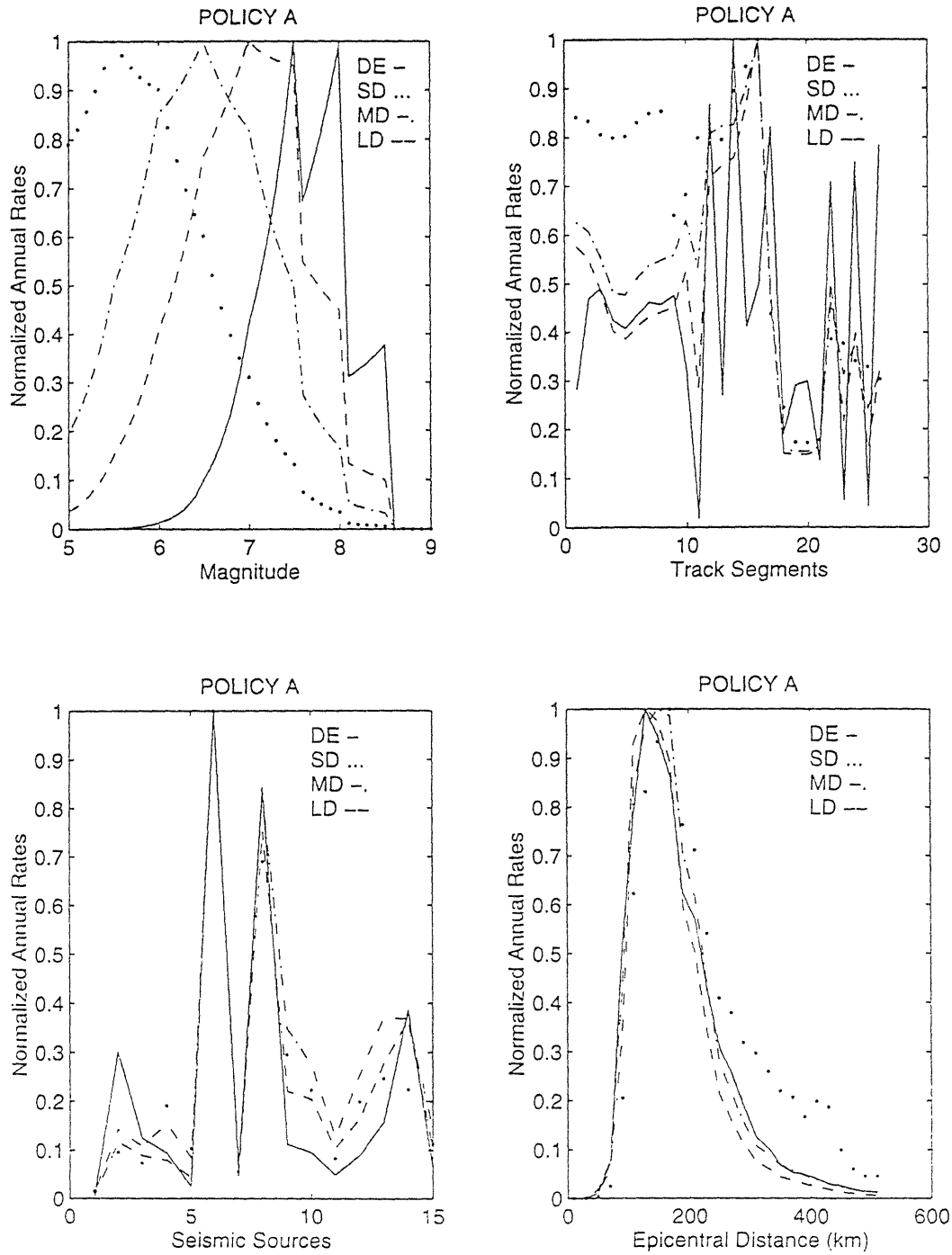


Figure 6.2: Normalized risk decomposition for $(a^*, a_{t,loc}, A_{insp1}, A_{insp2}) = (40, 40, 80, 120\text{gals})$: (a) by earthquake magnitude, (b) along the track, (c) by seismic source, and (d) by epicentral distance.

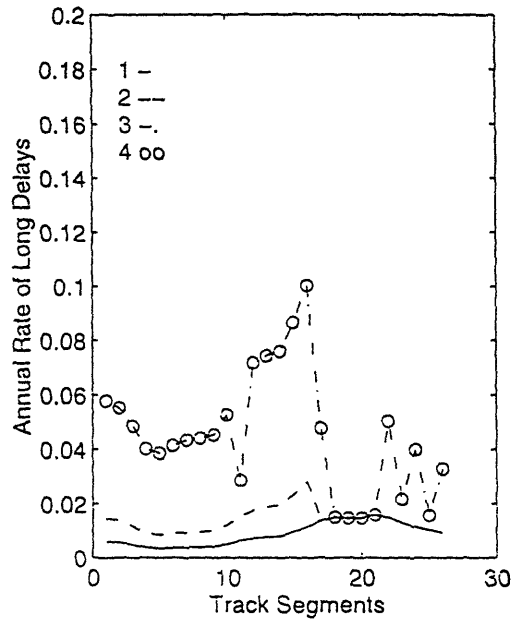
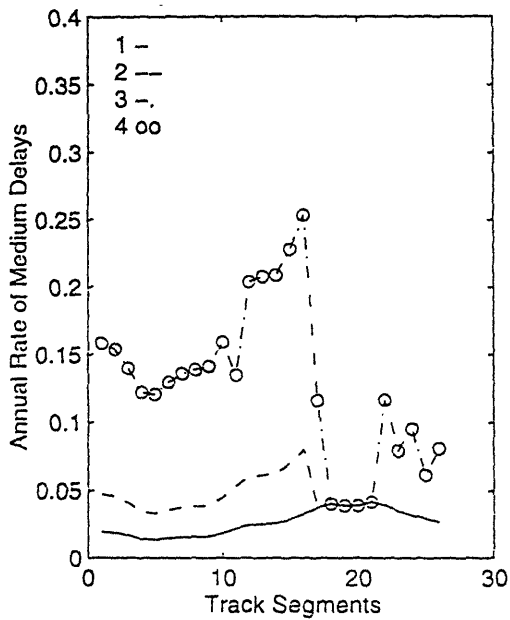
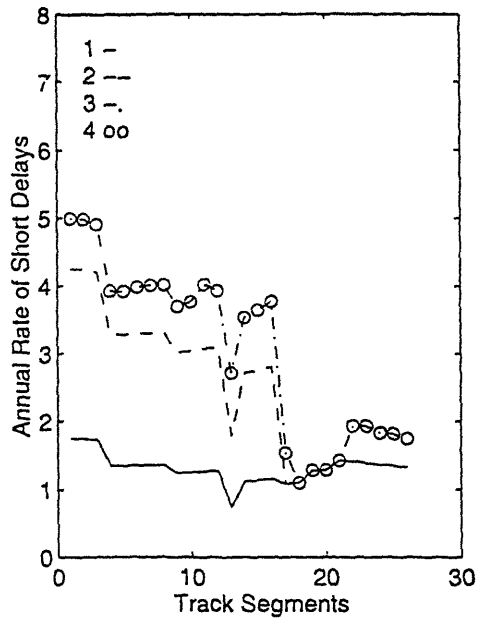
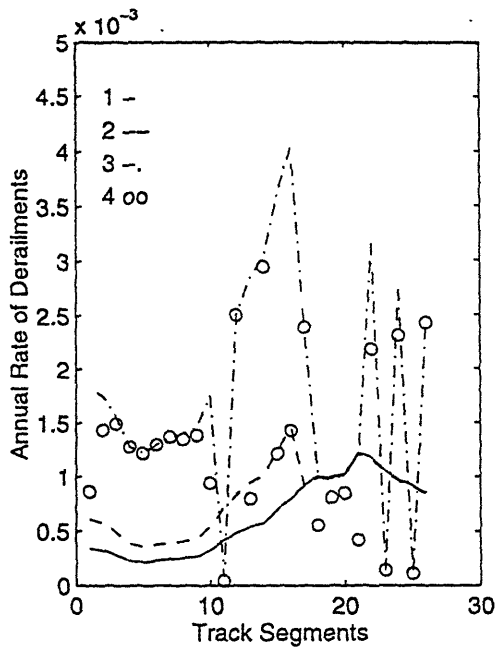


Figure 6.3: Distribution of risk along the track for $(a^*, a_{t,loc}, A_{insp1}, A_{insp2}) = (40, 40, 80, 120 \text{gals})$ for : case 1) same train frequency along entire line, soil type I all along line, no tunnels, case 2) same as case 1, but actual train frequency considered, case 3) same as case 2, but actual soil types considered, case 4) same as case 3 but tunnels considered (most realistic or base-case).

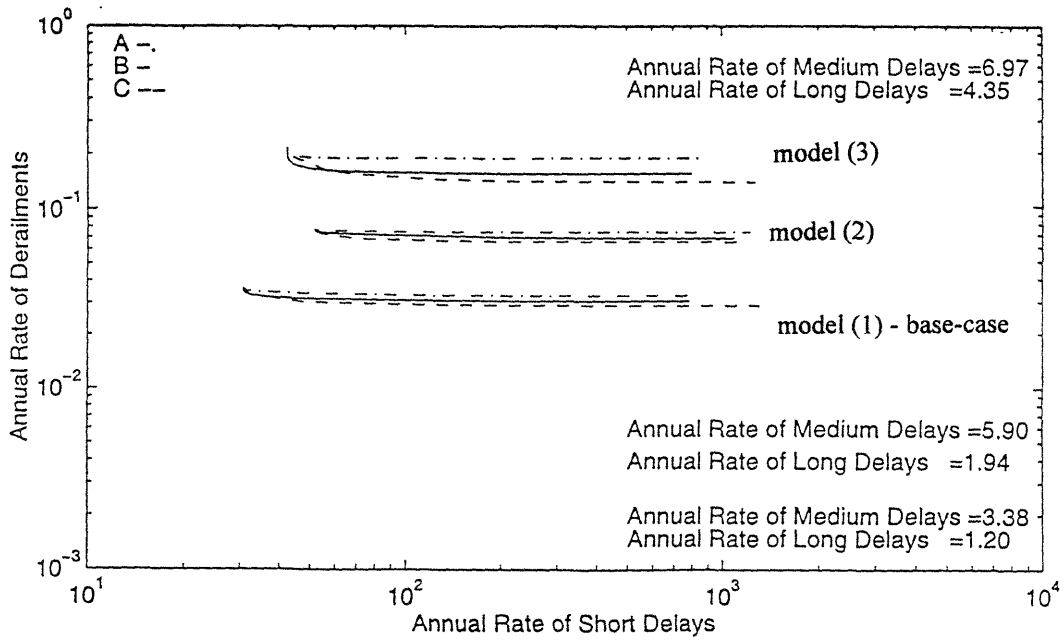
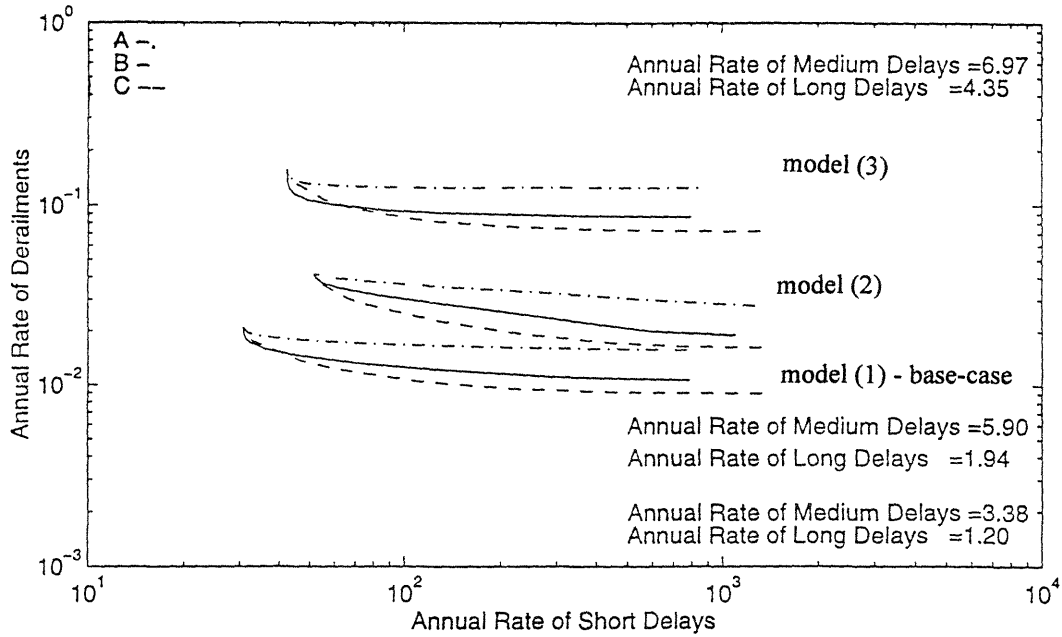


Figure 6.4: Annual rates of derailments and various delays, for coastal systems A, B and C and $(a_{t,loc}, A_{insp1}, A_{insp2})=(40, 80, 120\text{gals})$ for: (1) “modified Kawashima” model, (2) original Kawashima model, and (3) “modified Kawashima” model adjusted to account for the Kobe earthquake.
 (a) excluding derailment risk due to resumption of service following short delays
 (b) including derailment risk due to resumption of service following short delays

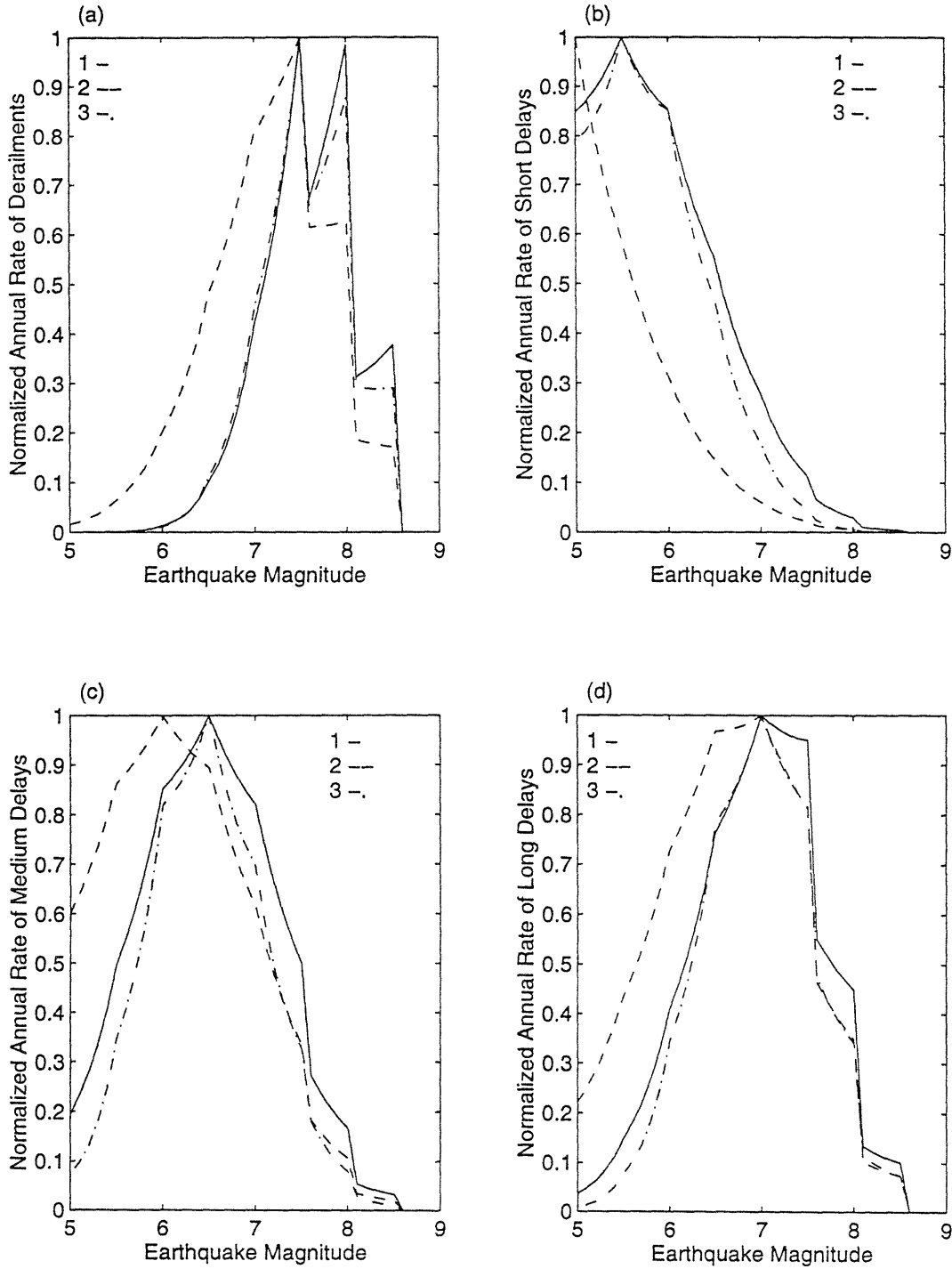


Figure 6.5: Normalized risk decomposition by earthquake magnitude, for $(\mathbf{a}^*, a_{t,loc}, A_{insp1}, A_{insp2}) = (40, 40, 80, 120\text{gals})$ for: (1) “modified Kawashima” model, (2) original Kawashima model and (3) “modified Kawashima” model adjusted to account for the Kobe earthquake.

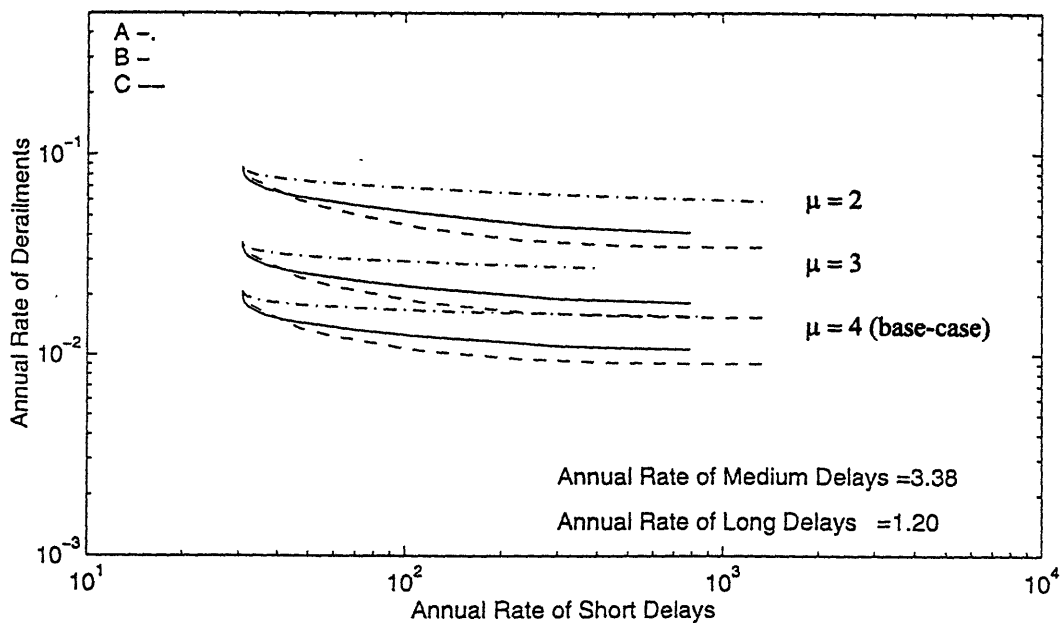
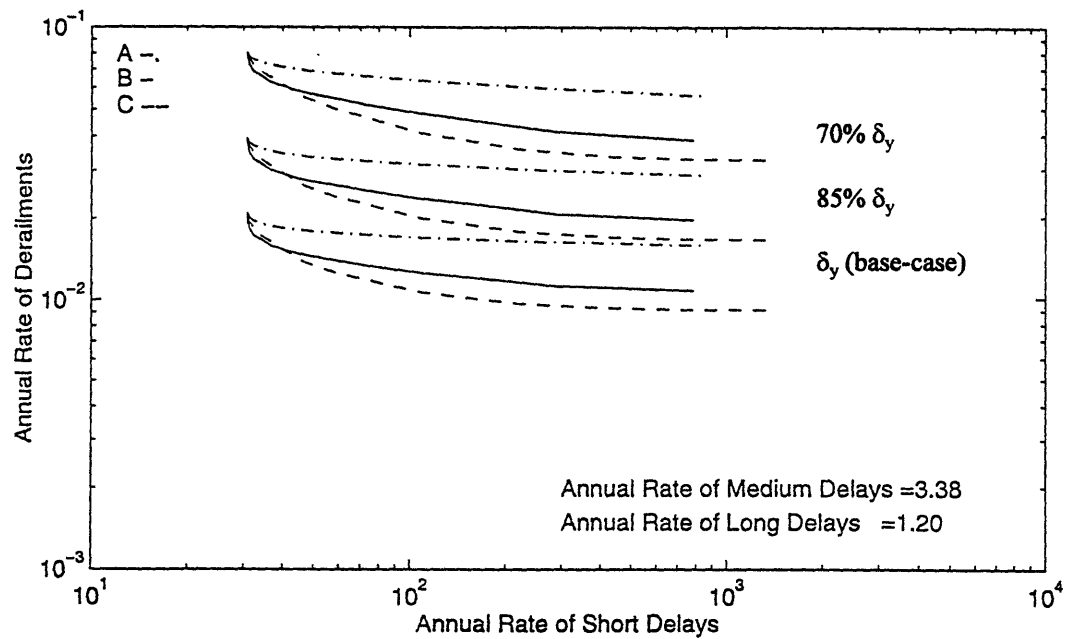


Figure 6.6: Annual rates of derailments and various delays, excluding derailment risk due to resumption of operation following short delays for coastal systems A, B and C and $(a_{t,loc}, A_{insp1}, A_{insp2}) = (40, 80, 120 \text{gals})$, if:
 (a) relative displacement at yielding, $\delta_y = (70\%, 85\%, 100\%)$ of base-case value
 (b) ductility ratio at failure, $\mu = 2, 3, 4$ (base-case value).

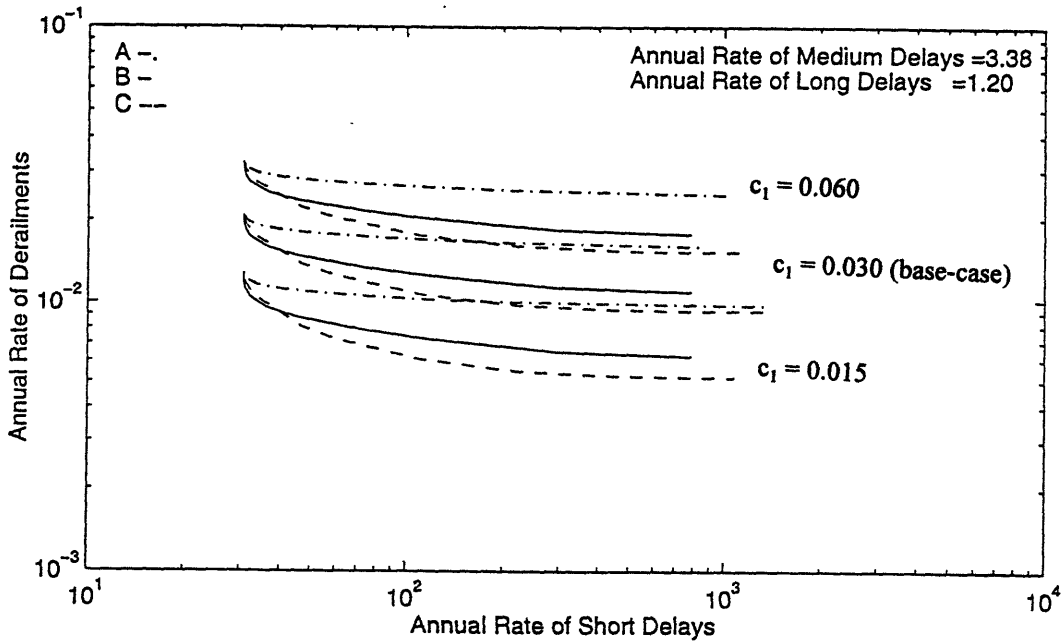
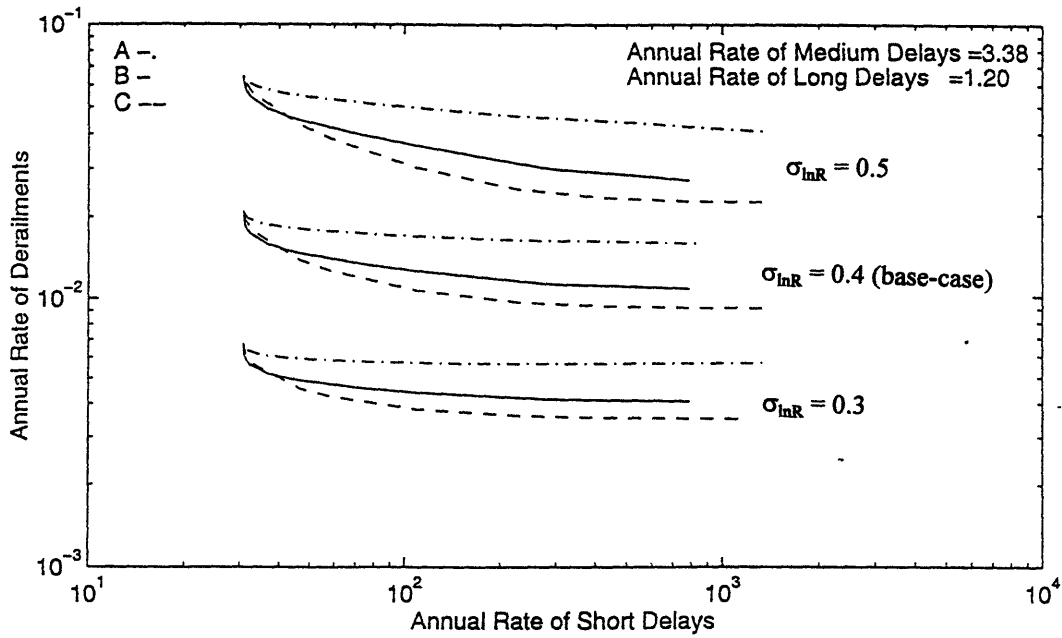


Figure 6.7: Annual rates of derailments and various delays, excluding derailment risk due to resumption of operation following short delays for coastal systems A, B and C and $(a_{t,loc}, A_{insp1}, A_{insp2}) = (40, 80, 120\text{gals})$, if:
 (a) uncertainty on resistance, $\sigma_{inR} = 0.3, 0.4$ (base-case value), 0.5 .
 (b) parameter controlling damage clustering, $c_1 = 0.015, 0.03$ (base-case value), 0.06

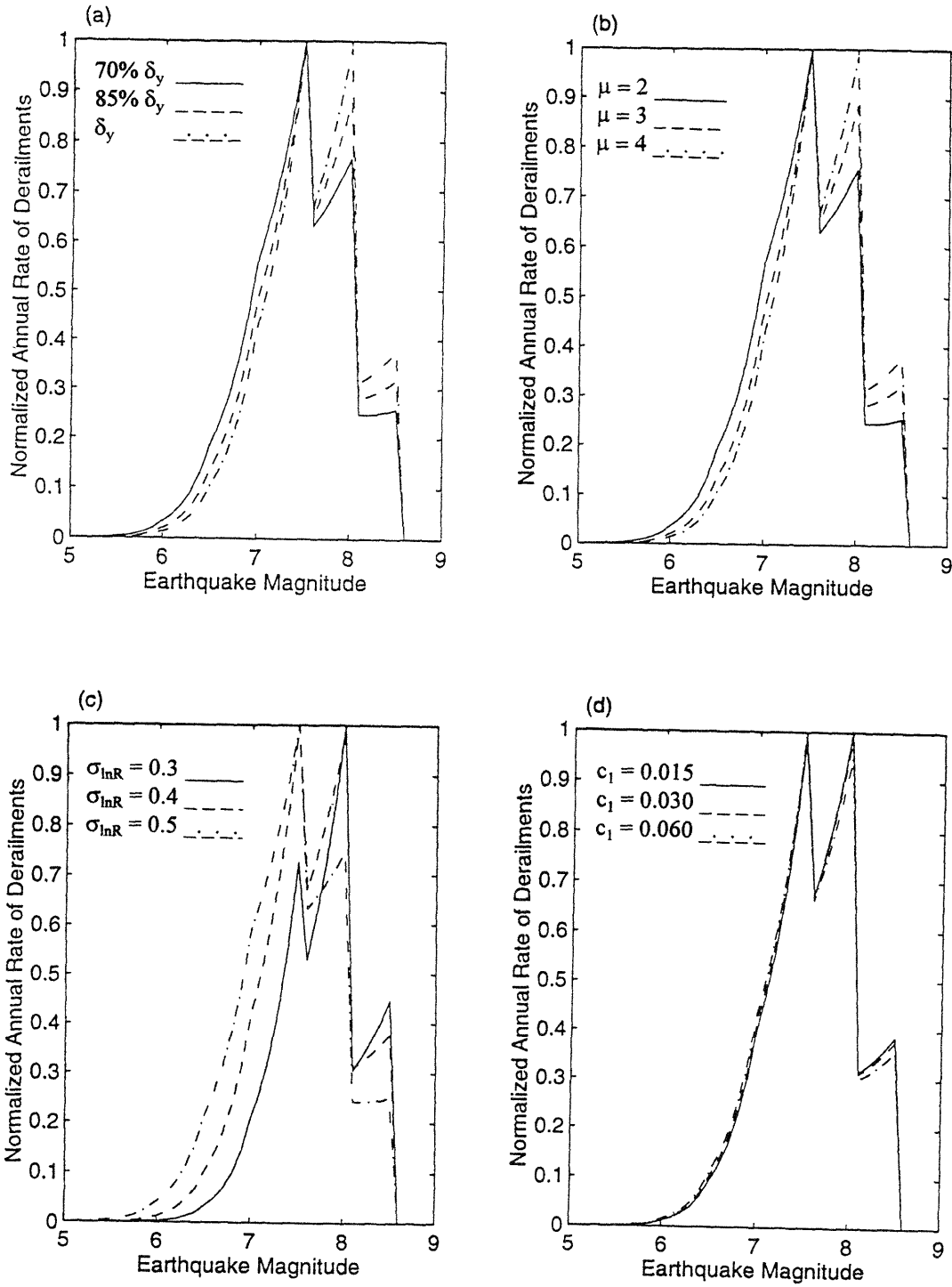


Figure 6.8: Normalized derailment risk decomposition, for $(a^*, a_{t,loc}, A_{insp1}, A_{insp2}) = (40, 40, 80, 120\text{gals})$, if:
 (a) $\delta_y = (70\%, 85\%, 100\%)$ of base-case value, (b) $\mu = 2, 3, 4$ (base-case value),
 (c) $\sigma_{inR} = 0.3, 0.4$ (base-case value), 0.5 , (d) $c_1 = 0.015, 0.03$ (base-case value), 0.06

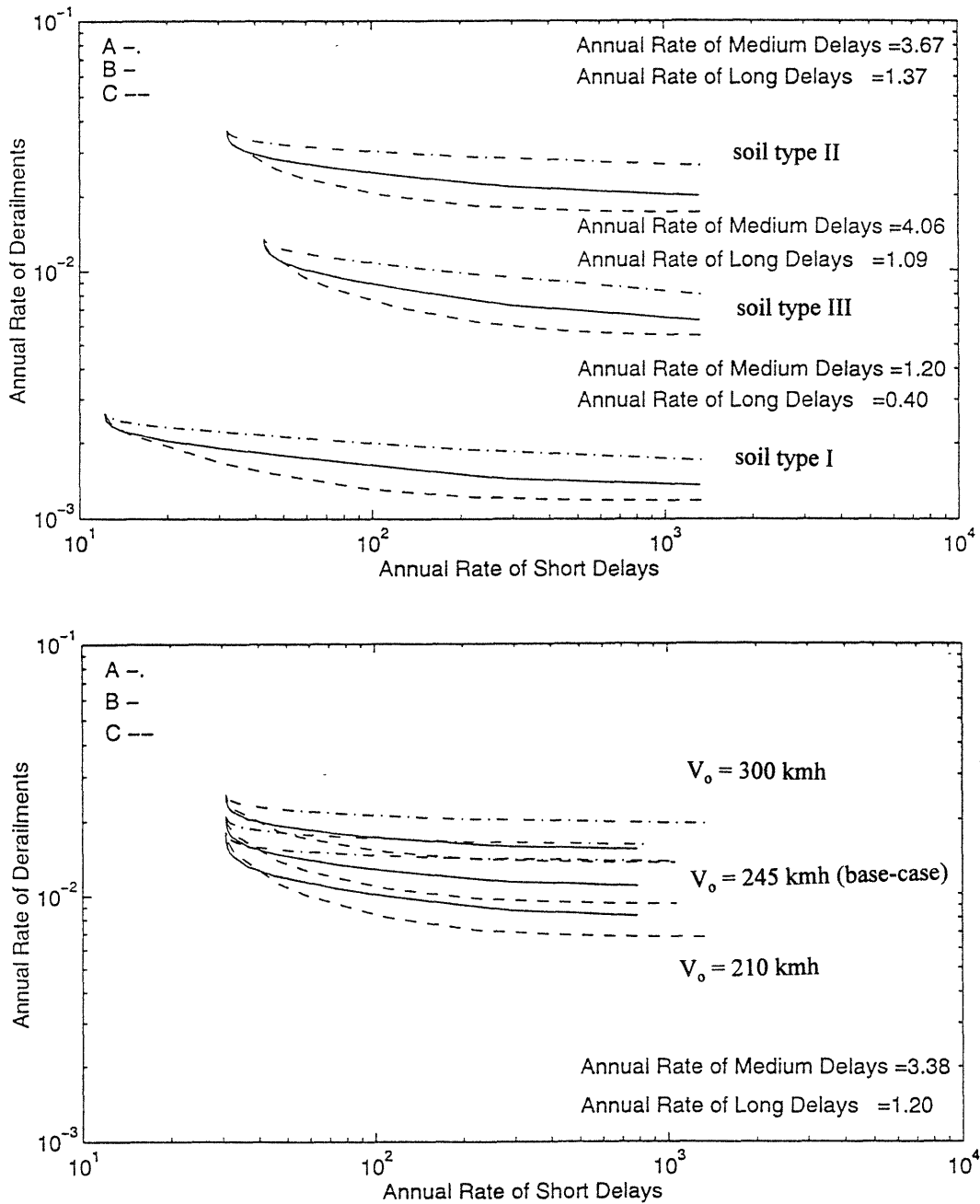


Figure 6.9: Annual rates of derailments and various delays, excluding derailment risk due to resumption of operation following short delays for coastal systems A, B and C and $(a_{t,loc}, A_{insp1}, A_{insp2}) = (40, 80, 120\text{gals})$, if: (a) soil type is I, II, III (Table 4.2) all along the line (b) maximum velocity, $V_o = 210\text{kmh}, 245\text{kmh}(\text{base-case value}), 300\text{kmh}$.

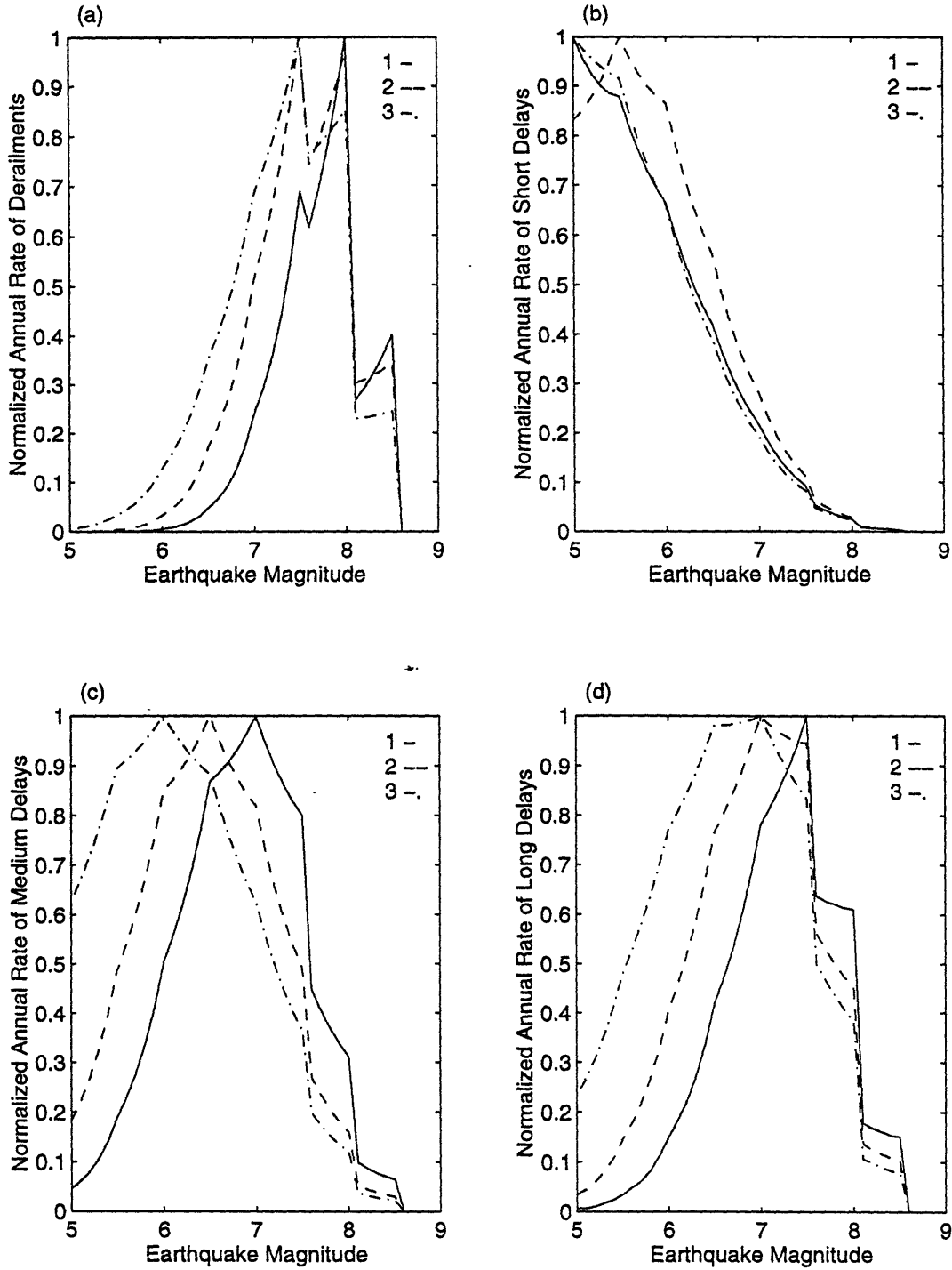


Figure 6.10: Normalized risk decomposition by earthquake magnitude, for $(\mathbf{a}^*, a_{t,loc}, A_{insp1}, A_{insp2}) = (40, 40, 80, 120\text{gals})$ if soil all along the line is: (1) type I, (2) type II, and (3) type III

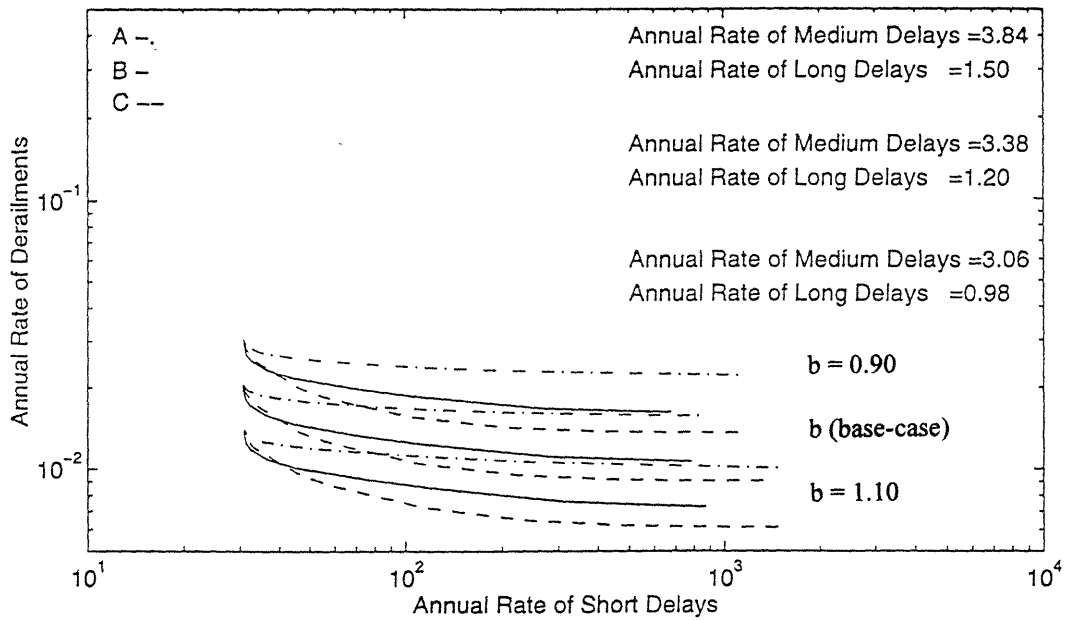
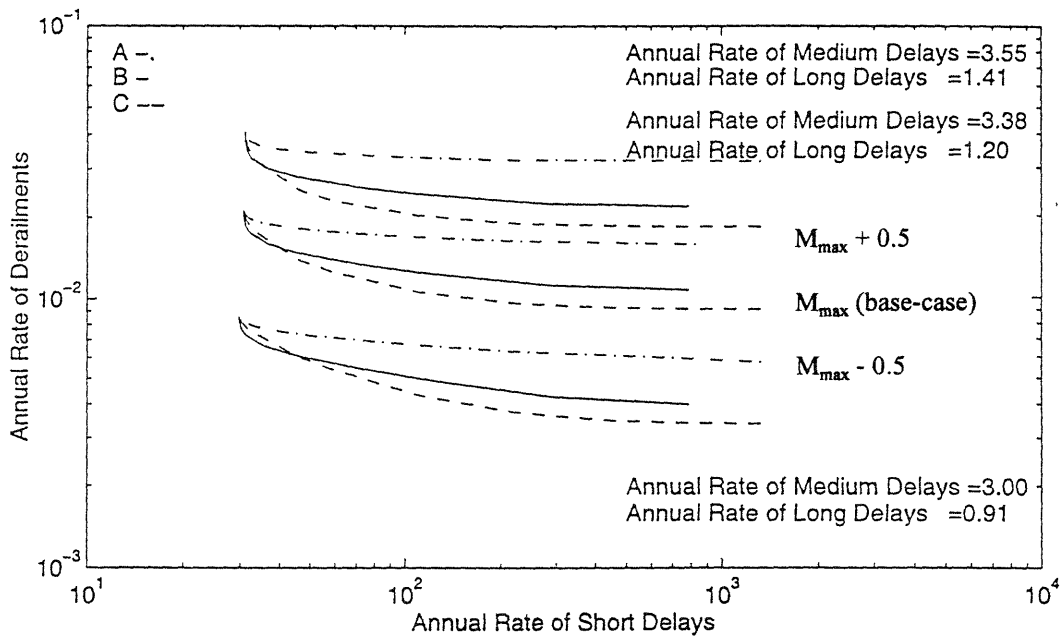


Figure 6.11: Annual rates of derailments and various delays, excluding derailment risk due to resumption of operation following short delays for coastal systems A, B and C and $(a_{t,loc}, A_{insp1}, A_{insp2})=(40, 80, 120\text{gals})$, if:
 (a) M_{max} of each seismic source is 0.5 higher/lower relative to base-case value
 (b) b -value of each seismic source is 0.9, 1.1 or base-case value.

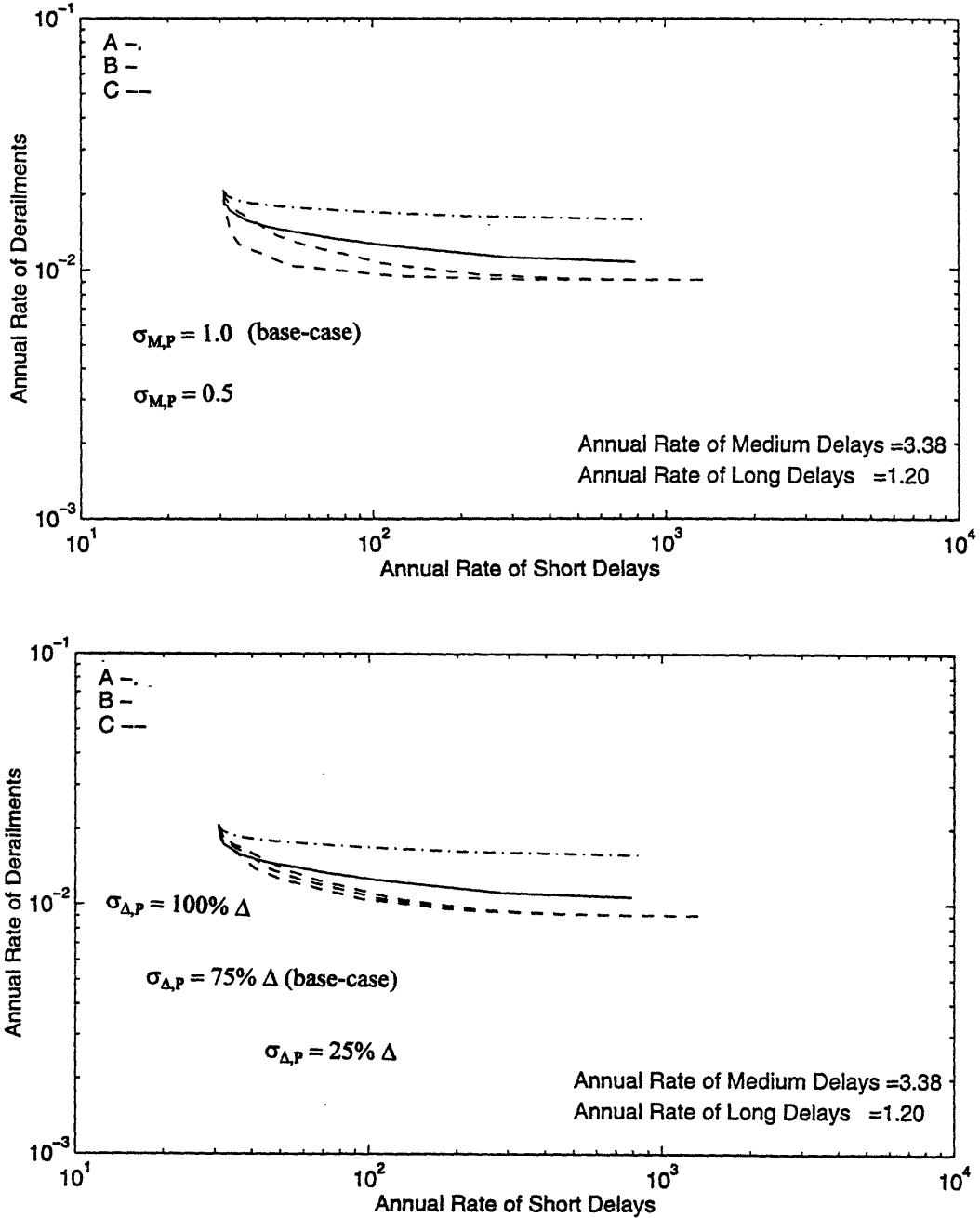


Figure 6.12: Annual rates of derailments and various delays, excluding derailment risk due to resumption of operation following short delays for coastal systems A, B and C and $(a_{t,loc}, A_{insp1}, A_{insp2}) = (40, 80, 120\text{gals})$ for the UrEDAS system accuracy of P-wave estimation of:
 (a) earthquake magnitude M : $\sigma_{M,P} = 0.5, 1.0$ (base-case value)
 (b) epicentral distance Δ : $\sigma_{\Delta,P} = 25\% \Delta, 75\% \Delta$ (base-case value), $100\% \Delta$

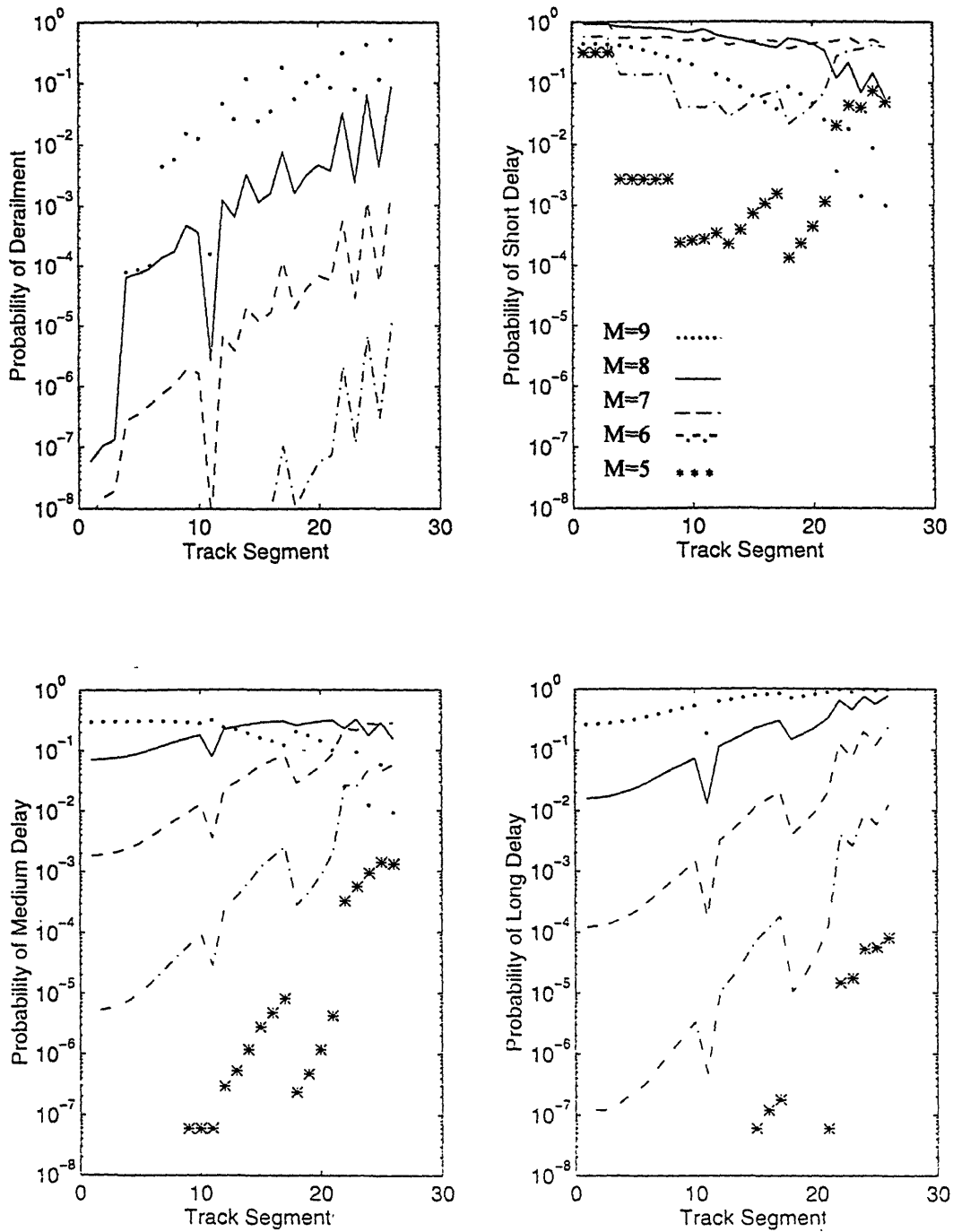


Figure 6.13: Conditional probability $P[E|M, \underline{x}, s, A]$ of event E along the line, for $(\mathbf{a}^*, a_{t,loc}, A_{insp1}, A_{insp2}) = (40, 40, 80, 120\text{gals})$ and earthquake magnitudes $M = 5 - 9$, [epicenter: 571km from $s=1$ and 135km from $s=26$]
 (a) E = derailment, (b) E = short delay, (c) E = medium delay, (d) E = long delay.

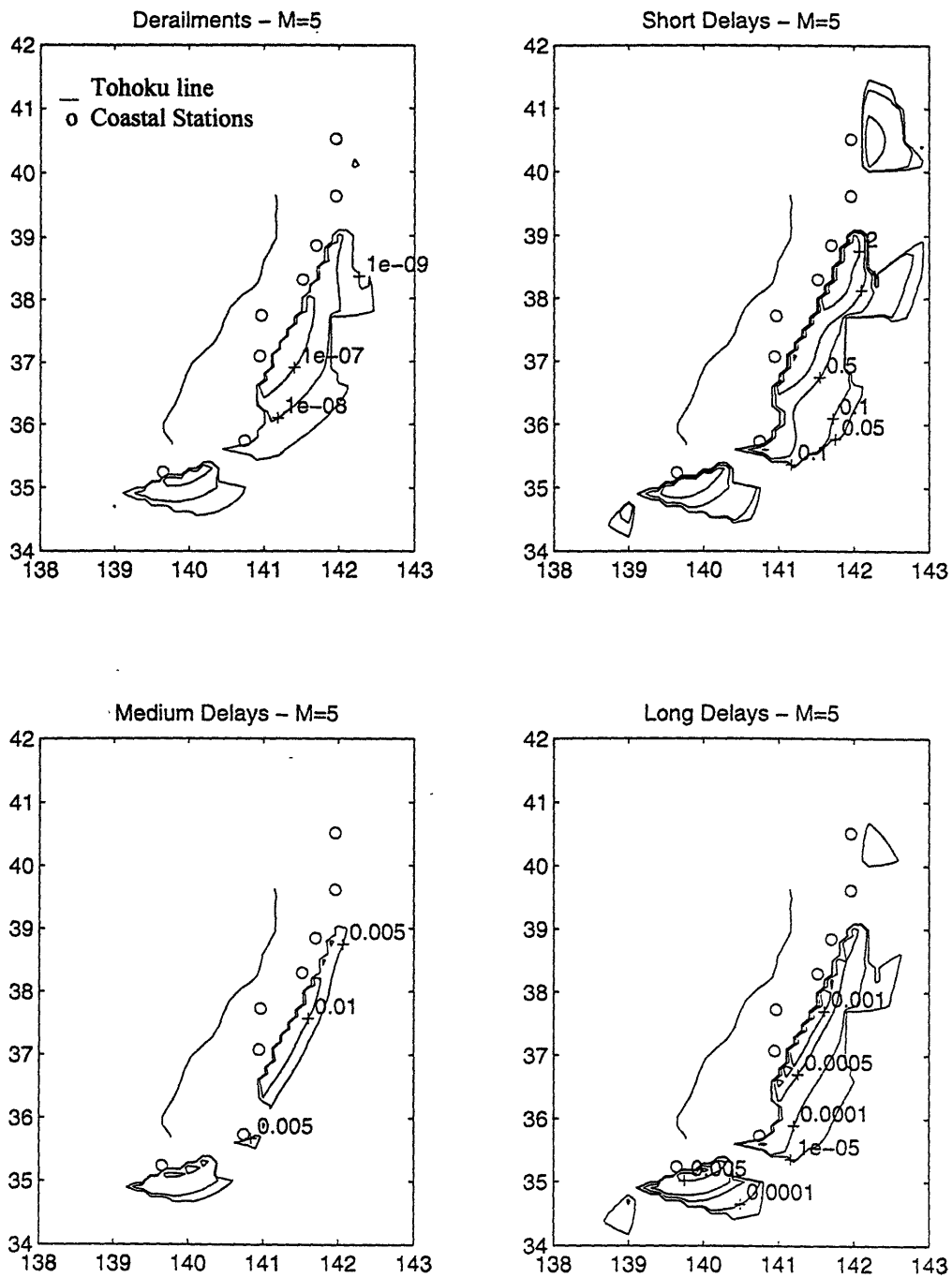


Figure 6.14: Expected number of events throughout the line, given earthquake of magnitude $M = 5$ occurring at map location, for $(a, a_{t,loc}, A_{insp1}, A_{insp2}) = (40, 40, 80, 120\text{gals})$, where events are: (a) derailments, (b) short delays, (c) medium delays, (d) long delays.

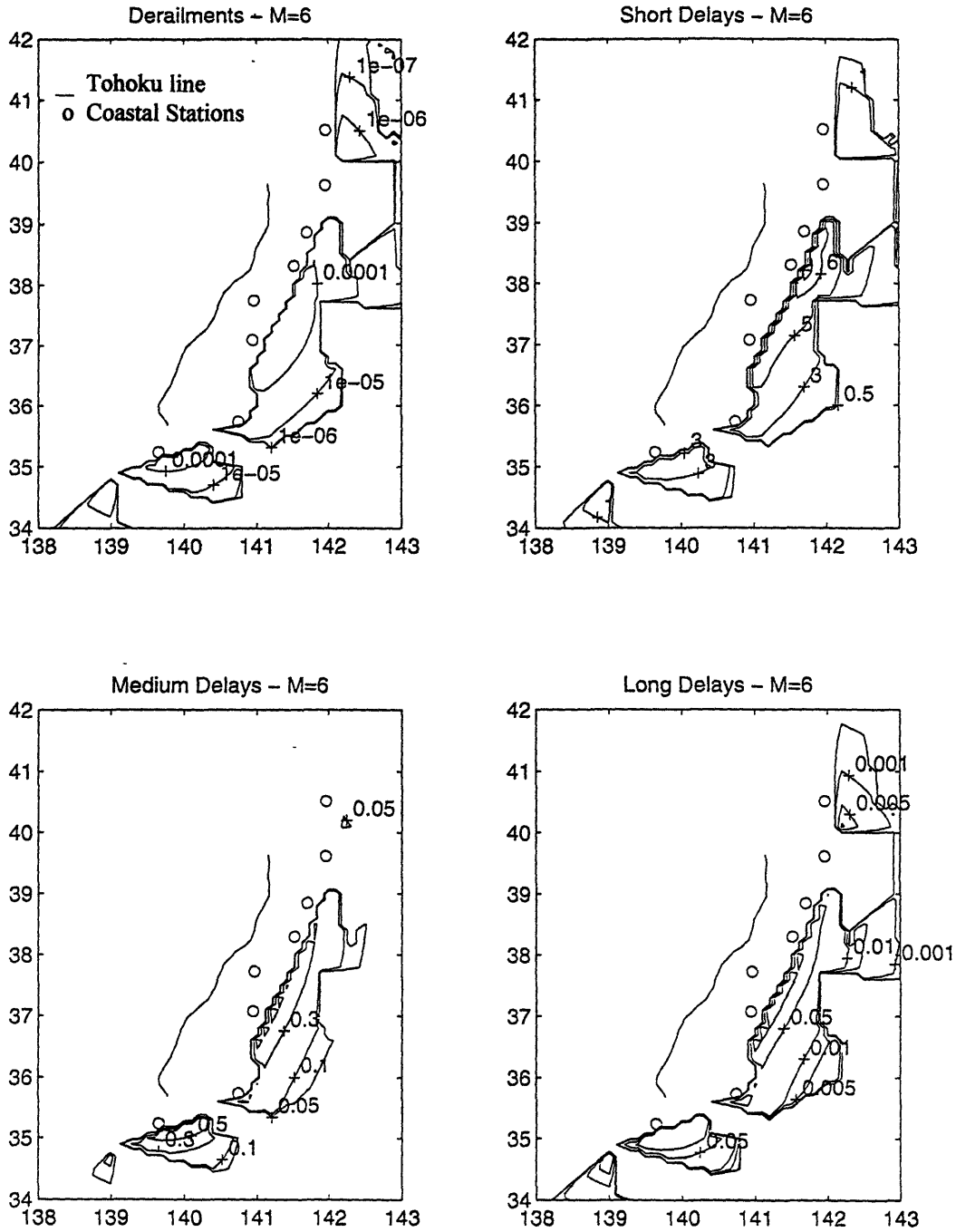


Figure 6.15: Expected number of events throughout the line, given earthquake of magnitude $M = 6$ occurring at map location, for $(a, a_{t,loc}, A_{insp1}, A_{insp2}) = (40, 40, 80, 120\text{gals})$, where events are: (a) derailments, (b) short delays, (c) medium delays, (d) long delays.

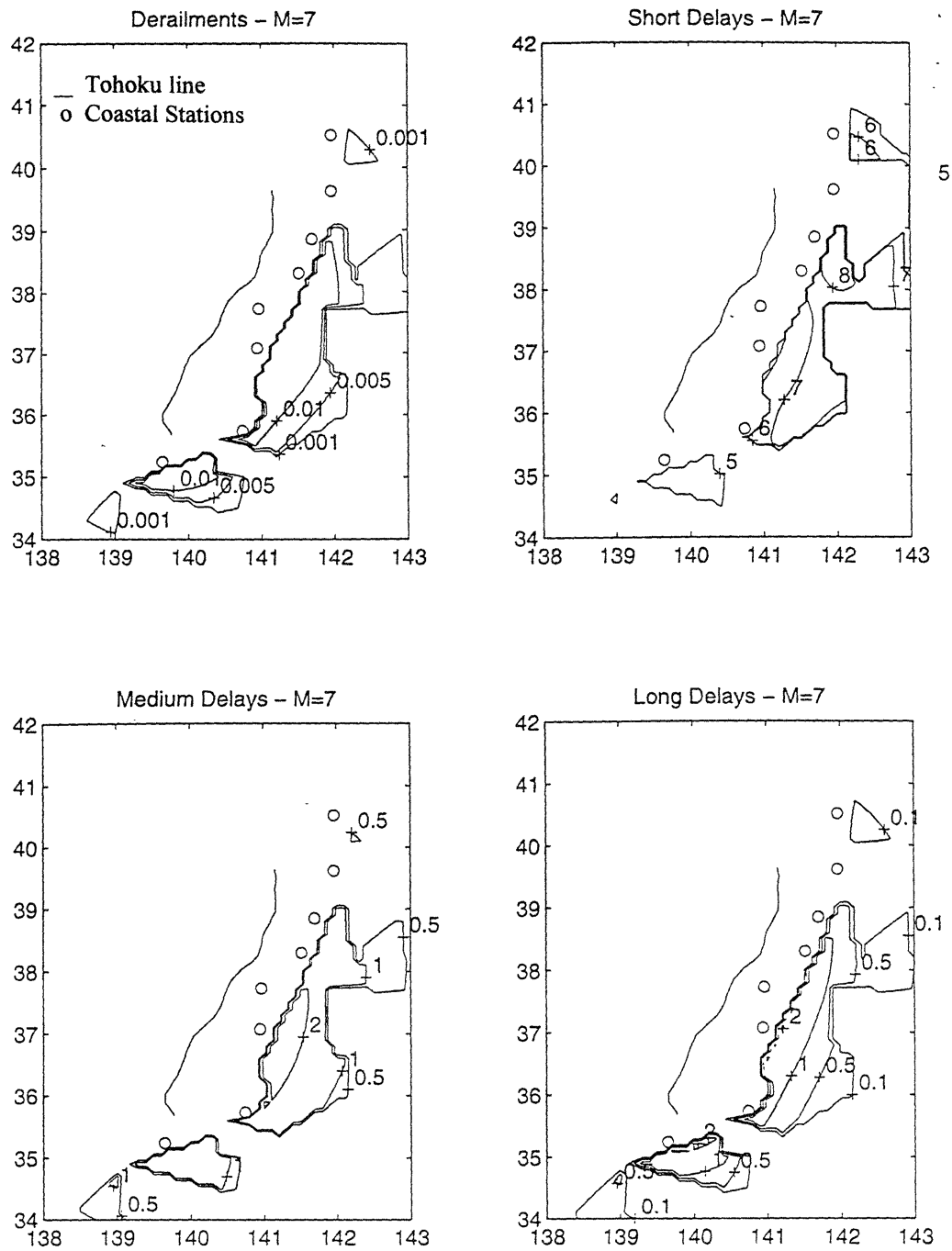


Figure 6.16: Expected number of events throughout the line, given earthquake of magnitude $M = 7$ occurring at map location, for $(a, a_{t,loc}, A_{insp1}, A_{insp2}) = (40, 40, 80, 120\text{gals})$, where events are: (a) derailments, (b) short delays, (c) medium delays, (d) long delays.

Chapter 7

Optimization of the Seismic Early Warning System

By choosing the most appropriate system and by modifying the operational parameters, the performance of the SEWS can be improved in the sense of reducing the current rate of delays, reducing the rate of derailments, or both. Optimization of the SEWS is pursued in a stepwise fashion, considering at each step the effect of modifying one additional parameter relative to the previous step. The parameters involved are: (a) the coastal system (A, B and C) and its trigger level (respectively, a^* , b^* and c^*), (b) the trigger and inspection levels of the wayside system, and (c) the seismic intensity parameter used by the wayside system (ground acceleration or spectral acceleration at the natural period of the viaduct). For reference, the estimated derailment and delay rates of the current SEWS systems (in trains/year) are:

- $\lambda_{DE} = 0.017$ (after resumption of service following short delays: 0.033)
- $\lambda_{SD} = 82.6$
- $\lambda_{MD} = 3.38$
- $\lambda_{LD} = 1.20$

As noted in Chapter 6, if the measure of seismic intensity used by the wayside system is peak ground acceleration a_{max} , the calculated value of λ_{DE} after resumption of operation following short delays rests on conservative assumptions and should be regarded as an upper bound. This is because we have assumed that a_{max} and the spectral acceleration S_a along the track are conditionally independent, given the earthquake magnitude and epicentral location. Another reason why such rate is not very accurate is that its value is sensitive to the fragility of the viaduct at low levels of ground motion, which is not well

known. The estimated derailment rates when S_a is used as ground motion intensity by the wayside system should be more accurate.

7.1 Optimization when the Wayside System Operates on a_{max}

In order to reduce the current high rate of short delays, one might consider increasing the trigger level of the present coastal system. All the rest remains the same. This action might be justified, as the risk of derailment is insensitive to the trigger level at the coast, a^* , whereas varying a^* can change the annual rate of short delays by orders of magnitude; see Figure 7.1. Using the results for coastal system A, one can see from Figure 7.1 that by raising the coastal parameter a^* above the current value of 40 gals, for example to 80gals, the rate of short delays can be reduced by 50%, with small increases in the derailment risk (about 5%). The benefits from this modification of the current SEWS system are however small relative to other modifications discussed below. The choice of a^* does not affect the rates of medium and long delays, which are determined entirely by the wayside system.

A second possible modification would be to raise the triggering level of the wayside system, $a_{t,loc}$, to the first track inspection level, A_{inspl} . Setting $a_{t,loc} = A_{inspl}$ would eliminate what we believe is a misconception in the current setting of the wayside system parameters, as there is no need for trains to be stopped if no track inspection is deemed necessary. The time delay between the instants when a truly strong motion exceeds 40 and 80 gals is very short and has no appreciable effect on the rate of derailment. If $a_{t,loc}$ is set to the current value of A_{inspl} (80 gals), then only the coastal system would produce short delays. These residual short delays are inevitable, given that ground motion intensity at the coastal stations and at the track are not deterministically related. The rate of short delays would become zero only if the coastal system was decommissioned.

Figure 7.2 compares the performance of the three coastal systems for $a_{t,loc}=A_{insp1}=80$ gals with that under the current setting ($a_{t,loc}=40$ gals, $A_{insp1}=80$ gals). Meaningful comparisons in this case should be in terms of the rates following resumption of operation; see Figure 7.2b. If the coastal system is operated with $a^* = 80$ gals, the rate of short delays drops to 11.7 trains/year, while the rate of derailments remains practically the same. Again, a change of $a_{t,loc}$ does not affect the rates of medium and long delays. A modification in this sense is considered definitely worthwhile. In all subsequent analyses, we have therefore set $a_{t,loc}=A_{insp1}$.

The effect of changing the inspection levels A_{insp1} and A_{insp2} (currently set at 80gals and 120gals) is shown in Figure 7.3, where results are presented for three settings: $(a_{t,loc}, A_{insp1}, A_{insp2}) = (80, 80, 120$ gals), $(100, 100, 140$ gals) and $(120, 120, 160$ gals). As one would expect, raising these levels produces higher rates of derailment, for any given value of λ_{SD} . However, the tradeoff is in this case with the rates of medium and long delays, which are reduced substantially. Moreover, after including the added risk due to derailments following short delays, the differences between coastal systems are insignificant; see the flat curves in Figure 7.3. This is attributed to the fact that, after resumption of service following short delays, almost all trains (except the medium and long delays) have covered the same track length (half the length between consecutive trains heading in the same direction) irrespective of whether they were stopped initially by the coastal system.

A more direct illustration of the tradeoff is provided in Figure 7.4 where, for System A and $a^* = 80$ gals, the values of the 4 annual rates after the resumption of operation of the short delays are plotted against A_{insp1} , while always keeping $A_{insp2} = A_{insp1} + 40$ gals. Plots for the other two coastal systems and for any other values of a^* are qualitatively similar. Table 7.1 indicates a possible alternative to the current setting of system A, as well as alternatives using systems B and C. These alternatives show that the effect of the coastal system and its trigger level, while nonzero, is not significant. More specifically,

system B outperforms system A, and System B may be outperformed by system C, in terms of the rates of derailments and short delays.

7.2 Optimization when the Wayside System Operates on S_a

A better measure of seismic intensity to use at the wayside is the response spectrum acceleration for $T = 0.4\text{sec}$ and 5% of critical damping. The performance of the SEWS after this modification is quantified in Figure 7.5 for the case when the triggering levels at the wayside are $(S_{at,loc}, S_{a,insp1}, S_{a,insp2})=(80, 160, 240\text{gals})$. A noteworthy difference relative to the use of a_{max} is that the added risk from service resumption after short delays is unnoticeable, at least for the relatively low value of $A_{insp1} = 160\text{gals}$ used in this figure. This is due to the fact that the low spectral accelerations that induce short delays produce insignificant track damage. Therefore, resumption of service following a short delay does not increase the risk of derailments by significant amounts. This effect of changing from an a_{max} -based to an S_a -based operation of the wayside system is a very significant step in the optimization procedure of this system.

In order to draw conclusions from a direct comparison of the performance of the SEWS with an a_{max} -based versus an S_a -based operation of the wayside system, we need to introduce comparable trigger and track inspection levels for a_{max} and S_a . By comparing the median attenuated values of a_{max} and S_a for different magnitudes we conclude that the levels of S_a are two times higher than those of a_{max} on average, given earthquake magnitude and epicentral distance; see Figures 4.4 and 4.5. Therefore, trigger and track inspection levels in terms of S_a twice as high as those in terms of a_{max} are considered comparable for the purpose of this study.

The general effect of this modification is presented in Figure 7.6. In this figure, we compare the a_{max} -based wayside system with $(a_{t,loc}, A_{insp1}, A_{insp2})=(80, 80, 120\text{gals})$ to the S_a -based system with $(S_{at,loc}, S_{a,insp1}, S_{a,insp2})=(160, 160, 240\text{gals})$. Regarding the rate of

derailments excluding the added risk from the resumption of service following short delays, the proposed change in the wayside system is not important when the coastal system triggers frequently but becomes significantly beneficial when the coastal system triggers rarely. Using S_a rather than a_{\max} can reduce the risk of derailments by as much as 50%. This decrease is due to the fact that S_a is a better parameter than a_{\max} to predict track damage. Therefore, earthquakes with high damage potential tend to trigger the wayside system when such systems operates on S_a . This is not the case when the wayside system operates on a_{\max} , given the low level of probabilistic dependence between a_{\max} and track damage. The increased protection from a wayside system operating on S_a also reduces the importance of the coastal system. This is shown in Figure 7.6, where the coastal trigger level is seen to have smaller effect on the derailment risk, when S_a is used by the wayside system.

Operating the wayside system on S_a is effective in reducing the derailment risk after the resumption of service following short delays (reduction of the total risk by about 50% relative to using a_{\max}). This condition is independent of the trigger level of the coastal system. Essentially, the risk of derailment from resumption of service after short delays has been eliminated.

The effect of changing the trigger and inspection levels of the wayside system is shown in Figure 7.7, where results are presented for $(S_{a,loc}, S_{a,insp1}, S_{a,insp2})=(160, 160, 240 \text{ gals})$, $(240, 240, 320 \text{ gals})$ and $(400, 400, 480 \text{ gals})$. The qualitative features of this figure are similar to those of Figure 7.3 for the case of an a_{\max} -based wayside system. There is, however, a very significant decrease in the rates of delays.

In order to identify the best setting of the coastal and wayside trigger parameters for an S_a -based wayside system, we observe that the value of the coastal parameter should be set to produce an annual rate of short delays in the (approximate) range of 1 to 100; having more than 100 expected short delays per year would probably result in inefficient performance of the system, while having fewer than 1/year would lead to a virtual

elimination of the coastal system. The latter action would probably be judged unwise in the case of a very large damaging event. Also, the value of the wayside trigger level, $S_{at,loc}$ should be set between 250 and 400 gals: setting $S_{at,loc} \leq 250$ gals is suboptimal as such conservative values do not appreciably reduce the risk of derailment, while $S_{at,loc} \geq 400$ gals produces what we consider as excessively high derailment risk. Figures 7.8 through 7.10 show the values of the derailment and delay rates within the above ranges of the coastal and local trigger parameters, for each of the three coastal systems. The derailment rates plotted in these figures include the risk from resumption of service following short delays. In all cases, the wayside parameters have the form : $(S_{at,loc}, S_{a,insp1}, S_{a,insp2}) = (S_{at,loc}, S_{at,loc}, S_{at,loc} + 80\text{gals})$. The following conclusions can be reached from examination of Figures 7.8 - 7.10 :

The annual rate of derailment is mainly a function of $S_{at,loc}$. The coastal system becomes influential only for low values of the coastal parameter. Coastal system C is somewhat more influential on the overall performance of the SEWS than system B, which in turn is more influential than system A.

The annual rate of short delays depends almost exclusively on the coastal trigger parameter. This rate increases slightly as $S_{at,loc}$ increases.

Medium and long delay rates are functions only of the wayside trigger levels. Their sum, $\lambda_{MD} + \lambda_{LD}$, is governed by A_{insp1} , whereas the relative value of the two rates is affected by A_{insp2} . Therefore, the setting of A_{insp2} should be based on the desirability of an on-train inspection (resulting in medium delays) versus on-foot inspection of the tracks (resulting in long delays). This decision should be based on the value of S_a recorded by the closest wayside accelerometer. To aid making this choice, we have estimated the probability of a train meeting damaged track in 35km (one half of the distance between trains traveling in the same direction), given S_a at the track. This probability is plotted in Figure 7.11 for the

range of the parameter c_1 that controls the spatial clustering of damage that we consider reasonable; see Section 6.1 and Figure 6.8b.

Table 7.2 gives the rates of derailment and of various delays for three specific settings of Systems A, B and C while the wayside system operates on S_a . These alternative systems, use identical settings of the S_a trigger levels for the wayside accelerometers. The results show that the effect of using different coastal systems, although not zero, is small.

By comparing Tables 7.1 and 7.2, one can see that using an S_a -based wayside system reduces very significantly all delays, in addition to reducing the derailment risk after resumption of operation following short delays by about 50%.

Annual Rates	Current : System A $a^* = 40\text{gals}$ (40, 80, 120 gals)⁽¹⁾	Alternative A1: System A $a^* = 60\text{ gals}$ (100,100,140gals)⁽¹⁾	Alternative B1: System B $b^* = 60\text{ gals}$ (100,100,140gals)⁽¹⁾	Alternative C1: System C $c^* = 3.20$ (100,100,140gals)⁽¹⁾
λ_{DE}	0.017 (0.033) ⁽²⁾	0.029 (0.038) ⁽²⁾	0.023 (0.037) ⁽²⁾	0.021 (0.036) ⁽²⁾
λ_{SD}	82.6	24.1	20.4	19.3
λ_{MD}	3.38	1.51	1.51	1.51
λ_{LD}	1.20	0.69	0.69	0.69

(1) The values in parentheses correspond to the setting of the wayside system : ($a_{t,loc}$, A_{insp1} , A_{insp2}).

(2) The values in parentheses correspond to the rate of derailments including the derailment risk due to resumption of service following short delays.

Table 7.1: Performance of alternative SEWS systems, using a_{max} as the intensity parameter at the wayside stations.

Annual Rates	Current : System A $a^* = 40\text{gals}$ (40, 80, 120 gals)⁽¹⁾	Alternative A2: System A $a^* = 80\text{ gals}$ (280,280,360gals)⁽¹⁾	Alternative B2: System B $b^* = 120\text{ gals}$ (280,280,360gals)⁽¹⁾	Alternative C2: System C $c^* = 4.00$ (280,280,360gals)⁽¹⁾
λ_{DE}	0.017 (0.033) ⁽²⁾	0.015 (0.015)	0.015 (0.015)	0.015 (0.015)
λ_{SD}	82.6	12.4	1.2	1.7
λ_{MD}	3.38	0.18	0.18	0.18
λ_{LD}	1.20	0.16	0.16	0.16

(1) The values in parentheses correspond to the setting of the wayside system : ($S_{at,loc}$, $S_{a,insp1}$, $S_{a,insp2}$).

(2) The values in parentheses correspond to the rate of derailments including the derailment risk due to resumption of service following short delays.

Table 7.2: Performance of alternative SEWS systems, using S_a as the intensity parameter at the wayside stations.

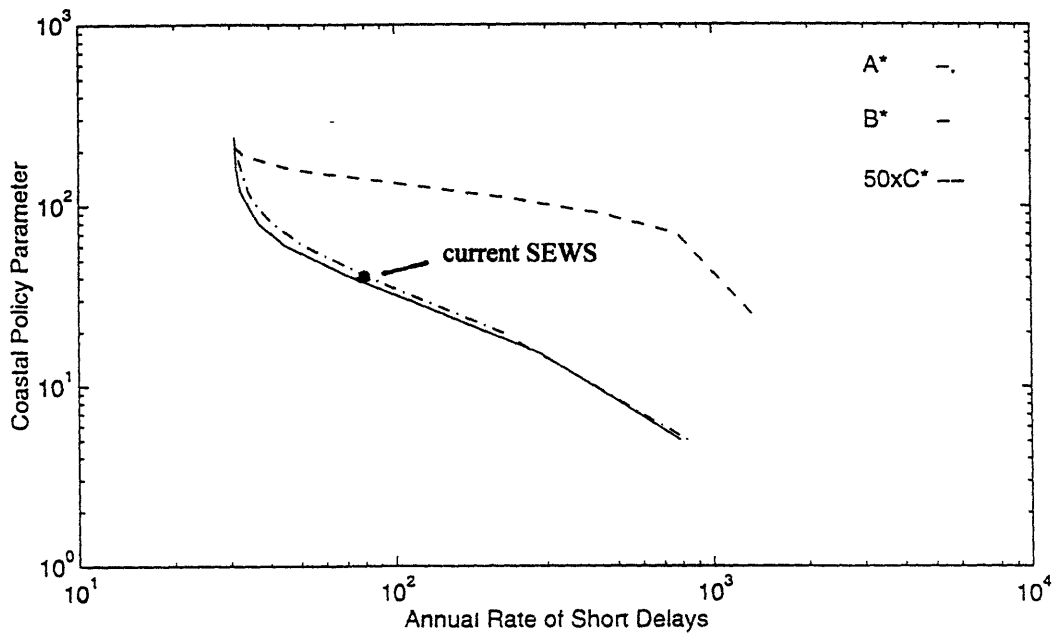
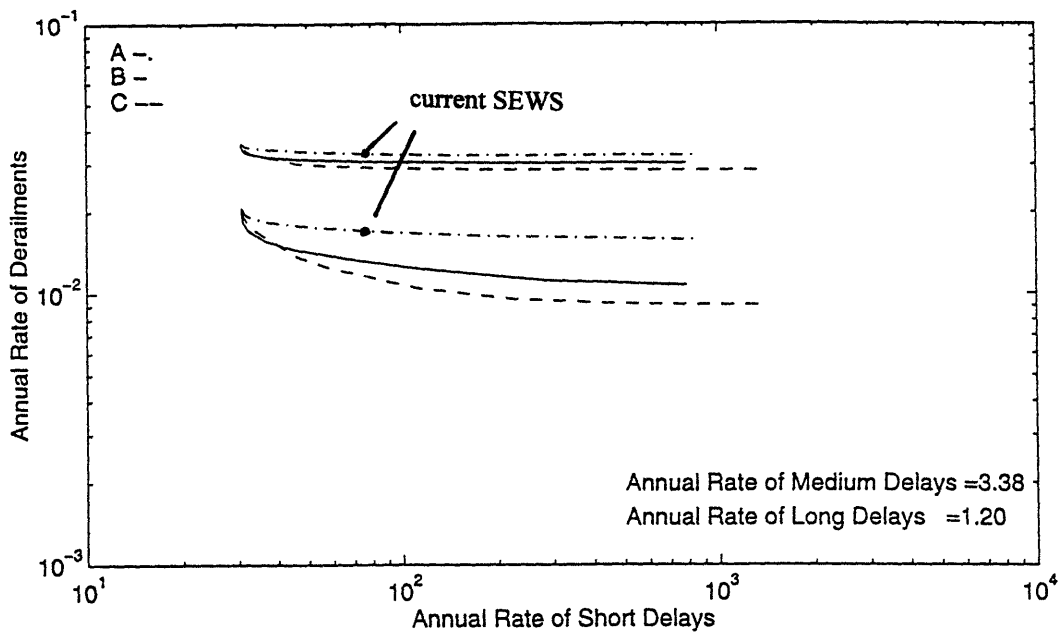


Figure 7.1: (a) Annual rates of derailments and various delays, excluding and including derailment risk due to resumption of operation following short delays, for coastal systems A, B and C and $(a_{t,loc}, A_{insp1}, A_{insp2})=(40, 80, 120\text{gals})$
 (b) Coastal trigger parameter versus annual rate of short delays, for coastal systems A, B and C and $(a_{t,loc}, A_{insp1}, A_{insp2})=(40, 80, 120\text{gals})$.

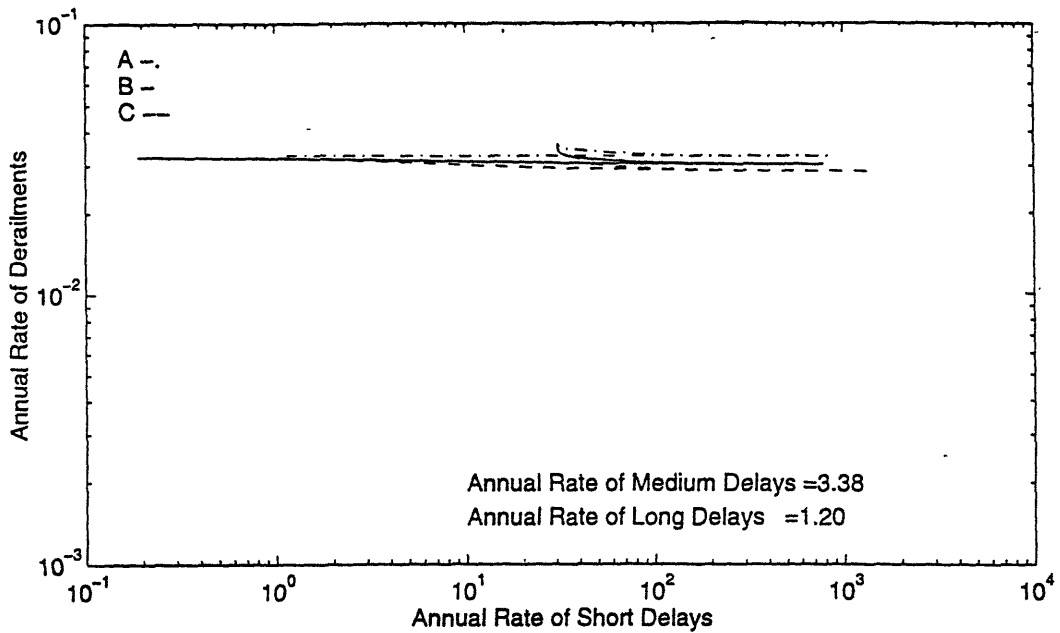
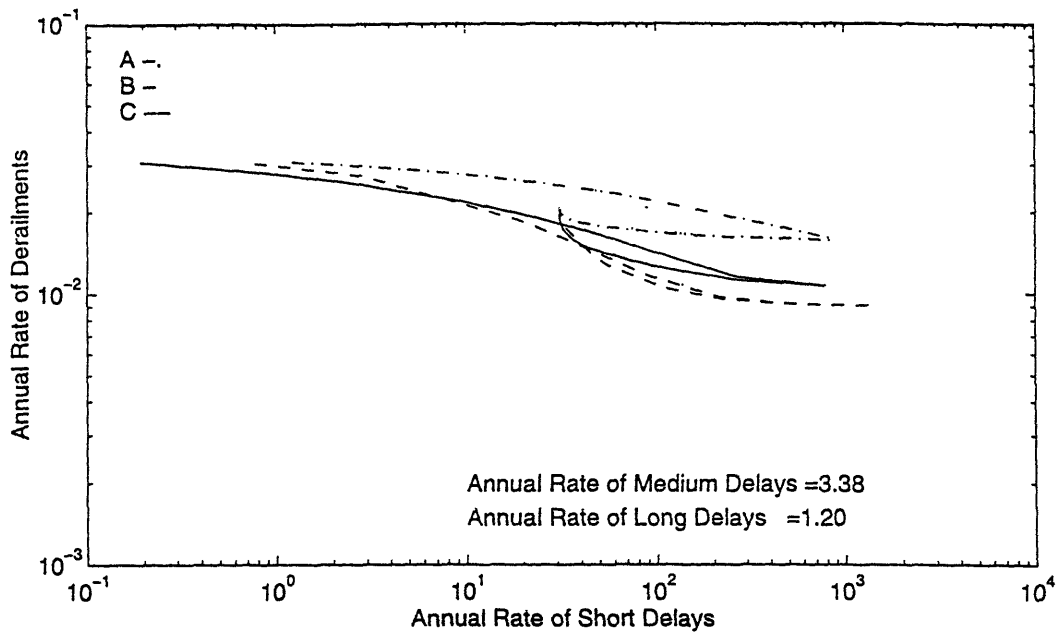


Figure 7.2: Annual rates of derailments and various delays, for coastal systems A, B, C and $(a_{t,loc}, A_{insp1}, A_{insp2}) = (40, 80, 120\text{gals})$ and $(80, 80, 120\text{gals})$
 (a) excluding derailment risk due to resumption of service following short delays
 (b) including derailment risk due to resumption of service following short delays

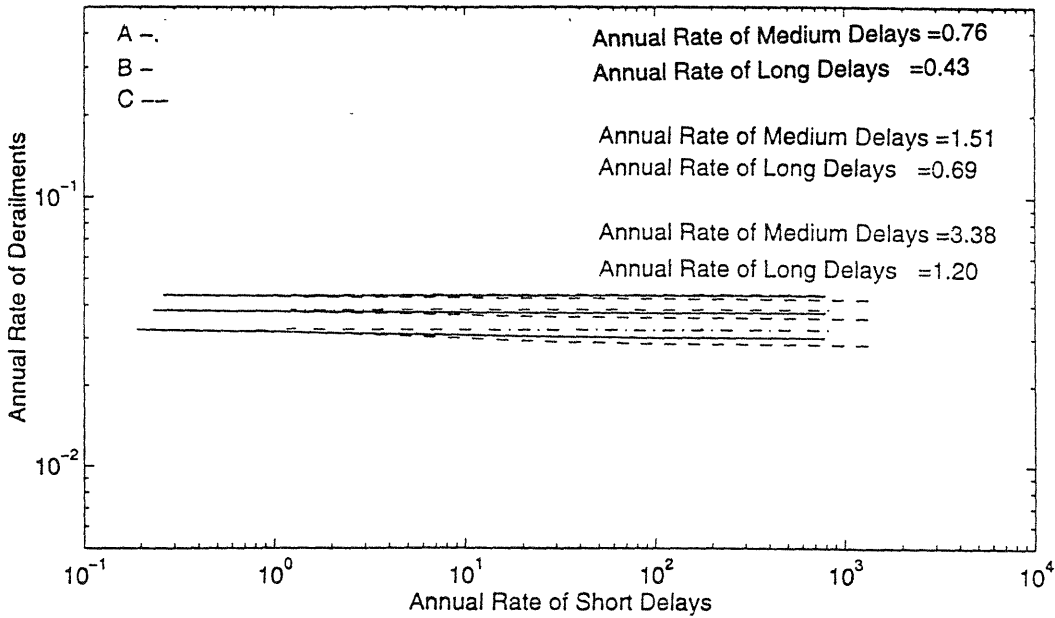
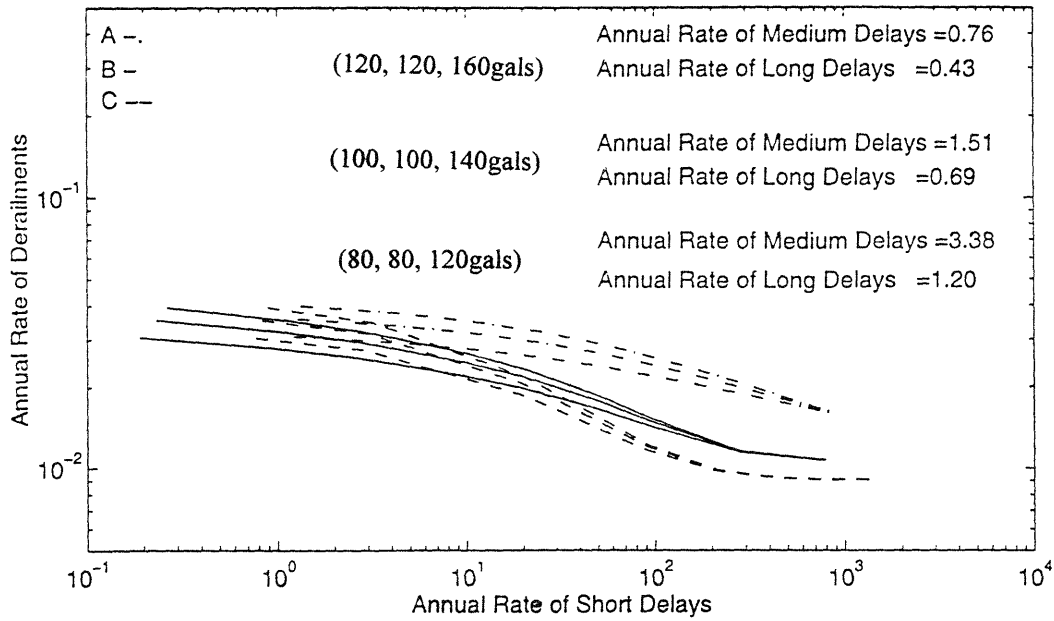


Figure 7.3: Annual rates of derailments and various delays, for coastal systems A, B and C and $(a_{t,loc}, A_{insp1}, A_{insp2}) = (80, 80, 120\text{gals}), (100, 100, 140\text{gals}),$ and $(120, 120, 160\text{gals})$.
 (a) excluding derailment risk due to resumption of service following short delays
 (b) including derailment risk due to resumption of service following short delays

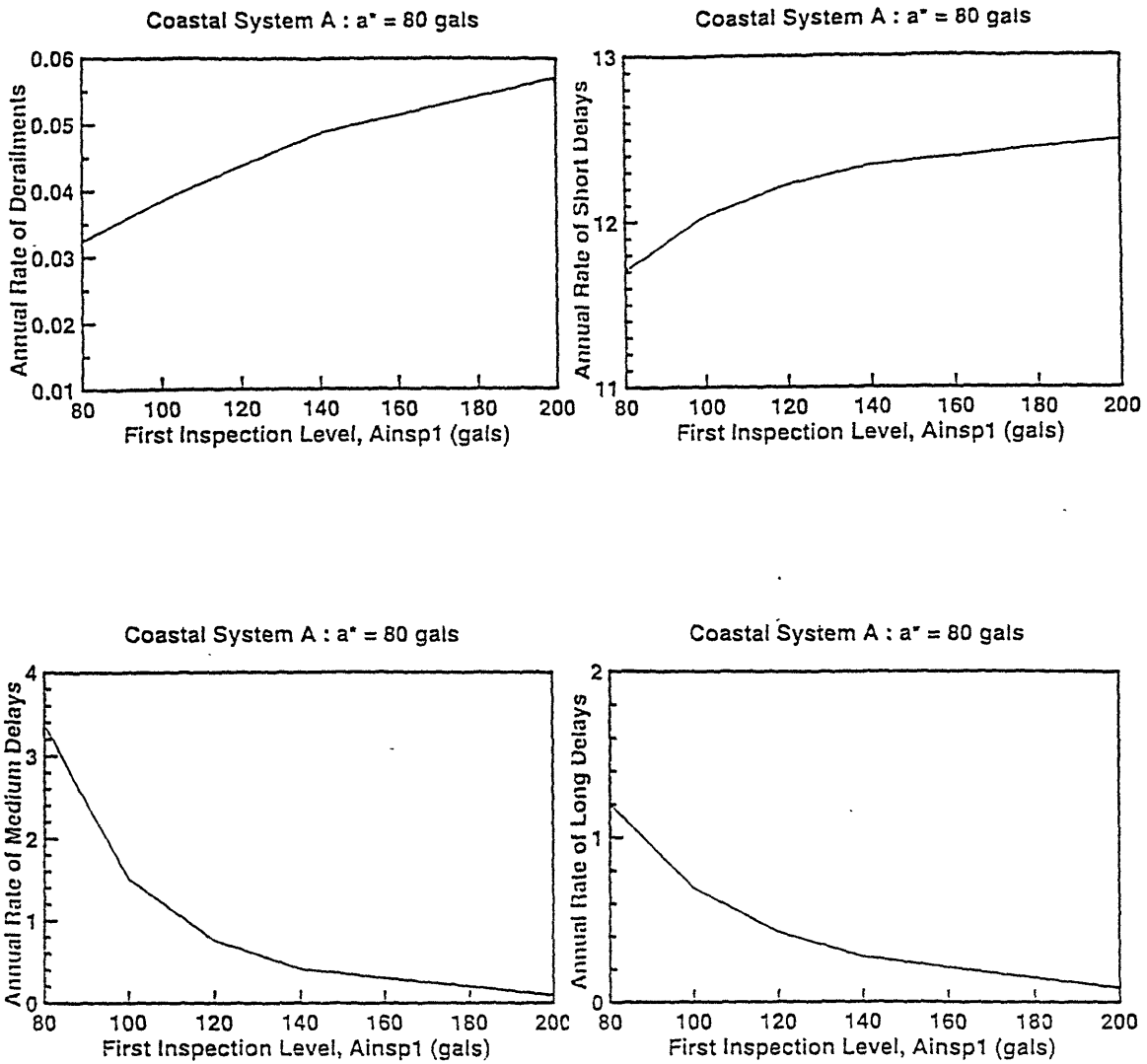


Figure 7.4: Expected number of event E versus A_{insp1} , for coastal system A, $a^* = 80$ gals, $a_{t,loc} = A_{insp1}$ and $A_{insp2} = A_{insp1} + 40$ gals and including derailment risk due to resumption of service following short delays, where E is: (a) E =derailments, (b) E =short delays, (c) E =medium delays, (d) E =long delays.

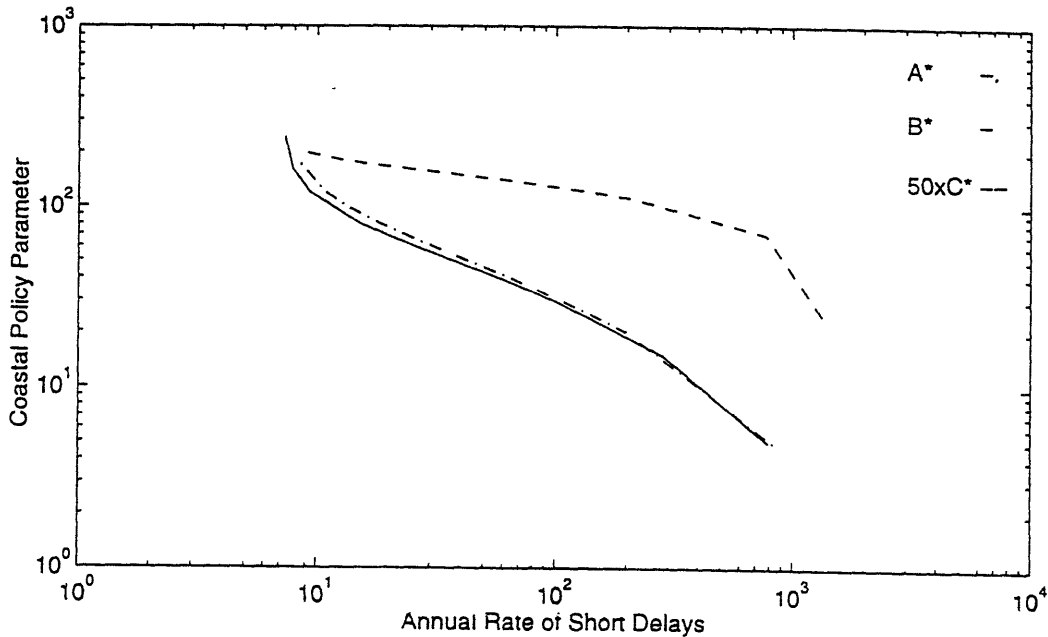
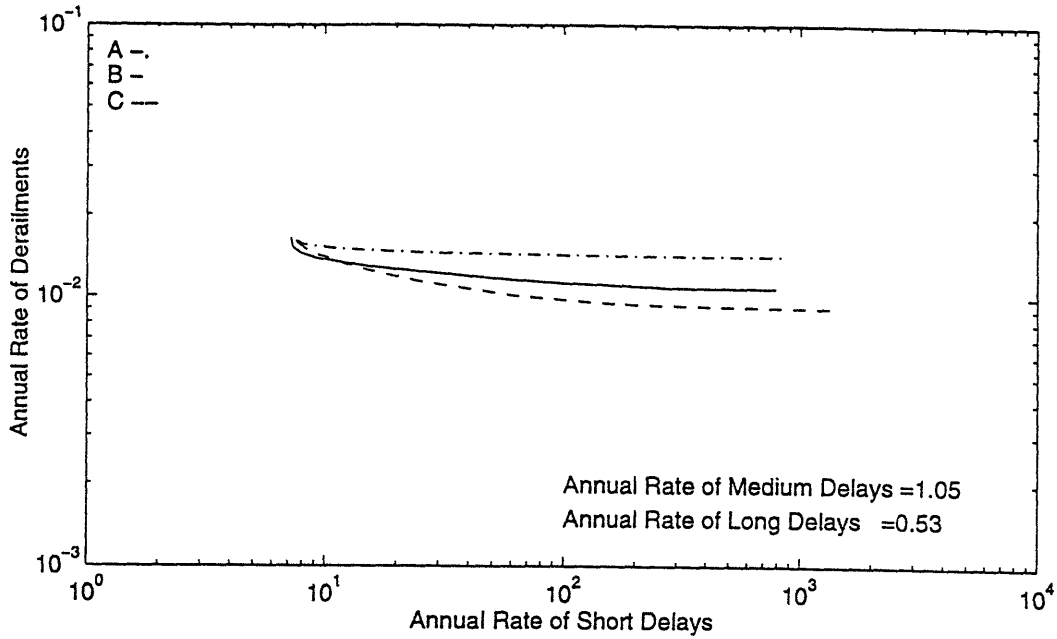


Figure 7.5: (a) Annual rates of derailments and various delays, excluding and including derailment risk due to resumption of operation following short delays, for coastal systems A, B, C and $(S_{at,loc}, S_{a,insp1}, S_{a,insp2})=(80, 160, 240\text{gals})$
 (b) Coastal trigger parameter versus annual rate of short delays, for coastal systems A, B and C and $(S_{at,loc}, S_{a,insp1}, S_{a,insp2})=(80, 160, 240\text{gals})$

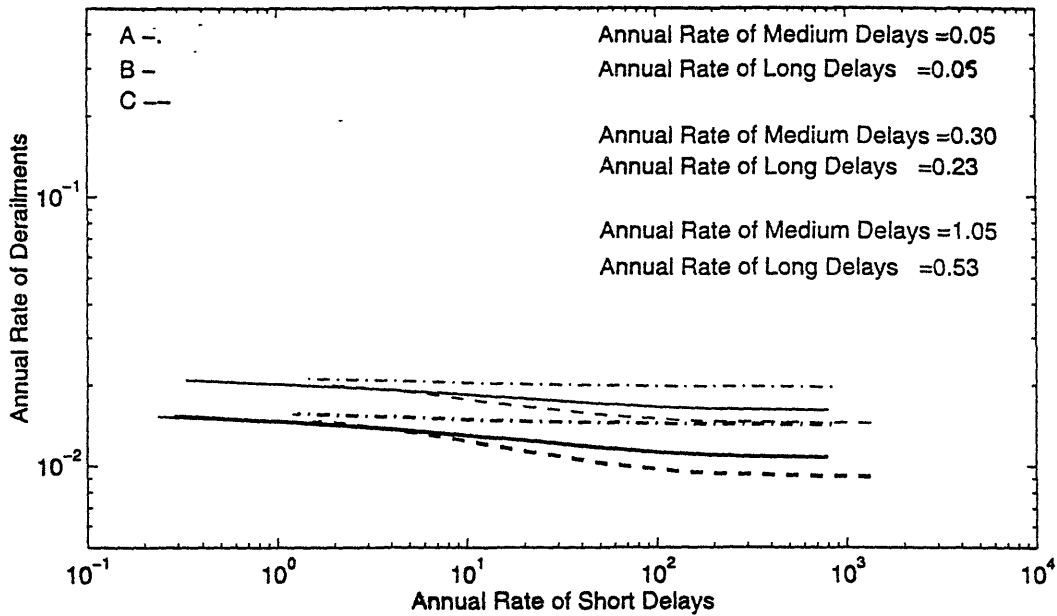
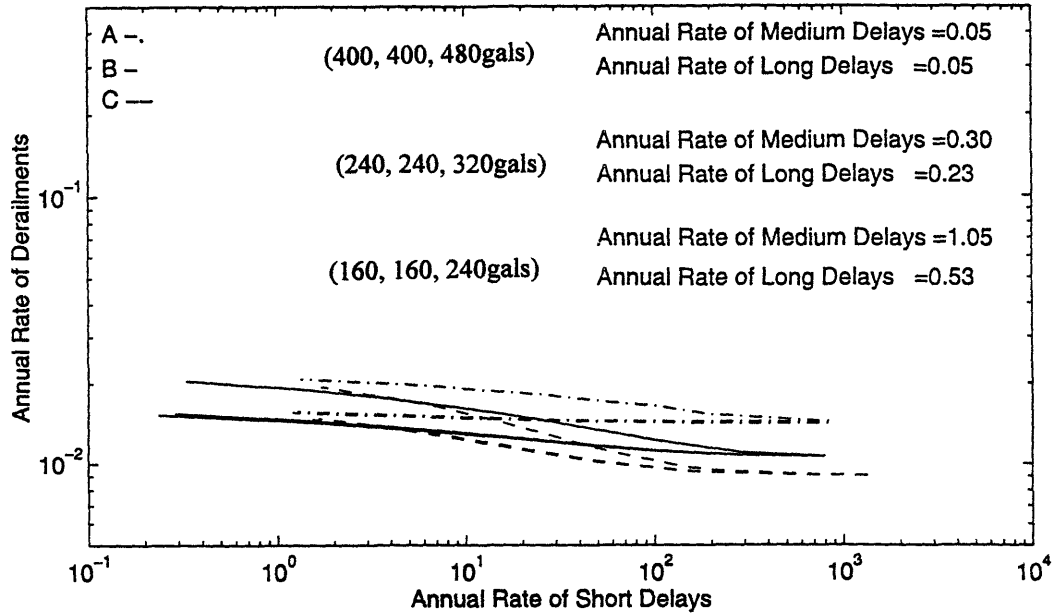


Figure 7.7: Annual rates of derailments and various delays, for coastal systems
 A, B, C and $(S_{at,loc}, S_{a,insp1}, S_{a,insp2}) = (160, 160, 240\text{gals}), (240, 240, 320\text{gals}), (400, 400, 480\text{gals})$.
 (a) excluding derailment risk due to resumption of service following short delays
 (b) including derailment risk due to resumption of service following short delays

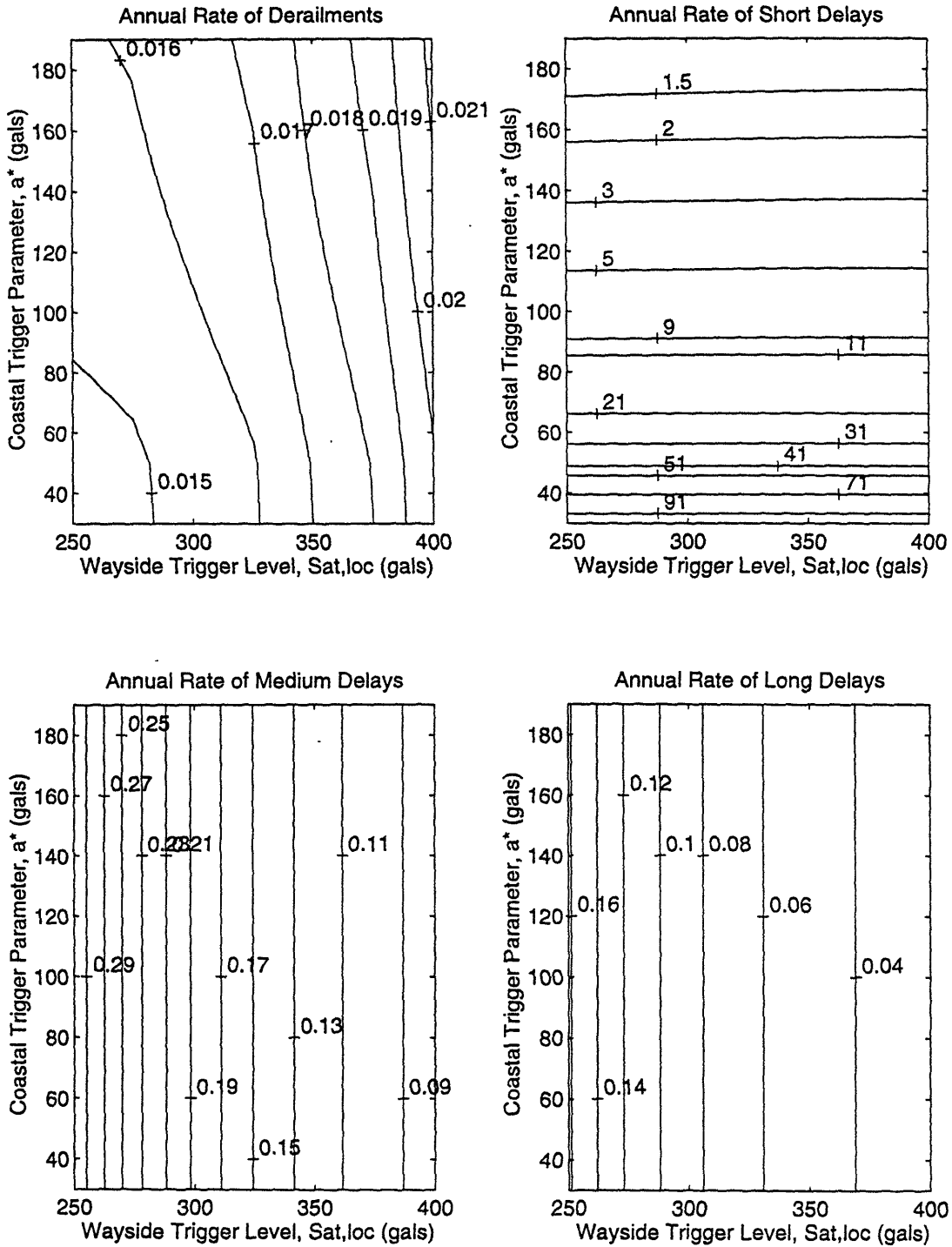


Figure 7.8: Annual rates of events throughout the line, as a function of a^* and $S_{at,loc}$ ($S_{a,insp1}=S_{at,loc}$ and $S_{a,insp2}=S_{a,insp1}+80$ gals), including derailment risk due to resumption of service following short delays, where events are: (a) derailments, (b) short delays, (c) medium delays, (d) long delays.

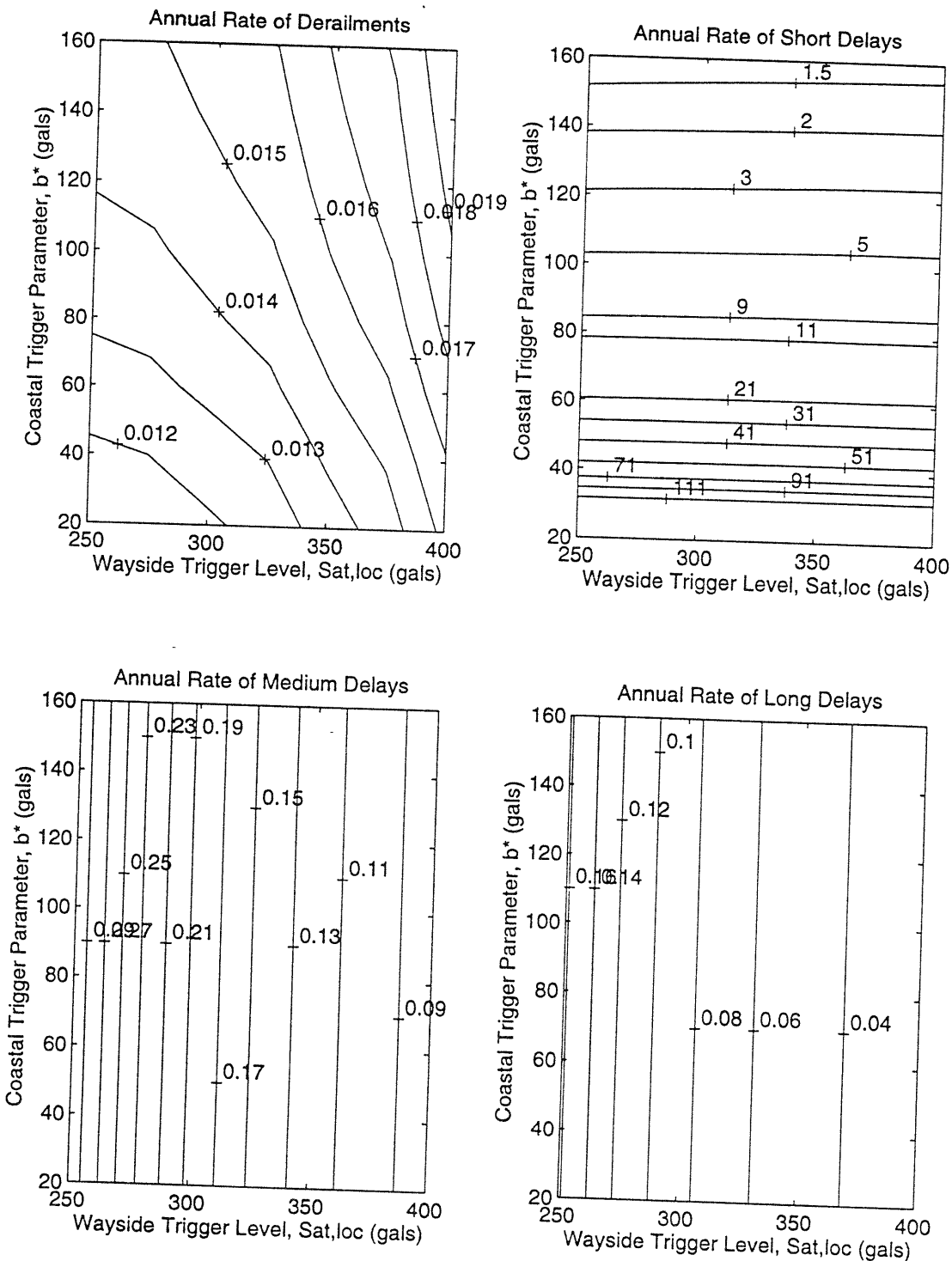


Figure 7.9: Annual rates of events throughout the line, as a function of b^* and $S_{at,loc}$ ($S_{a,insp1}=S_{at,loc}$ and $S_{a,insp2}=S_{a,insp1}+80$ gals), including derailment risk due to resumption of service following short delays, where events are: (a) derailments, (b) short delays, (c) medium delays, (d) long delays.

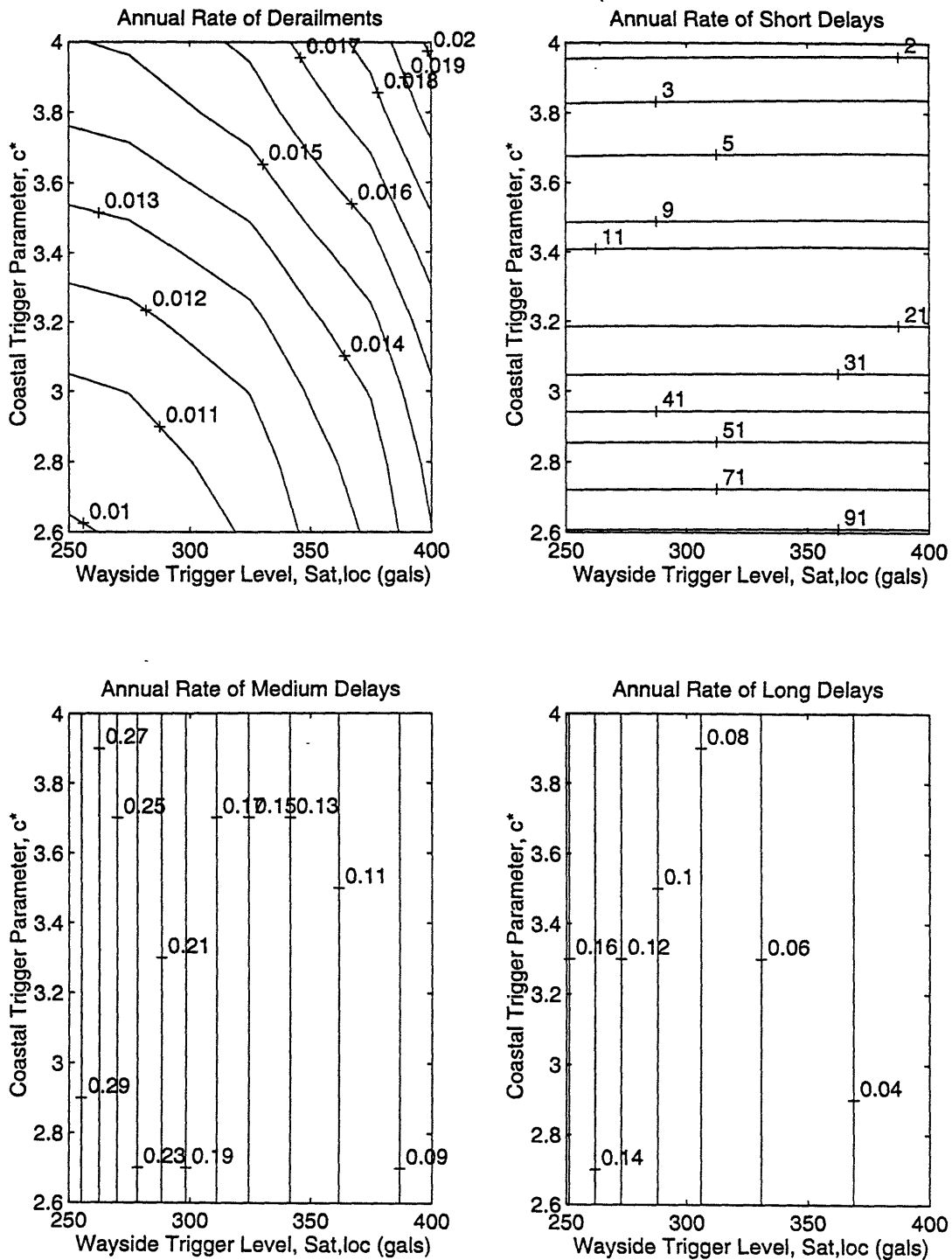


Figure 7.10: Annual rates of events throughout the line, as a function of c^* and $S_{at,loc}$ ($S_{a,insp1}=S_{at,loc}$ and $S_{a,insp2}=S_{a,insp1}+80\text{gals}$), including derailment risk due to resumption of service following short delays, where events are: (a) derailments, (b) short delays, (c) medium delays, (d) long delays.

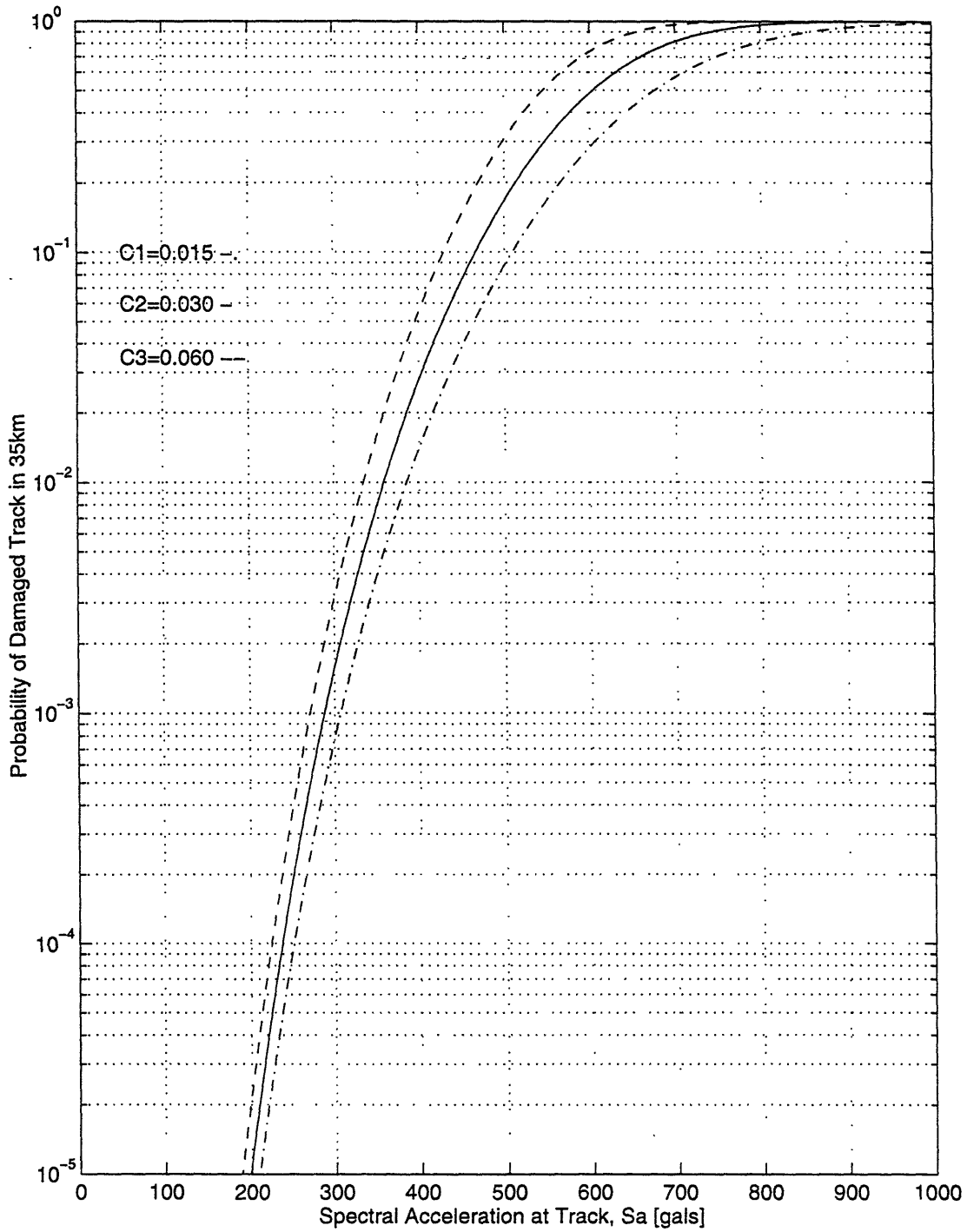


Figure 7.11: Probability of a train meeting damaged track in 35km, given spectral acceleration at the track, for $c_1 = 0.015, 0.03, 0.06$, i.e. a reasonable range of spatial clustering of damage.

Chapter 8

Conclusions

This study investigated the effectiveness of the current Seismic Early Warning System (SEWS) for the Tohoku Shinkansen and proposed alternatives for its future operation. The early warning system is composed of a set of accelerometers along the track (wayside system) and a set of accelerometers along the eastern coast of Honshu (coastal system), halfway between the track and the most dangerous offshore seismic sources. Each accelerometer of the wayside network may cause emergency braking of all trains within the track segment that it controls (total of 26 segments). In this way, trains do not continue travelling along potentially damaged tracks and thus the risk of derailment is reduced. The purpose of the coastal system is to further reduce the distance that trains travel over potentially damaged tracks by ordering emergency braking before the strong phase of ground motion arrives at the track. The current performance of the early warning system has been found to be sub-optimal. To improve it we have studied the effect of changing three characteristics of the early warning system: (1) the mode of operation of the coastal system, (2) the intensity parameter used at the wayside to make decisions about train stopping, inspection procedures and resumption of service and (3) the trigger levels for both the wayside and the coastal systems. Regarding the first characteristic, three alternative coastal systems (A, B and C) were considered. System A is the current system for which each coastal accelerometer controls a prespecified track section. Systems B and C allow any of the coastal accelerometers to cause emergency braking of trains anywhere along the Tohoku line, if the level of ground shaking calls for such an action. The difference between systems B and C is that the latter assumes that at the location of each of the coastal accelerometers there is the potential for issuing an earlier warning, i.e. upon the arrival of the P waves. A system that is capable of this early operation is the UrEDAS system (Nakamura, 1988 and 1989), which is based on real-

- 1) The estimated rate of derailments along the entire Tokyo-Morioka line under current operation of the SEWS system is 0.017 events/year excluding the risk during the resumption of service after short delays and about 0.033 if that additional risk is included. These values correspond roughly to 2-3 derailments occurring every 100 years.
- 2) For the present low trigger horizontal acceleration of the wayside system (40gals), the rate of derailments is insensitive to the type of coastal system. Under very conservative settings of the coastal parameters, coastal system B could reduce the risk of derailment by about 50% relative to system A, and system C could potentially reduce the risk by an additional 10%. These benefits are smaller for realistic settings of the coastal system parameters. Even smaller percentile differences among the three coastal systems are found if the risk of derailment after short delays is included; see Figure 6.1.
- 3) The setting of the coastal system may influence by several orders of magnitude the frequency of short delays. On the other hand, the coastal system does not affect the rate of medium and long delays; see Figure 6.1.
- 4) The current low setting of the trigger acceleration for the wayside system is the primary cause for the reduction of derailment risk by the present SEWS system. The track inspection levels determine the rates of medium and long delays; see Figure 6.1.

Regarding the decomposition of the annual rates by earthquake magnitude, seismic source and epicentral distance and the distribution of these rates along the Tohoku line, we have found that :

- 1) Derailments are caused for the most part by earthquake magnitudes from 7 to 8.5. Long, medium and short delays are caused mainly by earthquakes of magnitudes 7 ± 0.5 , 6.5 ± 0.5 and 5.5 ± 0.5 respectively; see Figure 6.2.
- 2) Most undesired events (derailments and various delays) are expected to occur within operational segments 12 through 16. Such events are most infrequent in operational segments 18 through 21. The variability of the risk along the Tohoku line is influenced mainly by the local soil conditions and by the fraction of track that runs in tunnels. An

additional factor is the traffic load and the proximity of the line to the main seismic sources; see Figures 6.2 and 6.3.

3) Seismic sources 6 and 8 contribute the most to the annual rate of all undesired events, whereas sources 1, 5, 7, 11, 15 contribute the least. These contributions are the combined effects of the proximity of the sources to the track and their seismic activity; see Figures 4.2 and 6.2.

4) Derailments and long delays are mostly caused by earthquakes with epicentral locations about 130 km from the track. The corresponding predominant epicentral distances for medium and short delays are around 150 and 160 km respectively; see Figure 6.2.

Seismic risk was found to be very sensitive to the value of the attenuation coefficients, the seismic fragility of the viaduct structure and the soil classification along the Tohoku line. More precisely :

1) The annual rates of derailment and long delays are very sensitive (factor of influence up to 8 and 3.6, respectively) to the form of the attenuation equation of earthquake ground motion, while the attenuation law affects marginally the rates of medium and short delays; see Figure 6.5.

2) The seismic fragility of the viaduct structure is very influential on the estimated rate of derailment. The fragility model is composed of various parameters. The most influential are the relative displacement of the viaduct deck at yielding, δ_y , and the uncertainty on the ultimate resistance in terms of spectral acceleration, σ_{lnR} , (up to factors of 4 and 3.5, respectively). The ductility ratio at failure, μ , and the spatial clustering of damaged track sections controlled by the parameter c_1 have moderate effects; see Figures 6.6 and 6.7.

3) The rates of derailment and long delays are very sensitive to the soil conditions along the Tohoku line (up to factors of 7 and 3, respectively), whereas the rates of medium and short delays are affected less by such conditions; see Figure 6.9a.

In contrast, seismic risk is not significantly sensitive to the speed of Shinkansen trains, to the seismicity parameters and the (M, \underline{x}) estimation accuracy of the UrEDAS system. More specifically, we have found that the speed of the trains has a small effect on the derailment risk. This varies by a factor of 1.3 on average, for either an increase to 300kmh or a decrease to 210kmh of the current operational speed of 245kmh. Moreover, a change in train speed was found not to affect any of the delay rates; see Figure 6.9b. Furthermore, the rate of derailment changes by a factor of about 2 with reasonable variations in the seismicity level, while the rates of various delays are even less sensitive to seismicity; see Figure 6.11. Finally, only the annual rate of short delays is moderately sensitive (potential reduction by 65%) to the magnitude estimation accuracy of the UrEDAS system using P waves. The annual rate of short delays is much less sensitive to the accuracy of estimation of the epicentral location \underline{x} for P waves. The estimation accuracy of the system has unimportant effects on the rate of derailment and does not affect the rates of medium and long delays which are completely controlled by the wayside system. The estimation accuracy of the UrEDAS system using S waves has no notable effect on the values of any of the rates. See Figure 6.12 for an illustration of these results.

Risk based on Scenario Analyses

For earthquakes of different magnitudes with fixed epicentral location, the probabilities of derailment and long delays increase monotonically and considerably with increasing earthquake magnitude. On the other hand, the probabilities of medium and short delays are not monotonic. Although the probabilities of all undesired events (derailments and various delays) show general trends along the line, there are abrupt increases and decreases in their values due mainly to local soil conditions and to the fraction of segment length in tunnels. For system A and for the case of derailments and short delays, these peaks and valleys are also influenced by the fixed assignment of track segments to the coastal stations; see Figure 6.13.

For the expected number of undesired events, as a function of earthquake magnitude and epicentral location, we find that the largest number of derailments would be expected from an offshore earthquake with epicentral location south of Tokyo (around E140°, N35°). A somewhat lower derailment risk is associated with events south-east of Sendai (around E141°30', N38°). These are also the events that cause the largest expected number of long delays; see Figures 6.14 - 6.17.

Optimization of the Seismic Early Warning System

The most beneficial changes to the current early warning systems in order of decreasing importance are:

Operate the wayside system on spectral acceleration S_a rather than peak ground acceleration a_{max} . Doing so reduces significantly the rates of derailments and of various delays. The benefit from changing the intensity parameter of the wayside system from a_{max} to S_a , is especially large if risk from the resumption of service after short delays is included. This is because S_a is a far better indicator of structural damage than a_{max} is; see Figure 7.6.

Set the wayside trigger level equal to the first track inspection level. Doing so reduces significantly the total number of short delays, which are then produced exclusively by the coastal system. In addition, if the coastal system was put out of operation, all short delays would be eliminated; see Figure 7.2.

Increase the wayside trigger and track inspection levels. This action reduces significantly the rates of medium and short delays, increases moderately the rate of derailments, and affects minimally the rate of short delays; see Figure 7.8. The value of the first track inspection level governs the total rate of medium or long delays. The relative allocation of this total rate to medium and long delays depends on the second track inspection level. Therefore, the setting of the second track inspection level should be based on the perceived necessity for on-train versus on-foot inspection of the track, as a function of the

value of S_a recorded at nearby stations. Figure 7.11 should be of aid in making this decision.

Increase the coastal trigger level, which reduces significantly the rate of short delays and increases only moderately the rate of derailments; see Figure 7.8

This study showed that the coastal system is relatively ineffective in reducing earthquake risk. Specifically, Systems B and C have comparable effectiveness and both outperform System A, but the overall benefit of changing the present system to B or C is marginal.

Overall, the recommended changes in the early warning system may reduce the annual rate of derailments by a factor of 2 and the total expected number of delayed trains by a factor of 40 on average; see Table 7.2.

Propagation of Delay along the Tohoku Line

Second order delay time, which is the aggregated delay time from all trains along the line due to the fact that trains are not able to proceed due to stopped or delayed trains ahead, increases the first order delay time by about 30%. First order delay time is the aggregated delay time from all trains along the line ignoring propagation of delay effects and corresponds to the rate of delayed and stopped trains as obtained in Chapters 6 and 7. Including third order delay, which corresponds to train cancellations, increases the first order delay time by a factor of about 2.

Future Work

The sensitivity results presented in Chapter 6 and summarized above point at the need to make a more detailed evaluation of several factors that affect the seismic risk of the Tohoku Shinkansen line. Priority areas of investigation appear to be : (a) the form and

coefficients of the attenuation law. (b) the seismic fragility of the viaduct structure, in particular the relative displacement at yielding, δ_y , the ductility ratio at yielding, μ , and the uncertainty on the seismic resistance, σ_{lnR} , and (c) the soil conditions and their potential seismic amplification along the line.

The present study is focused on offshore seismicity. Incorporation of inland seismicity would produce more accurate estimates of the total seismic risk, especially in the Tokyo region. A more detailed analysis of propagation of delays throughout the Tohoku Shinkansen is advisable. Such a study could take into account actual trains schedules and train and station locations.

References

- Annaka T., Nozawa Y. (1988), "A Probabilistic Model for Seismic Hazard Estimation in the Kanto District", Proceedings, Ninth World Conference on Earthquake Engineering, Tokyo, Japan, Vol II, article 2-1-13, pp 107 - 112.
- Boore D. M., Joyner W. B., Fumal T. E., (1993), "Estimation of Response Spectra and Peak Acceleration from Western North American Earthquakes: An Interim Report", U.S.G.S. Open - File Report 93 - 509, 72 pp.
- Der Kiureghian A., Crempien J. (1989), "An Evolutionary Model for Earthquake Ground Motion", Structural Safety, No 6, pp 235 - 246.
- Ejiri J., Goto Y. (1988), "Prediction of Earthquake Accelerograms of Stiff Ground Based on Nonstationary AR-MA Process", Proceedings, Ninth World Conference on Earthquake Engineering, Tokyo, Japan, Vol II, article 3-7-6, pp 807 - 812.
- Fujiwara T., Nakamura Y. (1980), "New Automatic Train Stopping System During Earthquake", Proceedings, Seventh World Conference on Earthquake Engineering, Constantinople, Turkey, Part II, pp 106 - 112.
- Fukushima Y., Tanaka T., Kataoka S. (1988), "A New Attenuation Relationship for Peak Ground Acceleration Derived from Strong - Motion Accelerograms", Proceedings, Ninth World Conference on Earthquake Engineering, Tokyo, Japan, Vol II, pp 343 - 348.
- Heaton T. (1985), "A Model for a Seismic Computerized Alert Network". Science, Volume 228, pp 987 - 990.
- Kanda J., Iwasaki R., Kitada Y. (1988), "Seismic Hazard Estimation Based on Earthquake Recurrence Rate in Comparison with Empirical Extreme value Distribution", Proceedings, Ninth World Conference on Earthquake Engineering, Tokyo, Japan, Vol II, article 2-1-9, pp 83 - 88.
- Kawashima K., Aizawa K., Takahashi K. (1984), "Attenuation of Peak Ground Motion and Absolute Acceleration Response Spectra", Proceedings, Eighth World Conference on Earthquake Engineering, San Fransisco, U.S.A., Vol 2, pp 257-264.
- Kobayashi K., Abe Y., Amaike F. (1988), "Magnitude Dependence and Attenuation Characteristics of Peak Ground Acceleration", Proceedings, Ninth World Conference on Earthquake Engineering, Tokyo. Japan. Vol II, article 3-2-11, pp 331 - 336.

- Murakami M., Penzien J. (1975), "Nonlinear Response Spectra for Probabilistic Seismic Design and Damage Assessment of Reinforced Concrete Structures", UC Berkeley, Report No. EERC 75-38, November.
- Nakamura Y. (1988), "On the Urgent Earthquake Detection and Alarm System (UrEDAS)", Proceedings, Ninth World Conference on Earthquake Engineering, Tokyo, Japan, Vol III, article 13-2-12.
- Nakamura Y. (1989), "Earthquake Alarm System for Japan Railways", Japanese Railway Engineering, No 109, March.
- NCEER Bulletin (1995), "Preliminary Report from the Hyogo-ken Nambu Earthquake of January 17, 1995", Vol 9, Number 1, January.
- Osteraas J., Krawinkler H. (1990), "Seismic Design Based on Strength of Structures", Proceedings, Fourth U.S. National Conference on Earthquake Engineering, Palm Springs, California, pp 955-964.
- NIBS (1994), "Development of a Standardized Earthquake Loss Estimation Methodology", Draft Technical Manual (95% Submittal, RMS Inc.), Vol II-7, California, pp 33 - 52.
- Takada T., Hwang H.H.M., Shinozuka M. (1988), "Response Modification Factor for Multiple-Degree-of-Freedom Systems", Proceedings, Ninth World Conference on Earthquake Engineering, Tokyo, Japan, Vol V, pp 129-134.
- Takada T., Ghosn M., Shinozuka M., (1989), "Response Modification Factors for Buildings and Bridges", Proceedings, Fifth International Conference on Structural Safety and Reliability, ICOSSAR '89, San Francisco, California.
- Takemura M., Ishida H., Amano A., Mizutani M. (1989), "A Seismic PRA Procedure in Japan and Its Application to a Building Performance Safety Estimation", Proceedings, Fifth International Conference on Structural Safety and Reliability, pp 621 - 628.
- Tomatsu Y., Katayama T. (1988), "An On-Line Graphic Computer Program <ERISA-G> and its Application to Seismic Macro-Zonation of Japan", Proceedings, Ninth World Conference on Earthquake Engineering, Tokyo, Japan. Vol II, article 2-2-10, pp 181 - 186.
- Umino N., Sacks S. (1993), "Magnitude-Frequency Relations for Northeastern Japan", Bulletin of the Seismological Society of America, Vol. 83, No. 5, pp 1492 - 1506.

Utsu T. (1974), "Space - Time Pattern of Large Earthquakes Off the Pacific Coast of the Japanese Islands", Journal of Physics of the Earth, Vol 22, pp 325 - 342.

Yamabe K., Kanai K. (1988), "An Empirical Formula on the Attneuation of the Maximum Acceleration of Earthquake Motions", Proceedings, Ninth World Conference on Earthquake Engineering, Tokyo, Japan. Vol II, article 3-2-12, pp 337 - 342.

Appendix I

Additional Tables and Figures

Appendix I contains the following: (a) tables that give the point estimates of the trigger parameter $\gamma(i,s,R)$ of System B (see Chapter 3) and, (b) figures that are qualitatively similar to the ones presented in Chapters 6 and 7. These are presented for a more complete interpretation of the performance of the early warning system for the Tohoku Shinkansen. The figures convey the following main results: (a) Changing from the current coastal system A to coastal systems B or C leads to a more uniform distribution of short delays along the line; see Figures I-1 and I-2, (b) Changing from peak ground acceleration to response spectrum acceleration as the measure of seismic intensity at the wayside system increases the contribution of higher earthquake magnitudes to the rates of all undesired events (derailments and various delays); see Figures I-3, I-4 and I-5, (c) Including the risk of derailments after resumption of trains following short delays reduces the differences in performance of different coastal systems; see Figures I-6 through I-10 and (d) Changing from the current coastal system A to coastal systems B and C alleviates most abrupt “jumps” in the conditional probability of short delays along the line, as this is no longer a function of the scope of control of the coastal accelerometers; see Figures I-11 and I-12.

i=1	i=2	i=3	i=4	i=5	i=6	i=7	i=8
3.84	2.57	1.75	1.42	1.12	0.96	0.73	0.61
3.82	2.55	1.74	1.41	1.11	0.96	0.72	0.61
3.78	2.53	1.72	1.40	1.10	0.95	0.71	0.60
3.71	2.48	1.69	1.37	1.08	0.93	0.70	0.59
3.61	2.41	1.65	1.33	1.05	0.91	0.68	0.58
3.47	2.32	1.58	1.28	1.01	0.87	0.66	0.55
3.32	2.22	1.52	1.23	0.97	0.83	0.63	0.53
3.17	2.12	1.45	1.18	0.93	0.80	0.60	0.51
3.03	2.03	1.39	1.13	0.89	0.77	0.58	0.49
2.89	1.94	1.33	1.08	0.85	0.73	0.55	0.47
2.10	1.41	0.97	0.78	0.62	0.53	0.40	0.34
2.63	1.76	1.21	0.98	0.77	0.67	0.50	0.43
2.50	1.68	1.15	0.94	0.74	0.64	0.48	0.41
2.36	1.59	1.09	0.89	0.70	0.60	0.46	0.38
2.21	1.49	1.02	0.83	0.66	0.57	0.43	0.36
2.12	1.43	0.98	0.80	0.63	0.54	0.41	0.35
2.03	1.37	0.94	0.77	0.61	0.52	0.39	0.33
3.50	2.36	1.63	1.32	1.05	0.90	0.68	0.58
3.34	2.25	1.56	1.27	1.00	0.86	0.65	0.55
3.15	2.13	1.47	1.20	0.95	0.82	0.62	0.52
2.90	1.96	1.36	1.11	0.88	0.76	0.57	0.48
1.50	1.02	0.71	0.58	0.46	0.39	0.30	0.25
1.09	0.74	0.52	0.42	0.33	0.29	0.22	0.18
1.36	0.93	0.64	0.52	0.42	0.36	0.27	0.23
1.00	0.69	0.48	0.39	0.31	0.27	0.20	0.17
1.30	0.89	0.62	0.50	0.40	0.34	0.26	0.22

Table I-1: System B: values of $\gamma(i, s, R)$ for earthquakes originating from “sector of origin” $R=1$.
[Columns: coastal station, $i=1-8$; Rows: segment, $s=1-26$]

i=1	i=2	i=3	i=4	i=5	i=6	i=7	i=8
2.13	2.57	2.09	1.71	1.24	1.08	0.78	0.61
2.12	2.57	2.08	1.71	1.24	1.08	0.78	0.61
2.11	2.55	2.07	1.70	1.24	1.07	0.78	0.61
2.07	2.50	2.03	1.67	1.21	1.05	0.76	0.60
2.01	2.43	1.97	1.62	1.18	1.02	0.74	0.58
1.92	2.33	1.89	1.55	1.13	0.98	0.71	0.56
1.84	2.22	1.80	1.48	1.08	0.93	0.68	0.53
1.75	2.12	1.72	1.41	1.03	0.89	0.65	0.51
1.68	2.03	1.65	1.35	0.98	0.85	0.62	0.49
1.59	1.92	1.56	1.28	0.93	0.81	0.59	0.46
1.14	1.38	1.12	0.92	0.67	0.58	0.42	0.33
1.42	1.72	1.40	1.15	0.83	0.72	0.53	0.41
1.36	1.64	1.33	1.10	0.80	0.69	0.50	0.39
1.29	1.55	1.26	1.04	0.76	0.66	0.48	0.37
1.20	1.44	1.17	0.97	0.70	0.61	0.44	0.35
1.14	1.37	1.11	0.92	0.67	0.58	0.42	0.33
1.08	1.31	1.06	0.88	0.64	0.55	0.40	0.32
1.89	2.27	1.85	1.53	1.11	0.97	0.70	0.55
1.83	2.20	1.80	1.48	1.08	0.94	0.68	0.53
1.74	2.10	1.71	1.41	1.03	0.90	0.65	0.51
1.63	1.97	1.61	1.33	0.97	0.84	0.61	0.48
0.88	1.06	0.87	0.72	0.52	0.46	0.33	0.26
0.67	0.81	0.66	0.55	0.40	0.35	0.25	0.20
0.87	1.05	0.86	0.71	0.52	0.45	0.33	0.26
0.66	0.80	0.66	0.55	0.40	0.35	0.25	0.20
0.88	1.07	0.88	0.73	0.53	0.46	0.34	0.26

Table I-2: System B: values of $\gamma(i, s, R)$ for earthquakes originating from “sector of origin” $R=2$.
[Columns: coastal station, $i=1-8$; Rows: segment, $s=1-26$]

i=1	i=2	i=3	i=4	i=5	i=6	i=7	i=8
1.47	2.54	3.44	2.61	1.56	1.27	0.82	0.61
1.46	2.53	3.42	2.60	1.55	1.27	0.82	0.60
1.45	2.51	3.40	2.59	1.54	1.26	0.81	0.60
1.42	2.45	3.31	2.52	1.50	1.23	0.79	0.59
1.37	2.36	3.19	2.43	1.45	1.18	0.76	0.56
1.29	2.23	3.01	2.29	1.37	1.12	0.72	0.53
1.22	2.10	2.83	2.16	1.29	1.06	0.68	0.50
1.15	1.98	2.66	2.03	1.22	1.00	0.65	0.48
1.09	1.87	2.50	1.92	1.15	0.94	0.61	0.45
1.01	1.73	2.32	1.78	1.07	0.88	0.57	0.42
0.72	1.22	1.63	1.26	0.76	0.62	0.40	0.30
0.88	1.49	1.99	1.53	0.93	0.76	0.49	0.36
0.83	1.41	1.87	1.44	0.87	0.72	0.47	0.34
0.77	1.31	1.73	1.34	0.82	0.67	0.44	0.32
0.70	1.19	1.56	1.22	0.74	0.61	0.40	0.29
0.65	1.10	1.44	1.13	0.69	0.57	0.37	0.27
0.61	1.03	1.34	1.05	0.65	0.53	0.35	0.26
1.06	1.78	2.31	1.82	1.12	0.93	0.61	0.45
1.04	1.73	2.25	1.78	1.10	0.91	0.60	0.44
0.99	1.65	2.14	1.70	1.05	0.87	0.57	0.42
0.95	1.58	2.04	1.63	1.01	0.84	0.55	0.41
0.52	0.87	1.12	0.90	0.56	0.46	0.30	0.22
0.41	0.68	0.88	0.71	0.44	0.36	0.24	0.18
0.56	0.94	1.22	0.98	0.60	0.50	0.33	0.24
0.45	0.74	0.97	0.78	0.48	0.40	0.26	0.19
0.62	1.03	1.35	1.08	0.66	0.55	0.36	0.26

Table I-3: System B: values of $\gamma(i, s, R)$ for earthquakes originating from “sector of origin” $R=3$.
[Columns: coastal station, $i=1-8$; Rows: segment, $s=1-26$]

i=1	i=2	i=3	i=4	i=5	i=6	i=7	i=8
0.89	1.37	2.22	2.95	1.84	1.54	0.88	0.60
0.89	1.37	2.21	2.94	1.84	1.54	0.88	0.60
0.88	1.36	2.20	2.93	1.83	1.53	0.87	0.59
0.86	1.33	2.14	2.85	1.78	1.49	0.85	0.58
0.82	1.27	2.05	2.72	1.70	1.43	0.82	0.56
0.77	1.19	1.92	2.55	1.59	1.34	0.77	0.52
0.72	1.12	1.80	2.37	1.49	1.25	0.72	0.49
0.68	1.05	1.68	2.22	1.39	1.17	0.67	0.46
0.64	0.99	1.58	2.08	1.31	1.10	0.63	0.43
0.59	0.91	1.45	1.90	1.20	1.01	0.58	0.40
0.41	0.63	1.01	1.32	0.84	0.71	0.41	0.28
0.50	0.77	1.23	1.60	1.02	0.86	0.50	0.34
0.48	0.74	1.16	1.52	0.97	0.82	0.48	0.32
0.45	0.70	1.09	1.42	0.92	0.78	0.45	0.31
0.42	0.64	1.00	1.30	0.84	0.72	0.42	0.28
0.39	0.60	0.93	1.20	0.79	0.67	0.39	0.27
0.37	0.57	0.88	1.14	0.75	0.64	0.38	0.25
0.67	1.02	1.59	2.05	1.35	1.16	0.68	0.46
0.68	1.04	1.61	2.08	1.38	1.18	0.69	0.47
0.70	1.06	1.65	2.14	1.42	1.22	0.71	0.48
0.71	1.08	1.67	2.18	1.45	1.25	0.72	0.49
0.40	0.62	0.96	1.26	0.84	0.72	0.42	0.28
0.34	0.51	0.80	1.05	0.70	0.60	0.34	0.23
0.47	0.72	1.14	1.50	0.99	0.85	0.49	0.33
0.39	0.59	0.93	1.23	0.81	0.69	0.40	0.27
0.54	0.82	1.30	1.73	1.14	0.97	0.55	0.38

Table I-4: System B: values of $\gamma(i, s, R)$ for earthquakes originating from “sector of origin” $R=4$.
 [Columns: coastal station, $i=1-8$; Rows: segment, $s=1-26$]

i=1	i=2	i=3	i=4	i=5	i=6	i=7	i=8
0.56	0.81	1.31	2.14	2.63	2.35	0.92	0.58
0.55	0.80	1.30	2.13	2.62	2.34	0.92	0.58
0.55	0.80	1.29	2.11	2.60	2.32	0.91	0.57
0.53	0.77	1.24	2.04	2.51	2.24	0.88	0.55
0.50	0.73	1.17	1.93	2.37	2.11	0.83	0.52
0.46	0.67	1.08	1.77	2.17	1.94	0.76	0.48
0.42	0.61	0.98	1.61	1.98	1.77	0.70	0.44
0.38	0.56	0.90	1.48	1.81	1.62	0.64	0.40
0.35	0.51	0.83	1.36	1.67	1.49	0.59	0.37
0.31	0.46	0.74	1.21	1.48	1.33	0.52	0.33
0.21	0.31	0.50	0.81	1.00	0.89	0.35	0.22
0.25	0.37	0.60	0.98	1.20	1.07	0.42	0.27
0.25	0.36	0.58	0.94	1.15	1.04	0.41	0.26
0.24	0.35	0.56	0.92	1.13	1.01	0.40	0.25
0.23	0.33	0.54	0.88	1.08	0.97	0.38	0.24
0.22	0.32	0.52	0.85	1.04	0.94	0.37	0.23
0.22	0.32	0.52	0.85	1.04	0.94	0.37	0.23
0.41	0.59	0.95	1.56	1.91	1.73	0.68	0.43
0.45	0.65	1.05	1.72	2.11	1.91	0.75	0.47
0.50	0.73	1.17	1.91	2.35	2.12	0.84	0.52
0.54	0.79	1.27	2.07	2.55	2.30	0.91	0.57
0.34	0.49	0.79	1.29	1.58	1.43	0.56	0.35
0.29	0.42	0.67	1.10	1.36	1.22	0.48	0.30
0.41	0.60	0.97	1.59	1.96	1.76	0.69	0.43
0.34	0.50	0.81	1.32	1.63	1.46	0.57	0.36
0.48	0.70	1.13	1.85	2.28	2.05	0.81	0.50

Table I-5: System B: values of $\gamma(i, s, R)$ for earthquakes originating from “sector of origin” $R=5$.
[Columns: coastal station, $i=1-8$; Rows: segment, $s=1-26$]

i=1	i=2	i=3	i=4	i=5	i=6	i=7	i=8
0.41	0.55	0.78	1.06	1.31	1.87	1.10	0.59
0.40	0.55	0.78	1.06	1.31	1.86	1.10	0.59
0.41	0.55	0.78	1.06	1.31	1.87	1.10	0.59
0.40	0.55	0.77	1.04	1.29	1.84	1.09	0.58
0.38	0.52	0.73	0.99	1.22	1.74	1.03	0.55
0.36	0.49	0.69	0.93	1.14	1.61	0.96	0.52
0.34	0.46	0.64	0.87	1.07	1.51	0.91	0.49
0.32	0.44	0.62	0.83	1.02	1.44	0.87	0.47
0.31	0.42	0.59	0.80	0.98	1.38	0.84	0.45
0.29	0.39	0.55	0.75	0.91	1.29	0.79	0.42
0.21	0.28	0.40	0.53	0.65	0.92	0.57	0.30
0.27	0.36	0.51	0.68	0.83	1.19	0.74	0.39
0.27	0.36	0.51	0.69	0.84	1.20	0.75	0.40
0.28	0.38	0.53	0.71	0.87	1.25	0.78	0.41
0.29	0.39	0.54	0.73	0.90	1.31	0.82	0.43
0.29	0.39	0.55	0.74	0.92	1.34	0.84	0.44
0.29	0.40	0.56	0.75	0.93	1.36	0.85	0.45
0.55	0.74	1.04	1.40	1.74	2.56	1.60	0.83
0.59	0.80	1.12	1.51	1.89	2.78	1.73	0.90
0.63	0.86	1.20	1.62	2.04	3.01	1.86	0.97
0.67	0.91	1.27	1.72	2.17	3.21	1.98	1.03
0.40	0.54	0.76	1.03	1.30	1.93	1.19	0.62
0.33	0.45	0.63	0.85	1.08	1.61	0.98	0.51
0.46	0.63	0.89	1.20	1.52	2.26	1.38	0.72
0.38	0.51	0.72	0.98	1.24	1.84	1.12	0.58
0.52	0.71	1.00	1.35	1.71	2.54	1.55	0.80

Table I-6: System B: values of $\gamma(i, s, R)$ for earthquakes originating from “sector of origin” R=6.
[Columns: coastal station, i=1-8; Rows: segment, s=1-26]

i=1	i=2	i=3	i=4	i=5	i=6	i=7	i=8
0.20	0.25	0.31	0.38	0.47	0.64	1.30	0.69
0.20	0.25	0.32	0.38	0.47	0.65	1.31	0.69
0.21	0.26	0.33	0.40	0.49	0.67	1.36	0.72
0.22	0.27	0.34	0.42	0.51	0.70	1.44	0.76
0.23	0.28	0.35	0.42	0.52	0.71	1.47	0.78
0.23	0.28	0.35	0.42	0.52	0.71	1.47	0.79
0.23	0.28	0.35	0.43	0.52	0.72	1.49	0.81
0.24	0.29	0.37	0.44	0.54	0.74	1.56	0.85
0.25	0.31	0.39	0.47	0.57	0.78	1.66	0.90
0.26	0.32	0.40	0.48	0.59	0.81	1.74	0.95
0.20	0.25	0.31	0.38	0.46	0.63	1.37	0.74
0.27	0.34	0.42	0.51	0.63	0.85	1.86	1.01
0.29	0.35	0.44	0.53	0.66	0.89	1.96	1.07
0.31	0.38	0.47	0.57	0.70	0.96	2.11	1.14
0.33	0.40	0.50	0.61	0.75	1.02	2.27	1.22
0.35	0.43	0.53	0.64	0.79	1.08	2.40	1.29
0.35	0.44	0.54	0.66	0.81	1.11	2.47	1.33
0.67	0.82	1.02	1.23	1.53	2.08	4.66	2.50
0.71	0.87	1.09	1.31	1.62	2.21	4.95	2.65
0.74	0.91	1.14	1.38	1.71	2.33	5.23	2.79
0.78	0.96	1.20	1.44	1.79	2.44	5.49	2.92
0.46	0.56	0.70	0.85	1.05	1.43	3.22	1.71
0.37	0.45	0.57	0.68	0.85	1.16	2.60	1.38
0.50	0.62	0.78	0.94	1.16	1.59	3.57	1.89
0.40	0.49	0.62	0.75	0.93	1.27	2.85	1.51
0.55	0.67	0.84	1.01	1.26	1.72	3.87	2.04

Table I-7: System B: values of $\gamma(i, s, R)$ for earthquakes originating from “sector of origin” $R=7$.
 [Columns: coastal station, $i=1-8$; Rows: segment, $s=1-26$]

i=1	i=2	i=3	i=4	i=5	i=6	i=7	i=8
0.13	0.15	0.18	0.20	0.25	0.30	0.54	0.99
0.13	0.15	0.18	0.21	0.25	0.31	0.55	1.02
0.14	0.16	0.19	0.21	0.26	0.32	0.58	1.06
0.14	0.17	0.20	0.23	0.28	0.35	0.62	1.14
0.16	0.18	0.22	0.25	0.30	0.37	0.67	1.24
0.17	0.19	0.23	0.27	0.33	0.40	0.72	1.34
0.18	0.21	0.25	0.29	0.36	0.44	0.80	1.48
0.20	0.24	0.28	0.33	0.40	0.49	0.89	1.66
0.23	0.26	0.31	0.36	0.44	0.54	0.99	1.85
0.24	0.29	0.34	0.39	0.48	0.59	1.07	2.01
0.20	0.23	0.28	0.32	0.39	0.48	0.88	1.65
0.28	0.33	0.39	0.45	0.55	0.68	1.23	2.32
0.30	0.35	0.42	0.48	0.59	0.72	1.32	2.49
0.32	0.37	0.44	0.51	0.63	0.77	1.41	2.67
0.34	0.40	0.48	0.55	0.68	0.83	1.51	2.86
0.37	0.43	0.51	0.58	0.72	0.88	1.62	3.06
0.38	0.44	0.53	0.60	0.75	0.92	1.67	3.17
0.71	0.83	0.99	1.14	1.41	1.73	3.16	6.00
0.75	0.88	1.04	1.20	1.48	1.82	3.33	6.31
0.78	0.91	1.09	1.25	1.55	1.90	3.47	6.59
0.81	0.95	1.13	1.30	1.61	1.98	3.62	6.88
0.47	0.55	0.66	0.76	0.94	1.15	2.11	4.00
0.38	0.44	0.52	0.60	0.75	0.92	1.68	3.19
0.51	0.60	0.71	0.82	1.01	1.24	2.28	4.33
0.40	0.47	0.56	0.65	0.80	0.98	1.80	3.43
0.54	0.63	0.75	0.87	1.08	1.32	2.43	4.61

Table I-8: System B: values of $\gamma(i, s, R)$ for earthquakes originating from “sector of origin” $R=8$.
[Columns: coastal station, $i=1-8$; Rows: segment, $s=1-26$]

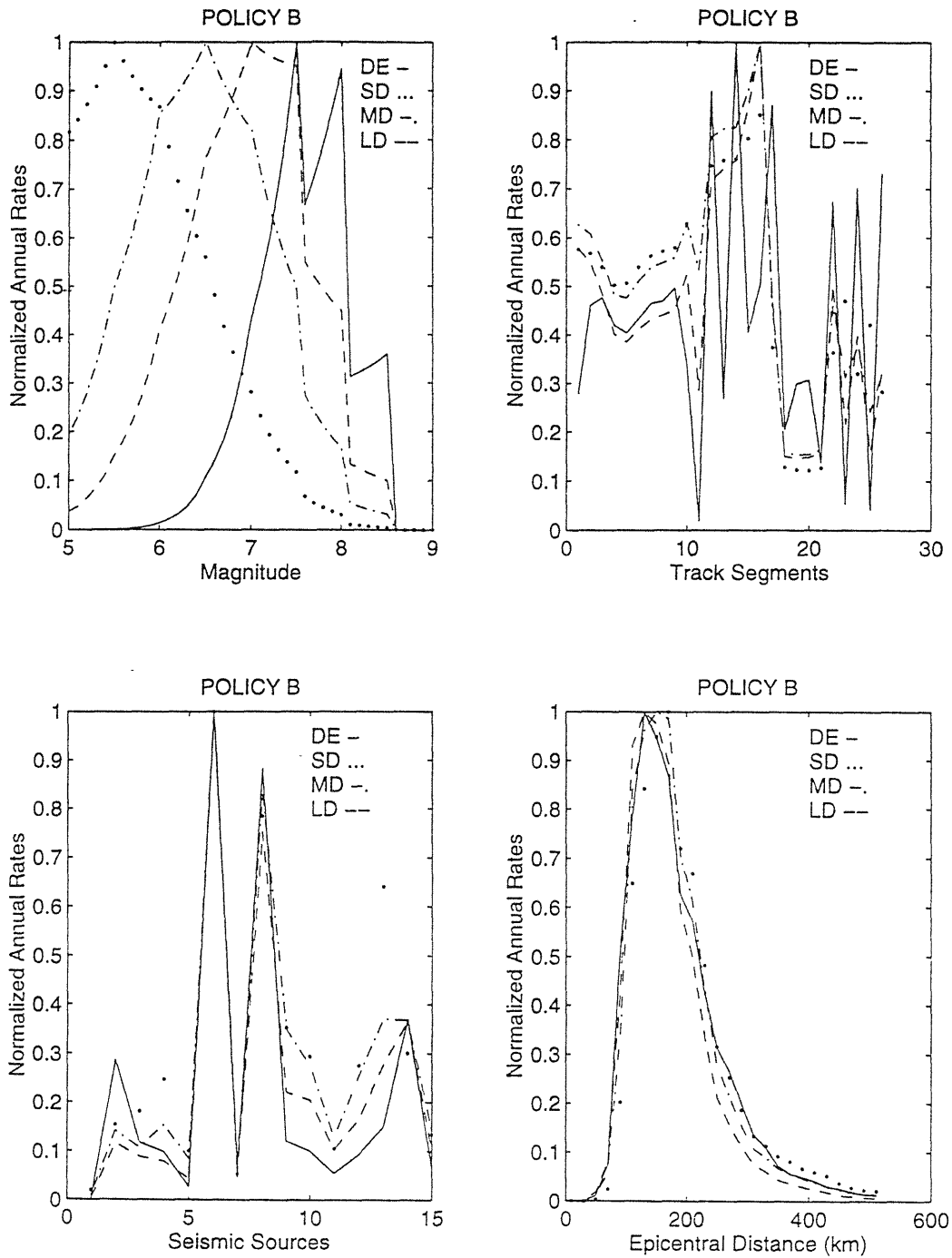


Figure I-1: Normalized risk decomposition for $(b^*, a_{t,loc}, A_{insp1}, A_{insp2}) = (40, 40, 80, 120\text{gals})$: (a) by earthquake magnitude, (b) along the track, (c) by seismic source, and (d) by epicentral distance [Figure similar to Figure 6.2]

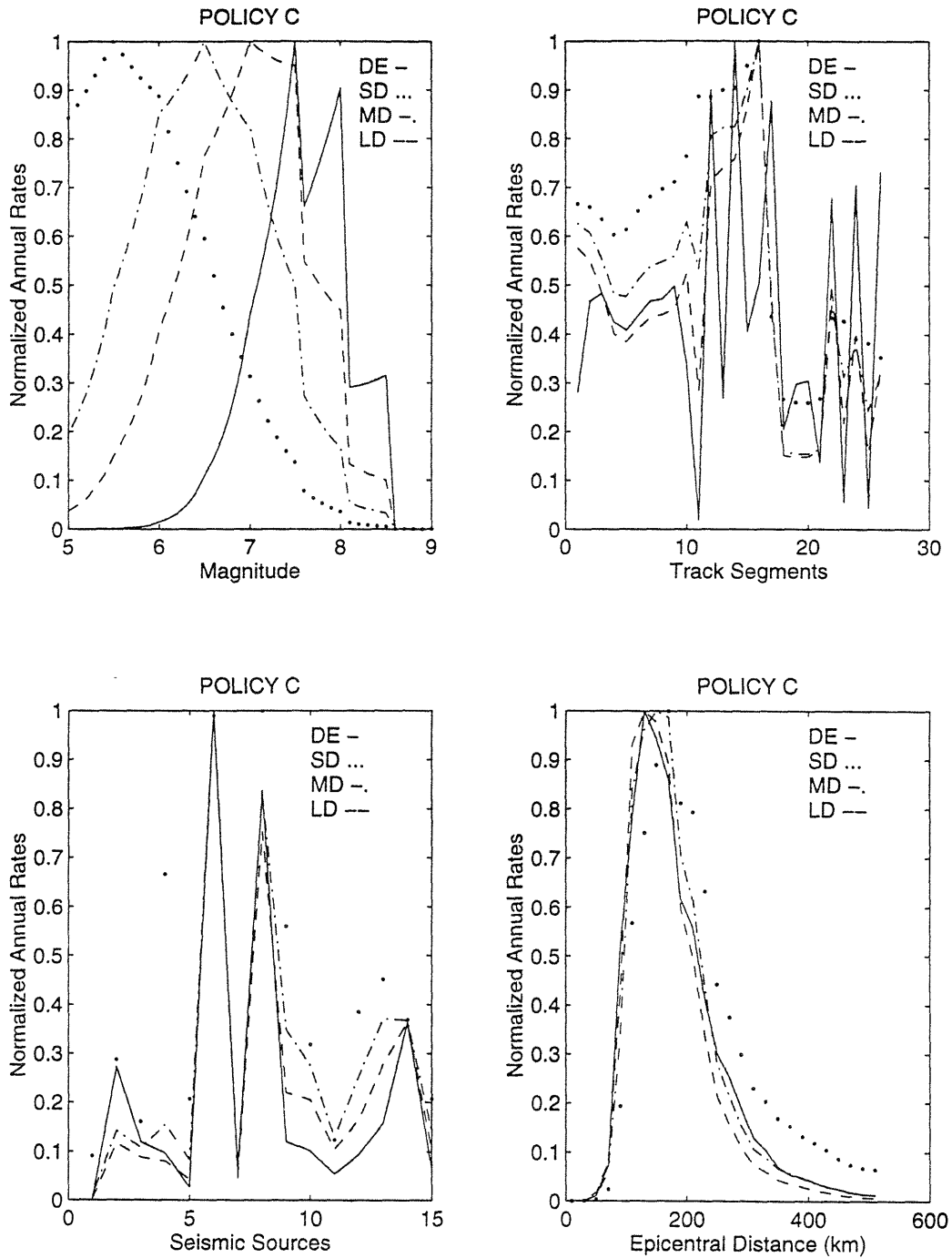


Figure I-2: Normalized risk decomposition for $(c^*, a_{t,loc}, A_{insp1}, A_{insp2}) = (3.0, 40gals, 80gals, 120gals)$: (a) by earthquake magnitude, (b) along the track, (c) by seismic source, and (d) by epicentral distance [Figure similar to Figure 6.2]

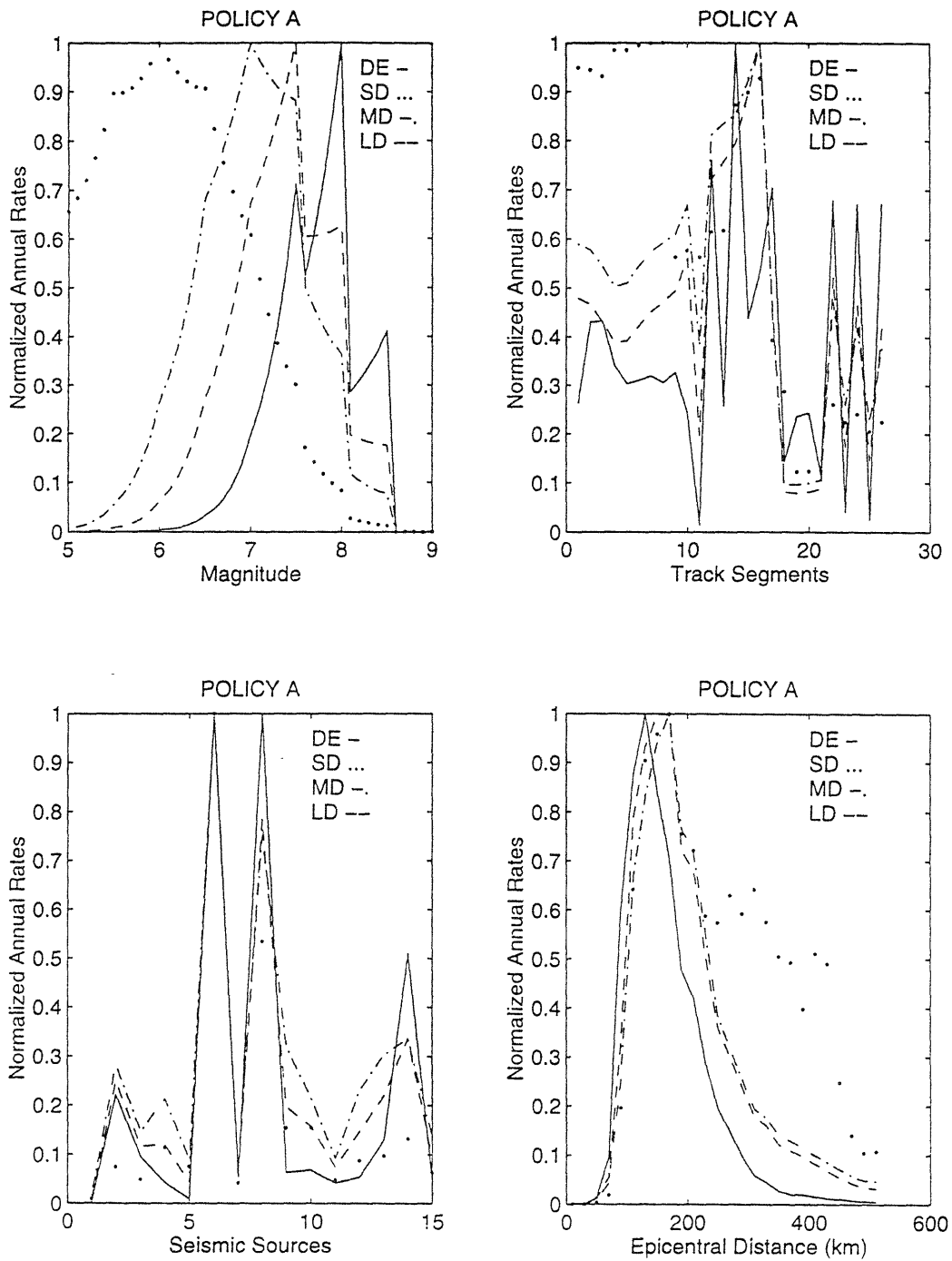


Figure I-3: Normalized risk decomposition-for $(\mathbf{a}^*, S_{a,tloc}, S_{a,insp1}, S_{a,insp2}) = (40, 80, 160, 240\text{gals})$: (a) by earthquake magnitude, (b) along the track, (c) by seismic source, and (d) by epicentral distance [Figure similar to Figure 6.2; notice the use of S_a at the wayside system]

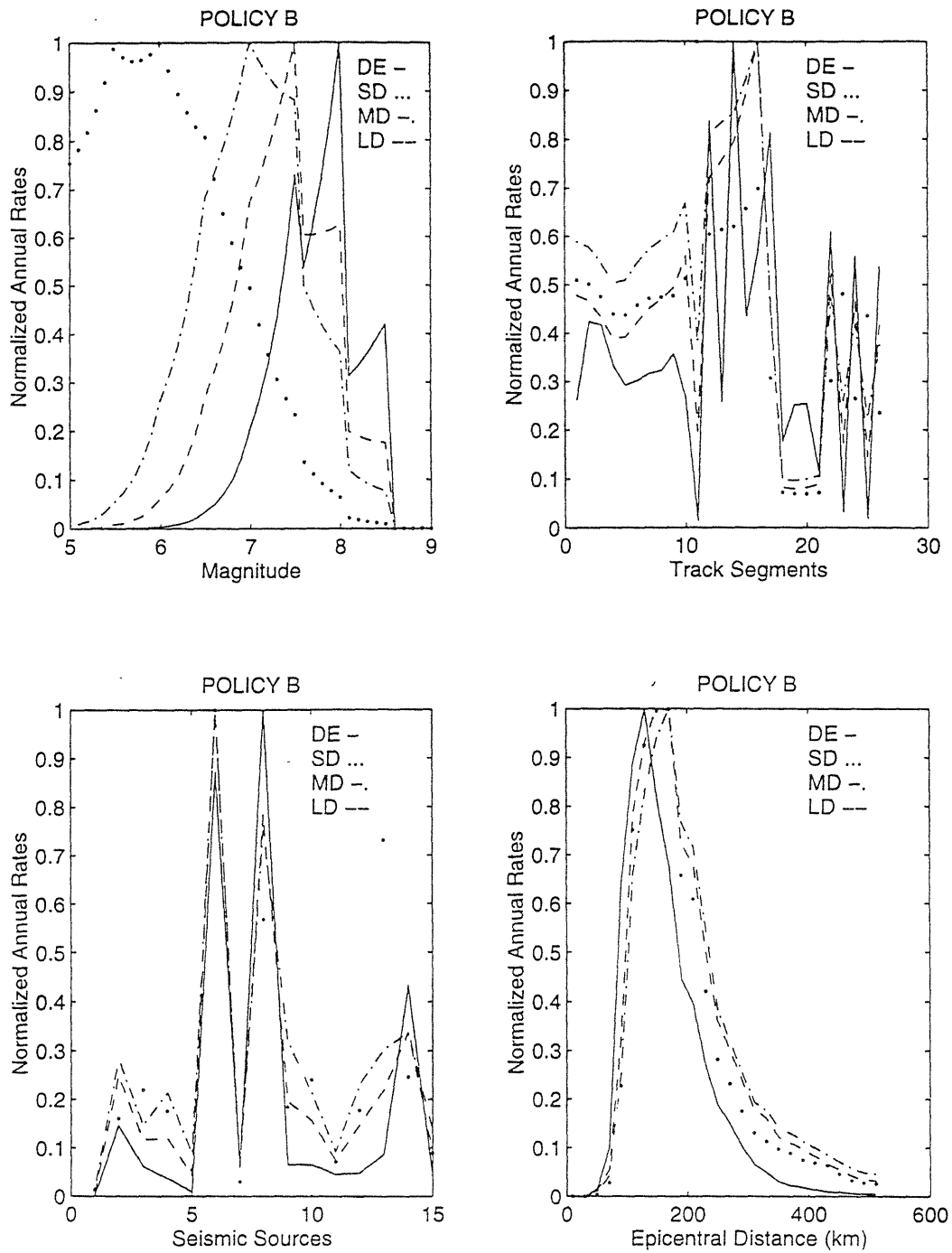


Figure I-4: Normalized risk decomposition for $(b^*, S_{a,tloc}, S_{a,insp1}, S_{a,insp2}) = (40, 80, 160, 240\text{gals})$: (a) by earthquake magnitude, (b) along the track, (c) by seismic source, and (d) by epicentral distance [Figure similar to Figure 6.2; notice the use of S_a at the wayside system]

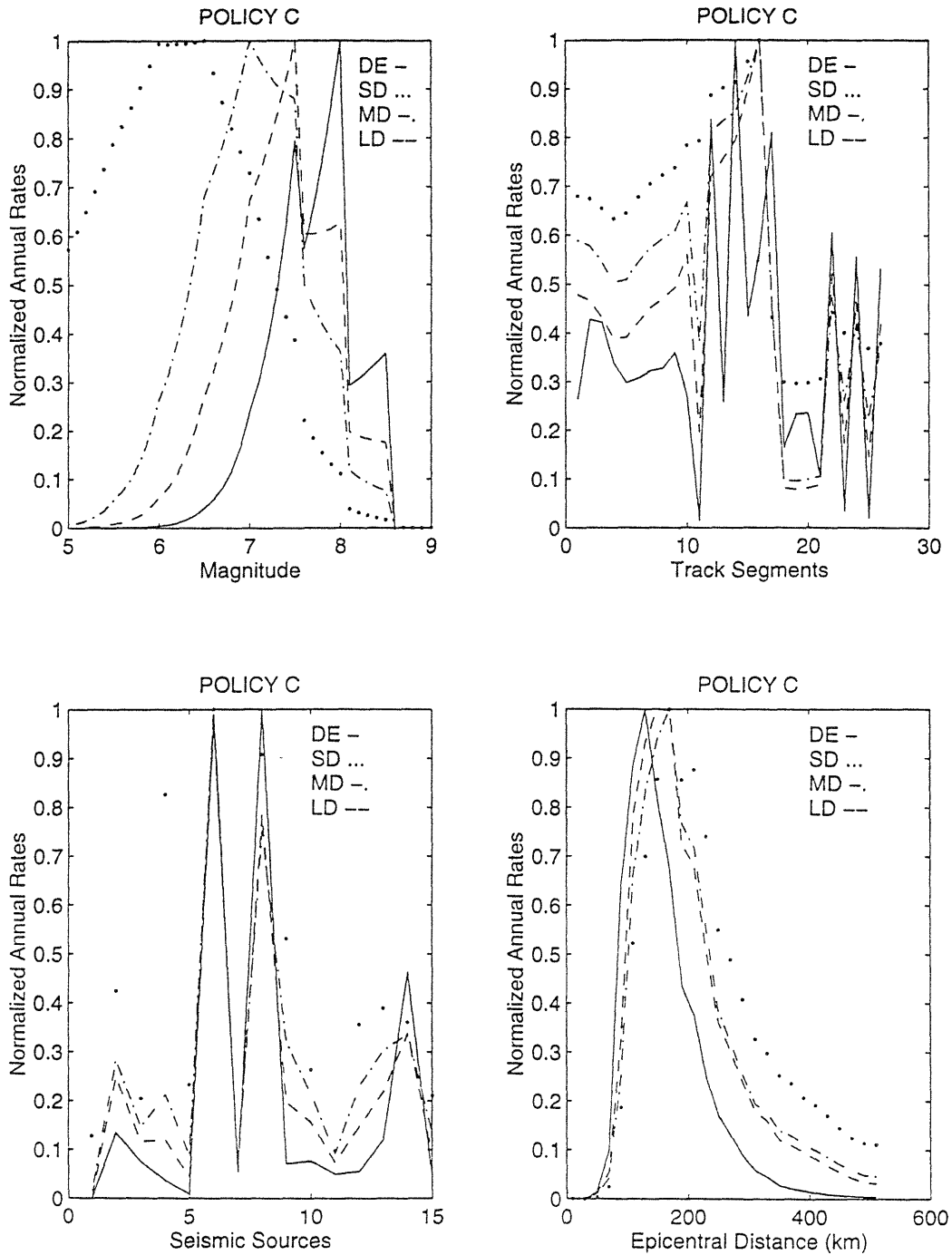


Figure I-5: Normalized risk decomposition for $(c^*, S_{a,tloc}, S_{a,insp1}, S_{a,insp2}) = (40, 80, 160, 240gals)$: (a) by earthquake magnitude, (b) along the track, (c) by seismic source, and (d) by epicentral distance [Figure similar to Figure 6.2; notice the use of S_a at the wayside system]

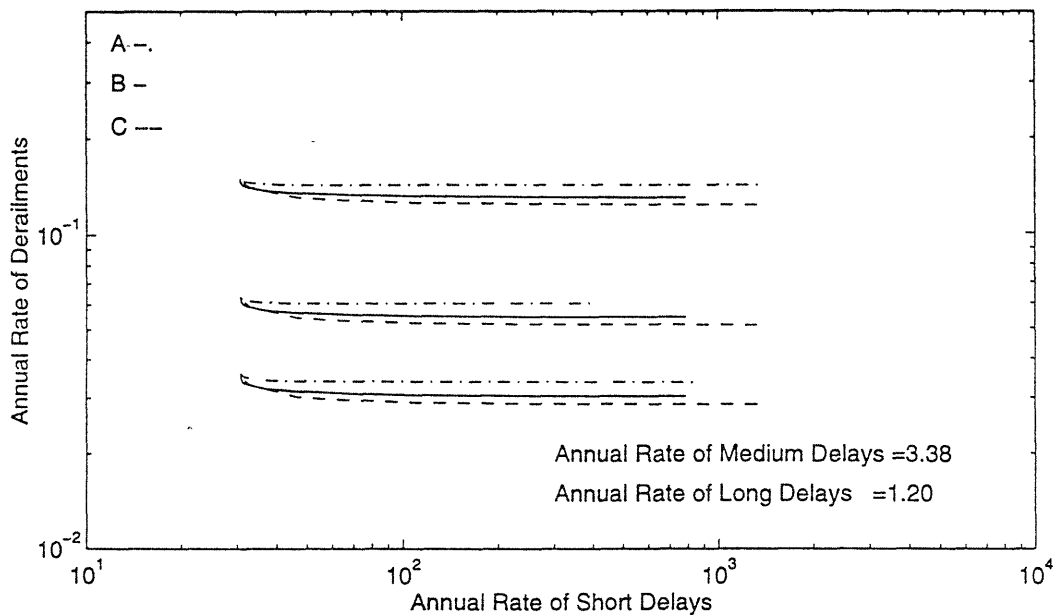
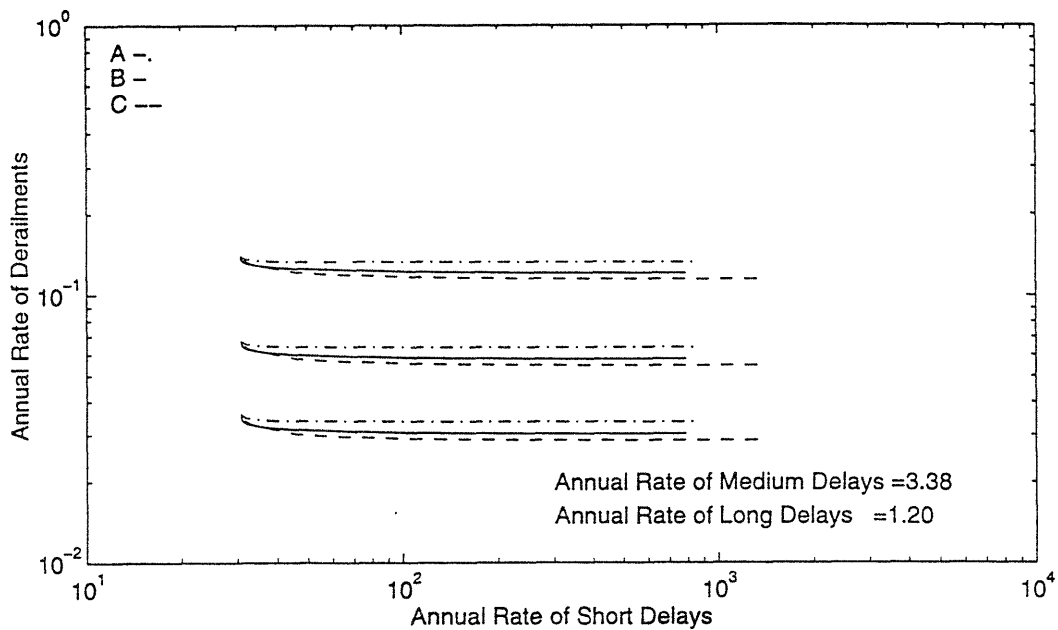


Figure I-6: Annual rates of derailments and various delays, including derailment risk due to resumption of operation following short delays for coastal systems A, B and C and $(a_{t,loc}, A_{insp1}, A_{insp2})=(40, 80, 120\text{gals})$, if:
 (a) relative displacement at yielding, $\delta_y = (70\%, 85\%, 100\%)$ of base-case value
 (b) ductility ratio at failure, $\mu = 2, 3, 4$ (base-case value)
 [Figure corresponds to cases illustrated in Figure 6.6]

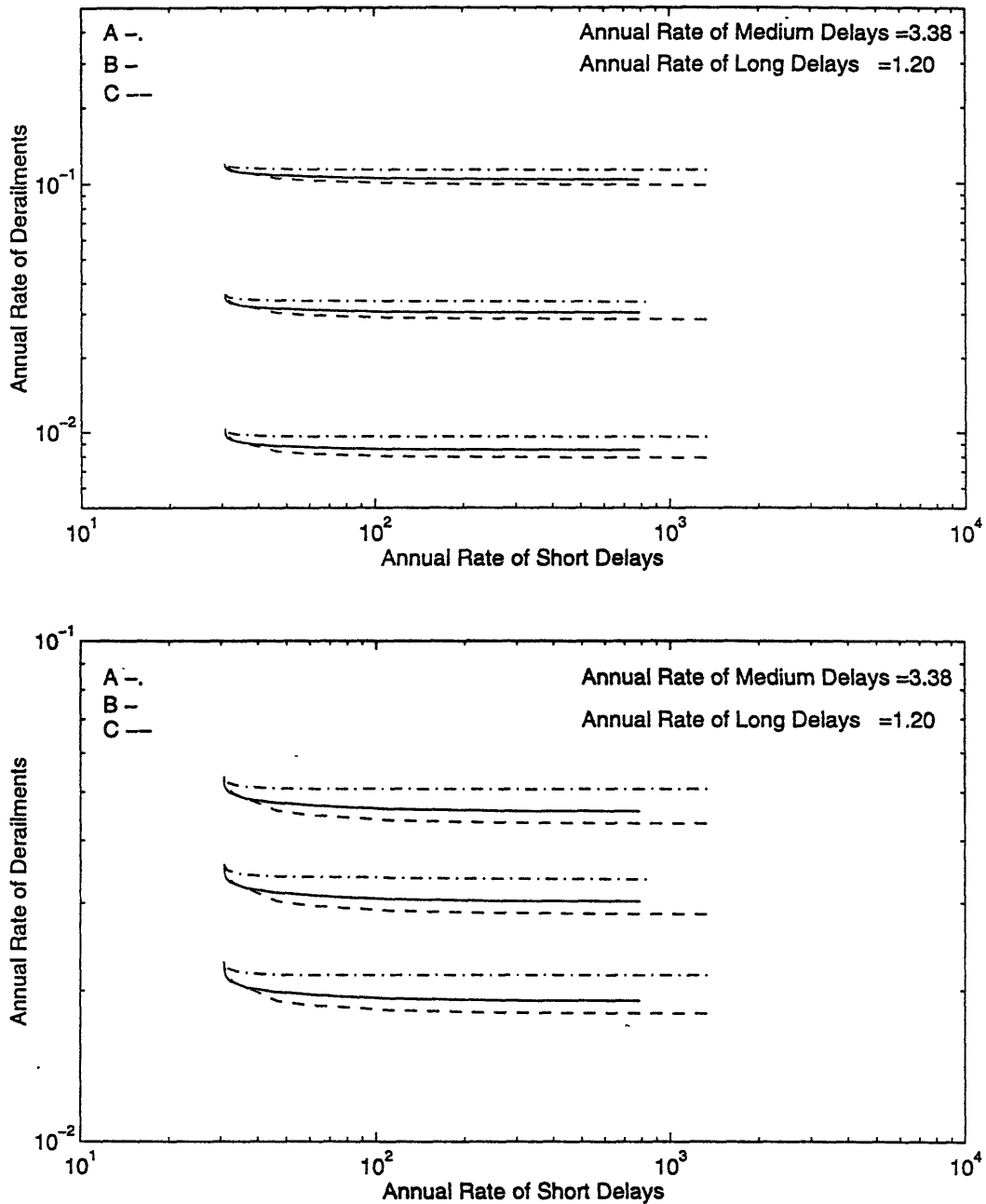


Figure I-7: Annual rates of derailments and various delays, including derailment risk due to resumption of operation following short delays for coastal systems A, B and C and $(a_{t,loc}, A_{insp1}, A_{insp2})=(40, 80, 120\text{gals})$, if:
 (a) uncertainty on resistance, $\sigma_{InR} = 0.3, 0.4(\text{base-case value}), 0.5$.
 (b) parameter controlling damage clustering, $c_1=0.015, 0.03(\text{base-case value}), 0.06$
 [Figure corresponds to cases illustrated in Figure 6.7]

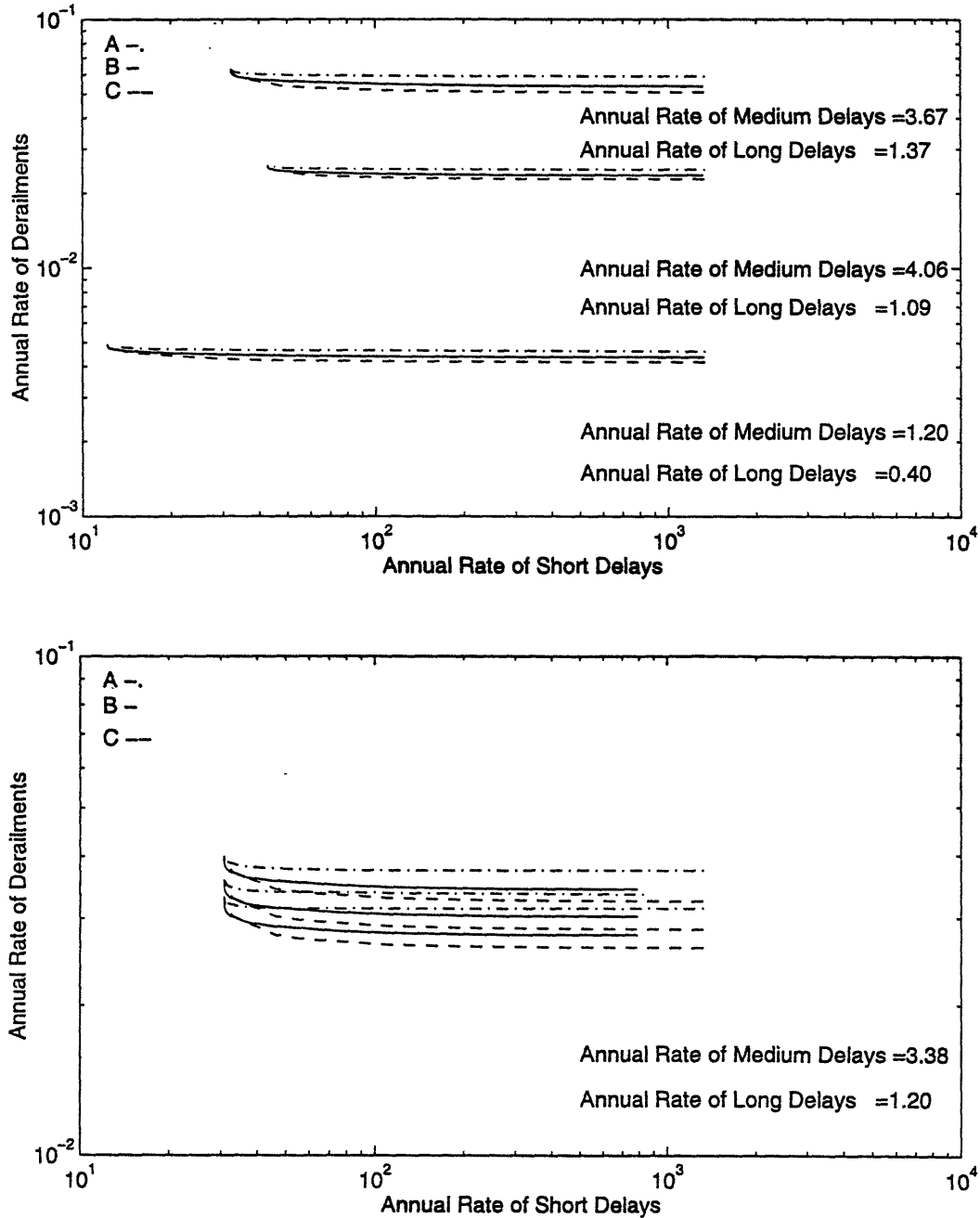


Figure I-8: Annual rates of derailments and various delays, including derailment risk due to resumption of operation following short delays for coastal systems A, B and C and $(a_{t,loc}, A_{insp1}, A_{insp2}) = (40, 80, 120\text{gals})$, if:
 (a) soil type is I, II, III (Table 4.2) all along the line
 (b) maximum velocity, $V_o = 210\text{kmh}, 245\text{kmh}(\text{base-case value}), 300\text{kmh}$
 [Figure corresponds to cases illustrated in Figure 6.9]

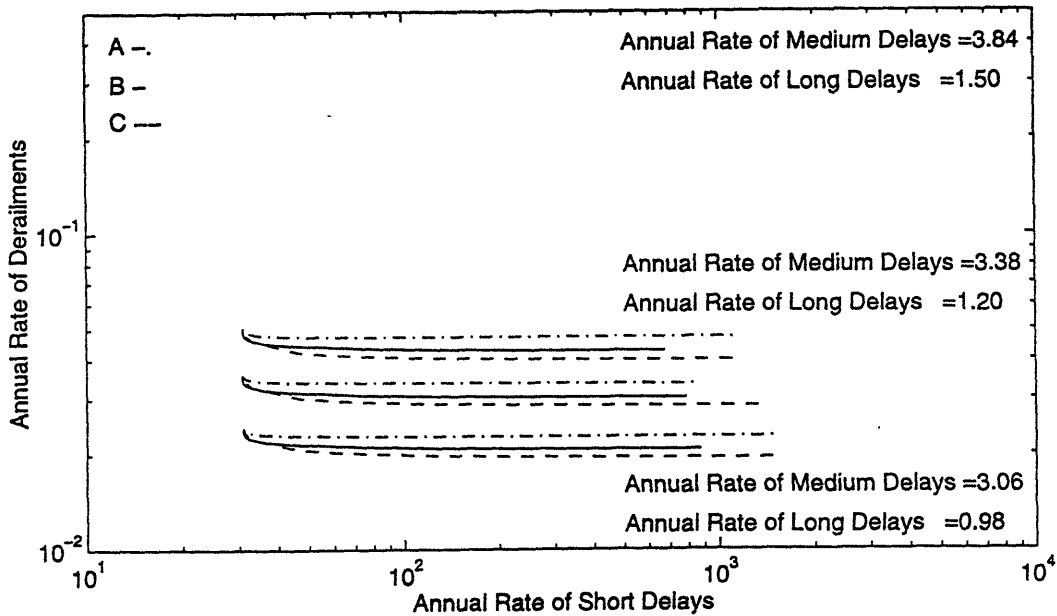
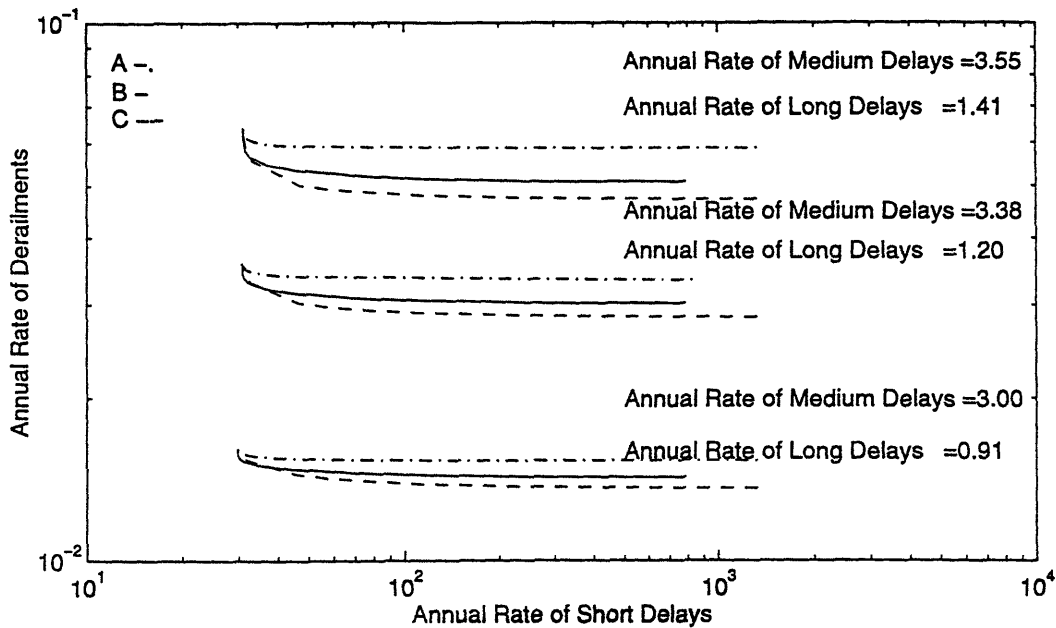


Figure I-9: Annual rates of derailments and various delays, including derailment risk due to resumption of operation following short delays for coastal systems A, B and C and $(a_{t,loc}, \bar{A}_{insp1}, A_{insp2})=(40, 80, 120\text{gals})$, if:
 (a) M_{max} of each seismic source is 0.5 higher/lower relative to base-case value
 (b) b -value of each seismic source is 0.9, 1.1 or base-case value
 [Figure corresponds to cases illustrated in Figure 6.11]

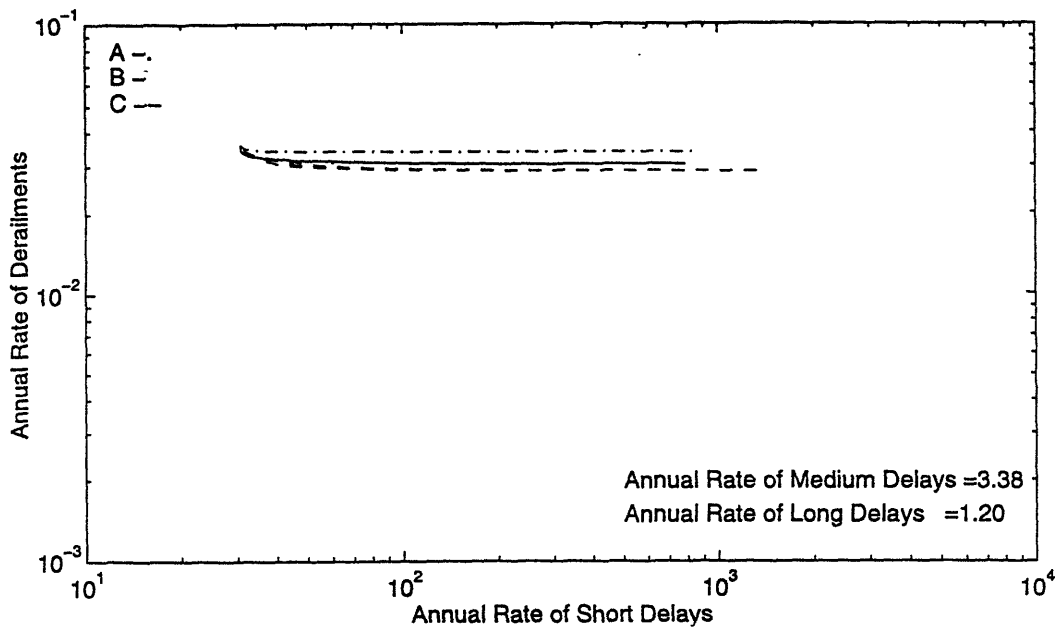
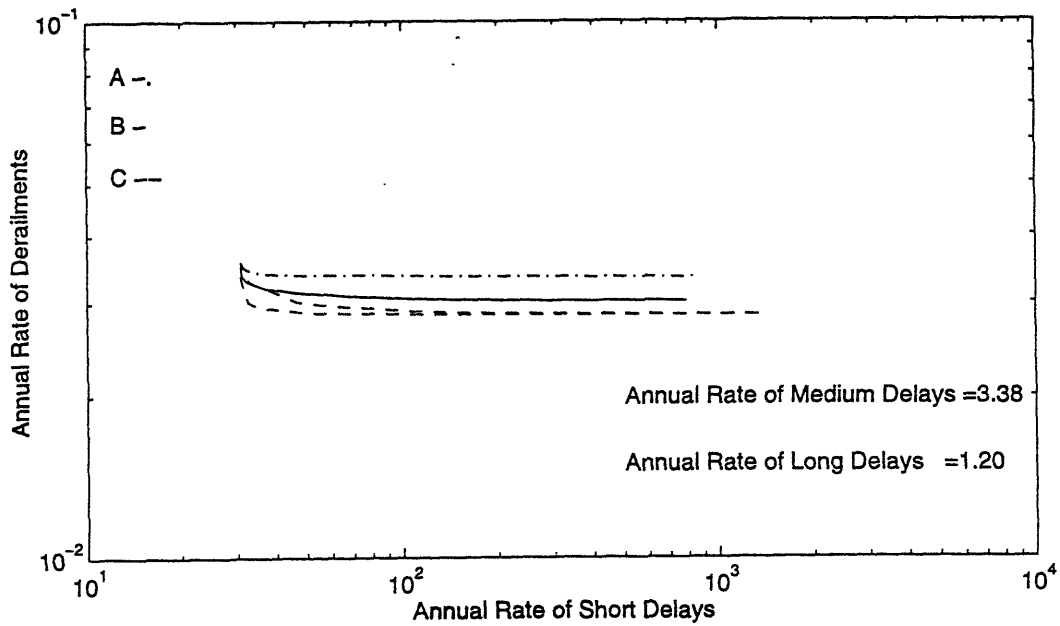


Figure I-10: Annual rates of derailments and various delays, including derailment risk due to resumption of operation following short delays for coastal systems A, B and C and $(a_{t,loc}, A_{insp1}, A_{insp2}) = (40, 80, 120\text{gals})$ for the UREDAS system accuracy of P-wave estimation of:
 (a) earthquake magnitude M : $\sigma_{M,P} = 0.5, 1.0$ (base-case value)
 (b) epicentral distance Δ : $\sigma_{\Delta,P} = 25\%\Delta, 75\%\Delta$ (base-case value), $100\%\Delta$
 [Figure corresponds to cases illustrated in Figure 6.12]

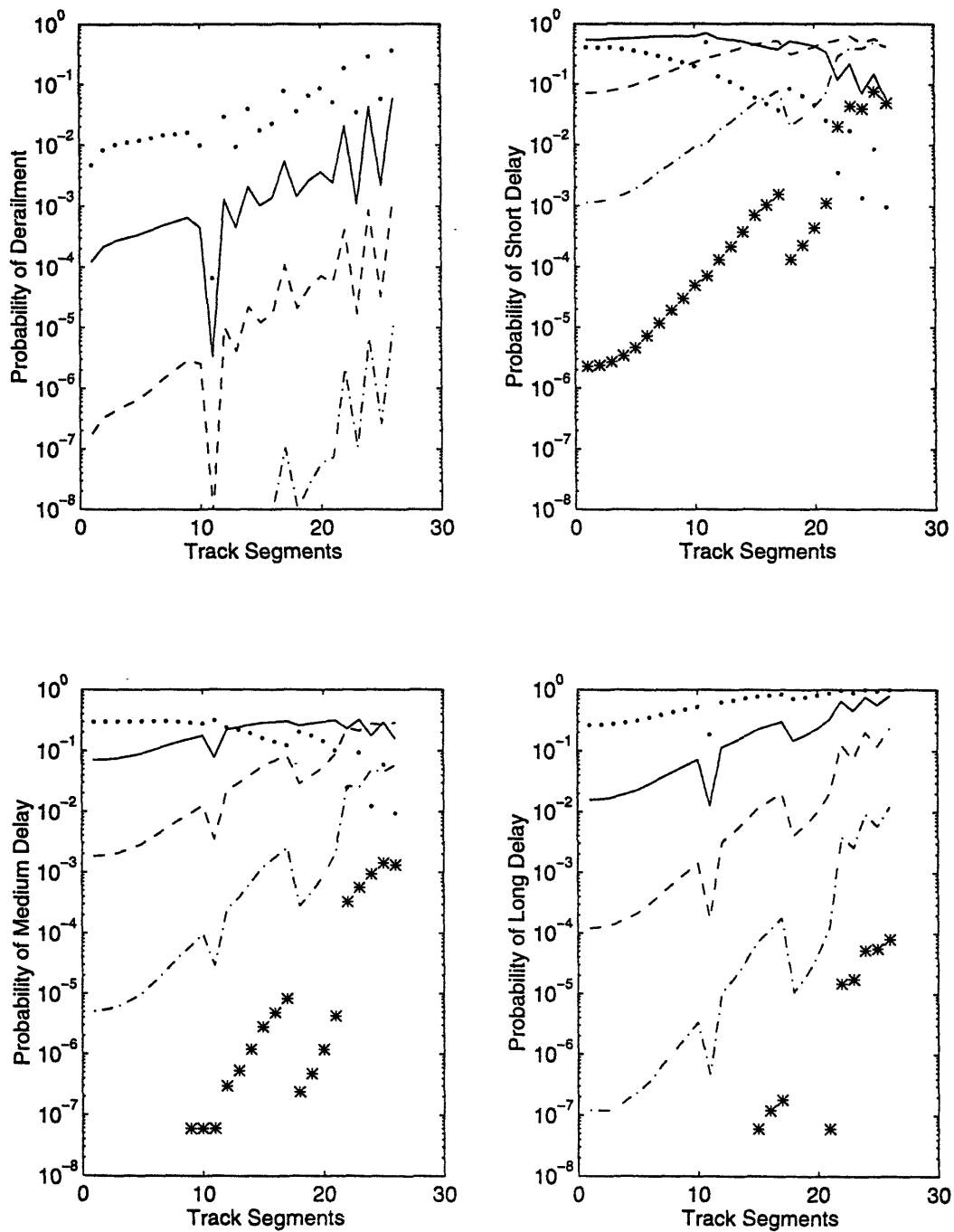


Figure I-11: Conditional probability $P[E|M, \underline{x}, s, B]$ of event E along the line, for $(b^*, a_{t,loc}, A_{insp1}, A_{insp2}) = (40, 40, 80, 120\text{gals})$ and earthquake magnitudes $M = 5 - 9$, [epicenter: 571km from $s=1$ and 135km from $s=26$]
 (a) E = derailment, (b) E = short delay,
 (c) E = medium delay, (d) E = long delay.
 [Figure similar to Figure 6.13, but for coastal system B]

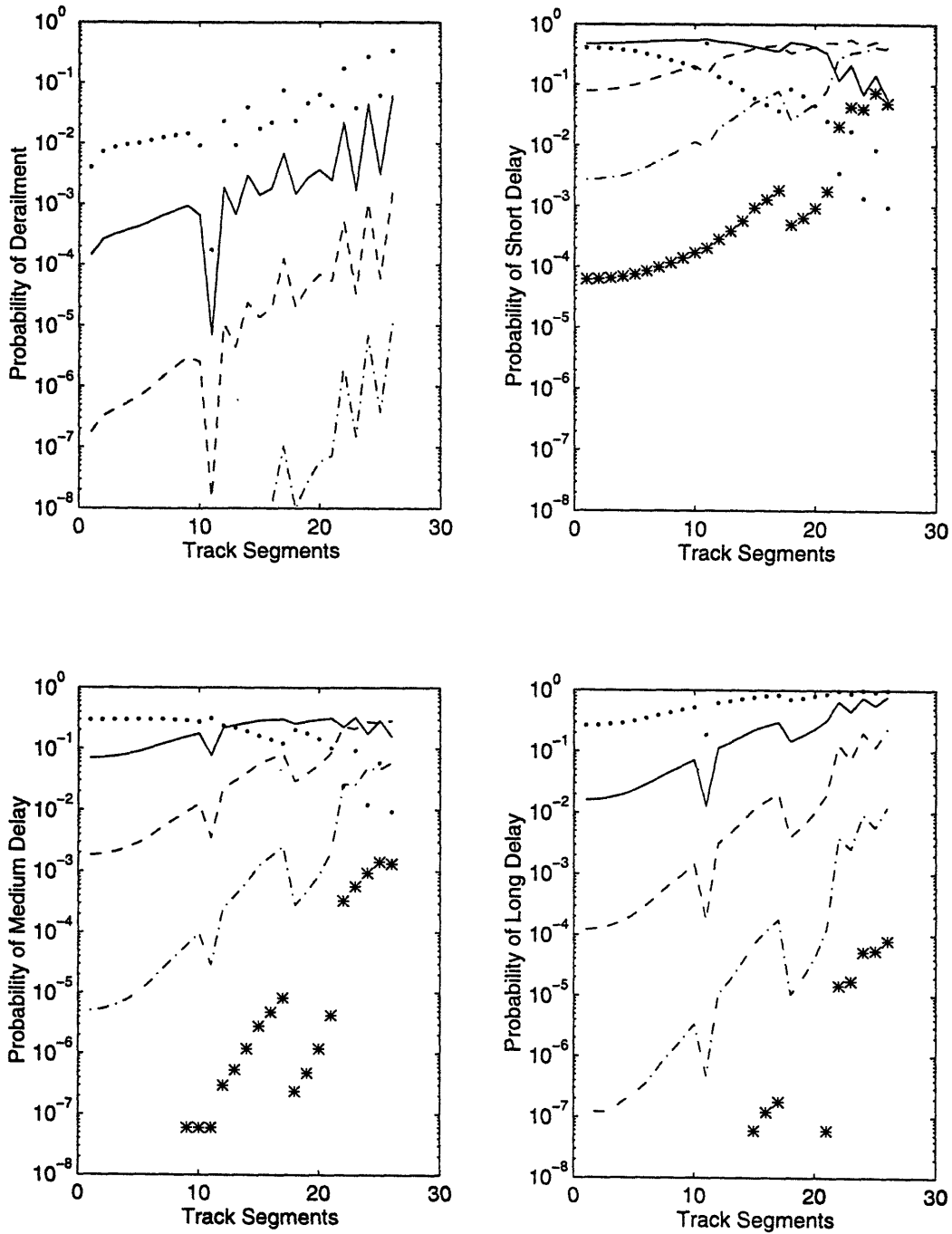


Figure I-12: Conditional probability $P[E|M, \underline{x}, s, C]$ of event E along the line, for $(\underline{c}, a_{t,loc}, A_{insp1}, A_{insp2}) = (3.0, 40\text{gals}, 80\text{gals}, 120\text{gals})$ and earthquake magnitudes $M = 5 - 9$, [epicenter: 571km from $s=1$ and 135km from $s=26$]
 (a) E = derailment, (b) E = short delay,
 (c) E = medium delay, (d) E = long delay.
 [Figure similar to Figure 6.13, but for coastal system C]

Appendix II

Propagation of Delay

Trains that have been cleared by the wayside system to resume regular operation after an earthquake may not be able to do so if there are trains stopped by the SEWS further along the line. This operational constraint increases the total number of delayed trains all along the Tohoku line. The magnitude of the increase is analyzed in this section under some simplifying assumptions, which however allow us to estimate the size of the effect and its dependence on various parameters. In our model, we consider a track 320km long composed of 16 operational segments of equal length, as a representation of the actual line between Tokyo and Sendai. Stations are assumed to be located every 2 operational segments. Traffic load is one of the most influential parameters in the propagation of delays along the line; here we consider three possible train frequencies : (a) one train in each operational segment (for a total of 16 trains, 8 in each direction of travel), (b) one train every two operational segments (total of 8 trains, 4 in each direction of travel) and (c) one train every three operational segments (total of 6 trains, 3 in each direction of travel). All trains are assumed to be located midway within the operational segment they occupy when they are stopped by the SEWS and are equally spaced in each direction; see Figure II-1.

A scenario-based approach is used to study the propagation of delays. Thus, earthquakes of different magnitudes ($M=5, 6, 7$ and 8) are considered to occur at different distances ($D=60, 100$ and 140km) from the midpoint of the track; see Figure II-1. We further assume that the accelerations measured by the wayside accelerometers are the median values given by the attenuation relations (Table 4.3). Moreover, given the fact that along this line we have predominantly soil type II (Table 4.2), we assume this to be true uniformly along the model line. The values of peak ground acceleration for soil type II

along the track, given M and \underline{x} , are presented in Figure II-2. Assuming that all trains along the line have been stopped by either the coastal or the wayside system, the total number of trains is subdivided into short, medium and short delay events, depending on the value of the two track inspection levels A_{insp1} and A_{insp2} and the median attenuated peak ground accelerations for soil type II. In this analysis, we consider constant track inspection levels, which correspond to the current settings, i.e. $A_{insp1}=80\text{gals}$ and $A_{insp2}=120\text{gals}$; see Figure II-2.

In order to compare different delay patterns, we calculate the total duration in minutes of each type of delay. We assume that on-foot inspection of the tracks (long delay) requires 30 minutes, during which the train remains stopped (JREast, personal communication). Following a short delay, we assume that the train is able to catch up by increasing its speed within the normal operational limits. After resumption of operation, such trains are assumed to operate with an average speed of 200kmh. Finally, in the case of a medium delay, trains continue operation at low speed (40kmh) until they reach the next vacant station. During this 30 minute period, a train traveling at 40kmh accumulates 24 minutes of delay compared to regular operation. In general, trains are being dispatched regularly from Tokyo and Sendai during this inspection period. These trains continue their travel until the furthest vacant station with a speed that depends on the level of acceleration recorded in each segment, i.e. 40 or 200kmh corresponding to medium or short delays. Trains are canceled if there are no vacant stations ahead or if the recorded accelerations call for on-foot inspection of the track segment immediately neighboring the dispatching stations. In order to account for train cancellations in the total delay time, we assign a nominal value of delay per cancelled train equal to 96 minutes. This is the time that a Shinkansen train needs to travel all the 320km of the line at a speed of 200kmh. Finally, we assume that no more than one train traveling in the same direction can be in the same 10km track section at any one time.

An example of the resumption of operation of the model line after the operation of the SEWS is presented in Figure II-3. This figure shows only half the total track (from 0 to

160km and operational segments 1-8) and only half of the trains due to symmetry. For an earthquake of $M=7$ and $D=60\text{km}$ (see Figure II-1), the recorded values of a_{max} compared to the two track inspection levels call for on-foot inspection in segments 7 and 8 (from 120 to 160km), for on-train inspection in segments 4, 5 and 6 (from 60 to 120km) and allow immediate resumption of regular operation of trains in segments 1, 2 and 3 (from 0 to 60km); see Figure II-2. Figure II-3 shows the locations of the 8 trains included in this track section versus time after resumption of operation. Of these 8 trains, 2 trains remain stopped for 30 minutes, 4 trains travel at low speed for some time, 1 train stops at a station until the track is cleared as there is no vacant station to proceed to and only 1 train resumes regular operation and reaches its destination without delay. Moreover, 2 trains are cancelled (12 and 24 minutes after resumption of service), while 36 minutes after resumption of service the first train is dispatched according to schedule. Scenarios of the same type are studied for different earthquake magnitudes and epicentral distances.

Results are presented in terms of the following quantities:

- **First order delay**, which is the aggregated delay time in minutes from all trains along the line, ignoring propagation of delay effects. This corresponds to the delays estimated in Chapters 6 and 7.
- **Second order delay**, which is the aggregated delay time in minutes from all trains along the line, due to the fact that the trains are not able to proceed due to stopped or delayed trains ahead. This second order delay does not include train cancellations.
- **Third order delay**, in number of trains as well as minutes, associated with train cancellations.

Results are also presented in terms of correction factors of the first order delay if we include second or both second and third order.

Results in Terms of Minutes of Total Delay

Under the simplifying assumptions we have just described, we have found that earthquakes of magnitudes 5 and 6 at distances 60, 100 and 140km from the track cause only short delays (see Figure II-2), which can be compensated by increasing the speed of trains after resumption of service. This is not the case for higher magnitudes. Table II-1 presents the delay results for distances $D=60, 100$ and 140km and earthquake magnitudes 7 and 8. Based on these results we conclude:

As the frequency of trains decreases, the total delay in terms of minutes along the line decreases as well. This is true for all orders of delay, their aggregate sums and for the number of cancelled trains. Moreover, total delays increase with earthquake magnitude. This is consistently observed for the total delay time along the line, however the first and second order delay times are sensitive to the location of trains along the line when they are stopped by the SEWS. An interesting result is that the number of cancelled trains is more sensitive to the frequency of trains than to earthquake magnitude and location. Finally, the dispatching policy of trains which governs cancellations (3rd order delay), is very significant in controlling the total delay time along the line.

Correction Factors of the First Order Delay

The correction factors of first order delay time to include second order or both second and third order delays are presented in Table II-2, for various magnitudes and epicentral distances. If one includes both types of delay propagation, there is at most a 4-fold increase in the value of the first order delay while on average we observe a 2-fold increase. If train cancellations are excluded, then the correction factor on the first order delay is around 1.3 on average with a peak value of 1.6.

Order of Delay	1 train per segment	1 train per 2 segments	1 trains per 3 segments	1 train per segment	1 train per 2 segments	1 train per 3 segments
D=60km	M=7			M=8		
1st	216	108	84	480	240	180
2nd	86	63	48	0	0	0
3rd(cancel) ¹	(4) 384	(2) 192	0	(4) 384	(2) 192	0
1st+2nd	302	171	132	480	240	180
1st+2nd+3rd	686	363	132	864	432	180
D=100km	M=7			M=8		
1st	156	78	48	420	210	120
2nd	68	46	18	30	15	15
3rd(cancel) ¹	(4) 384	0	0	(4) 384	(2) 192	0
1st+2nd	224	124	66	450	225	150
1st+2nd+3rd	608	124	66	834	417	150
D=140km	M=7			M=8		
1st	0	0	0	432	216	156
2nd	0	0	0	0	0	0
3rd(cancel) ¹	0	0	0	(4) 384	(2) 192	0
1st+2nd	0	0	0	432	216	156
1st+2nd+3rd	0	0	0	816	408	156

(1) in parentheses, the number of cancelled trains

Table II-1: Aggregate delay in terms of minutes for first, second and third order delays along the line, for earthquakes of magnitudes 7 and 8 occurring at 60, 100 and 140km from the center point of the model line.

Order of Delay	1 train per segment	1 train per 2 segments	1 trains per 3 segments	1 train per segment	1 train per 2 segments	1 train per 3 segments
D=60km	M=7			M=8		
incl 2nd	1.4	1.6	1.6	1.0	1.0	1.0
incl. 2nd+3rd	3.2	3.4	1.6	1.8	1.8	1.0
D=100km	M=7			M=8		
incl. 2nd	1.4	1.6	1.4	1.1	1.1	1.2
incl. 2nd+3rd	3.9	1.6	1.4	2.0	2.0	1.2
D=140km	M=7			M=8		
incl. 2nd	1.0	1.0	1.0	1.0	1.0	1.0
incl. 3rd	1.0	1.0	1.0	1.9	1.9	1.0

Table II-2: Factors of increase of the first order delay, after including second or both second and third order delay, for earthquakes of magnitudes 7 and 8 occurring 60, 100 and 140km from the central point of the model line.

POTENTIAL EPICENTERS OF EARTHQUAKES
with Respect to Model Line-1 train per segment

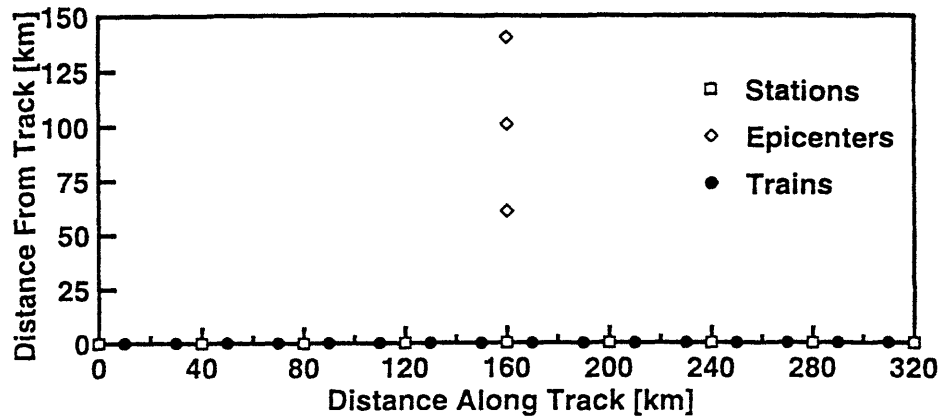


Figure II-1: Model line, train and station locations and potential epicenters of earthquakes used in the study of propagation of delay along the line [Figure for train frequency of 1 train per segment]

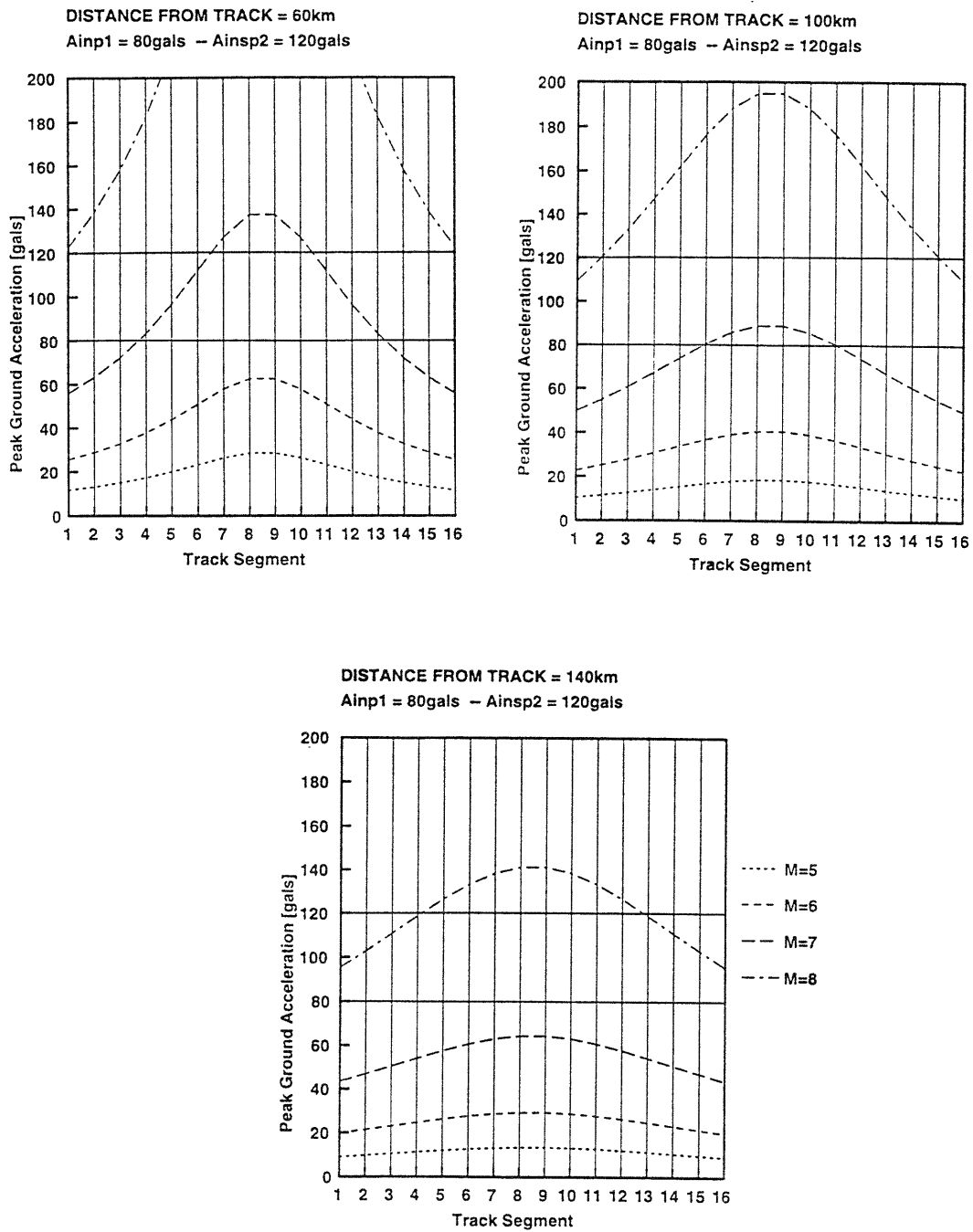


Figure II-2: Assumed recorded values of peak ground acceleration along the model line for $M = 5-8$, compared to track inspection levels: $A_{insp1}=80\text{gals}$ and $A_{insp2}=120\text{gals}$, for epicentral distances: (a) $D=60\text{km}$, (b) $D=100\text{km}$ and (c) $D=140\text{km}$.

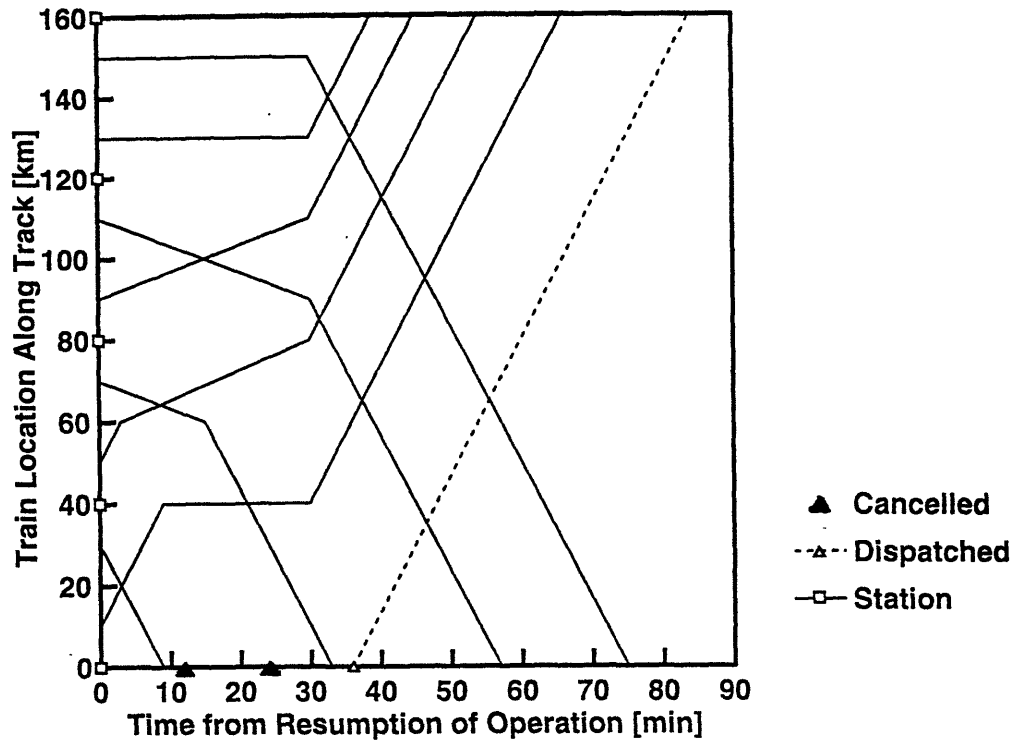


Figure II-3: Train location versus time after resumption of service of trains
 according to current track inspection levels: $A_{insp1}=80\text{gals}$ and $A_{insp2}=120\text{gals}$.
 for earthquake of $M=7$ at $D=60\text{km}$.
 [1. Figure presents half the total track and half the trains due to symmetry,
 2. Figure for train frequency of 1 train per segment]